HEAVY QUARKONIUM HADROPRODUCTION IN THE COLOR EVAPORATION MODEL

by

Christopher P. Smith

A thesis submitted in partial fulfillment of

the requirements for the degree of

Master of Science

(Physics)

DISTRIBUTION STATEMENT A
Approved for Public Release
Distribution Unlimited

at the

UNIVERSITY OF WISCONSIN – MADISON

2000

20000523 047

DTIC QUALITY INSPECTED 2

REPORT DOCUMENTATION PAGE

Form Approved OMB No. 0704-0188

Public reporting burden for this collection of information is estimated to average 1 hour per response, including the time for reviewing instructions, searching existing data sources, gathering and maintaining the data needed, and completing and reviewing this collection of information. Send comments regarding this burden estimate or any other aspect of this collection of information, including suggestions for reducing this burden to Department of Defense, Washington Headquarters Services, Directorate for Information Operations and Reports (0704-0188), 1215 Jefferson Davis Highway, Suite 1204, Arlington, VA 22202-4302. Respondents should be aware that notwithstanding any other provision of law, no person shall be subject to any penalty for failing to comply with a collection of information if it does not display a currently valid OMB control number. **PLEASE DO NOT RETURN YOUR FORM TO THE ABOVE ADDRESS.**

1. REPORT DATE *(DD-MM-YYYY)*	2. REPORT TYPE	3. DATES COVERED *(From - To)*
17-05-2000	Master of Science Thesis	N/A

4. TITLE AND SUBTITLE
Heavy Quarkonium Hadroproduction in the Color Evaporation Model

5a. CONTRACT NUMBER
N/A

5b. GRANT NUMBER
N/A

5c. PROGRAM ELEMENT NUMBER
N/A

6. AUTHOR(S)
CPT Christopher P. Smith

5d. PROJECT NUMBER
N/A

5e. TASK NUMBER
N/A

5f. WORK UNIT NUMBER
N/A

7. PERFORMING ORGANIZATION NAME(S) AND ADDRESS(ES)
N/A N/A

8. PERFORMING ORGANIZATION REPORT NUMBER
N/A

9. SPONSORING / MONITORING AGENCY NAME(S) AND ADDRESS(ES)
N/A N/A

10. SPONSOR/MONITOR'S ACRONYM(S)
N/A

11. SPONSOR/MONITOR'S REPORT NUMBER(S)
N/A

12. DISTRIBUTION / AVAILABILITY STATEMENT
Distribution is unlimited.

13. SUPPLEMENTARY NOTES
This is an MS thesis in theoretical physics. It was written while I was a graduate student at the University of Wisconsin - Madison under the Army's Advanced Civil Schooling Program.

14. ABSTRACT
The primary goal of this thesis is to test the predictions of the Color Evaporation Model against the available hadroproduction data on the bottomonium system. As a secondary effort, it also applies each test to the model's predictions for the charmonium system in order to confirm and extend previous results and to identify any differences between the two heavy quarkonium systems. The analysis leads to three significant results. First, although it shows that the model can account for most of the available hadroproduction data, it identifies two potentially important behaviors in the charmonium system that the model fails to explain. Second, it refutes two significant assumptions made in some previous formulations of the model. Finally, it introduces a potentially useful technique to estimate the numerical values of the model's non-perturbative factors for states on which experimental data is not available.

15. SUBJECT TERMS
Theoretical Physics; Elementary Particle Physics; High Energy Physics

16. SECURITY CLASSIFICATION OF:			17. LIMITATION OF ABSTRACT	18. NUMBER OF PAGES	19a. NAME OF RESPONSIBLE PERSON
a. REPORT	b. ABSTRACT	c. THIS PAGE			CPT Christopher P. Smith
Unclassified	Unclassified	Unclassified	N/A	117	19b. TELEPHONE NUMBER *(include area code)* 608-271-7086

Abstract

The primary goal of this thesis is to test the predictions of the Color Evaporation Model against the available hadroproduction data on the bottomonium system. As a secondary effort, it also applies each test to the model's predictions for the charmonium system in order to confirm and extend previous results and to identify any differences between the two heavy quarkonium systems. The analysis leads to three significant results. First, although it shows that the model can account for most of the available hadroproduction data, it identifies two potentially important behaviors in the charmonium system that the model fails to explain. Second, it refutes two significant assumptions made in some previous formulations of the model. Finally, it introduces a potentially useful technique to estimate the numerical values of the model's non-perturbative factors for states on which experimental data is not available.

Acknowledgements

Although I am the sole author listed on the cover of this thesis, it would be unjust for me to imply that I alone deserve the credit for its completion. I would never have been able to design and execute such a project without a great deal of assistance. The complete list of people who provided some form of support or advice is far too long to include. Thus, although I wish to offer my most sincere appreciation to everyone who helped me along the way, I will make explicit reference only to those whose contributions were most significant.

First, I want to thank Don Reeder, my thesis advisor, for his expert advice and his untiring patience. His experience and intuition were invaluable in selecting logical and productive courses of action at every point in the analysis. More importantly, although I gave him many reasons to conclude that I was a hopelessly inept physicist, he never made me feel like one.

Second, I would like to thank Francis Halzen for suggesting this topic and for lending me his technical expertise whenever I required it. His enthusiastic response to even the slightest progress was always a great source of encouragement.

Next, I want to express my appreciation to Eduardo Gregores for setting me on the correct path. Without his suggestions and his willingness to answer the most basic questions, I would not have known where to begin.

Last, but most importantly, I want to thank my wife, Julie, and my daughters, Shannon and Amanda, for their unconditional support. During the writing of this thesis, they were forced to sacrifice my attention and endure my unpleasant disposition for weeks at a time. In exchange, they offered only patience, love, and encouragement. I am truly fortunate to share my life with women such as these.

Table of Contents

List of Figures

List of Tables

Chapter 1

Introduction and Theoretical Background

One of the primary goals of science is to gain an understanding of nature at its most fundamental levels. At the vanguard of this quest is the discipline of elementary particle physics. Its practitioners seek to identify the most basic structureless units of matter and to describe the interactions between them. A century of extensive research has led them to believe that matter is composed of two different classes of elementary particles known as quarks and leptons. At accessible energy scales, these particles interact through three distinct fundamental forces called the strong, electro-weak, and gravitational interactions. Such a simple categorization, however, belies the number and diversity of the phenomena produced by these basic components and the complexity of the theories required to describe them. A detailed discussion of them all is beyond the scope of any one work. Accordingly, in this paper we will limit our attention to only one class of elementary particles, the quarks, and one of the fundamental forces, the strong interaction.

1.1 Quarks and Color

Quarks are structureless fermions with spin ½. Six different types or "flavors" of quarks are known to exist. The relevant properties of each type are listed in Table 1.1 (a). Each flavor

of quark has an associated anti-quark. As shown in Table 1.1 (b), the anti-quarks have the same masses as the corresponding quarks but their electric charges carry the opposite sign.

QUARKS			
Flavor	Symbol	Approximate Mass (GeV)	Electric Charge
Up	u	0.004	+2/3
Down	d	0.007	-1/3
Strange	s	0.135	-1/3
Charm	c	1.5	+2/3
Bottom	b	5	-1/3
Top	t	175	+2/3

(a)

ANTI-QUARKS			
Flavor	Symbol	Approximate Mass (GeV)	Electric Charge
Anti-Up	$\bar{u}$	0.004	-2/3
Anti-Down	$\bar{d}$	0.007	+1/3
Anti-Strange	$\bar{s}$	0.135	+1/3
Anti-Charm	$\bar{c}$	1.5	-2/3
Anti-Bottom	$\bar{b}$	5	+1/3
Anti-Top	$\bar{t}$	175	-2/3

(b)

Table 1.1: (a) Selected properties of the six quark flavors. (b) Selected properties of the corresponding anti-quarks. The mass values are taken from page 2 of Reference [1].

As these tables imply, the masses of the quarks are difficult to define. We will discuss this issue in more detail in Section 1.2.3. At this point, however, we note that it is conventional

to refer to those quarks with masses less than 1 GeV as light quarks and those with masses greater than 1 GeV as heavy quarks.

Quarks are distinguished from leptons by the fact that they possess an additional conserved quantum number known as "color". For any given quark, regardless of flavor, this quantum number has only three possible values. These values are equal in magnitude but they represent orthogonal unit vectors in an abstract, three-dimensional "color space". The three possible color states of the quark are referred to as red (R), green (G), and blue (B) while those of the anti-quark are called anti-red ($\overline{R}$), anti-green ($\overline{G}$), and anti-blue ($\overline{B}$). The logic behind this naming scheme will become evident in Section 1.2.3.

At the most basic level, it is this property of color that determines the nature of the strong interaction between two particles. The forces associated with the interaction act only on particles with non-zero color. Thus, quarks participate in strong interactions but leptons do not.

1.2 Strong Interactions and Quantum Chromodynamics

Elementary particle physicists suspect that all of the fundamental interactions in nature can be described by quantum field theories based on dynamical invariance under local phase or "gauge" transformations. The currently accepted "gauge theory" of the strong interaction is called Quantum Chromodynamics (QCD). It is derived from the requirement of invariance under local phase transformations of the color fields of quarks. Since color space has three dimensions, the corresponding symmetry group or "gauge group" is SU(3). Like the more familiar theory of Quantum Electrodynamics (QED), QCD is renormalizable. Unlike QED, however, it is "non-abelian". Formally, this means that the generators of the transformations

do not commute with each other. Physically, however, it has several very important consequences that we will discuss later in this section.

One of the hallmarks of any gauge theory is the introduction of a particle called a "gauge boson" which mediates the corresponding interaction. In QCD, the gauge boson is a massless, spin 1 particle called the gluon. The size of the gauge group requires the existence of eight types of gluons that differ only in their color wave functions. The explicit forms of these wave functions are given in Table 1.2. Note that each gluon carries both one unit of color and one unit of anti-color.

Gluon	Color Wave Function
1	$R\overline{G}$
2	$R\overline{B}$
3	$G\overline{R}$
4	$G\overline{B}$
5	$B\overline{R}$
6	$B\overline{G}$
7	$\sqrt{\frac{1}{2}}(R\overline{R} - G\overline{G})$
8	$\sqrt{\frac{1}{6}}(R\overline{R} + G\overline{G} - 2B\overline{B})$

Table 1.2: Gluon color wave functions.

QCD is a fascinating theory with many important and unusual properties. Only three of these properties, however, are critical to the analysis in this paper. Thus, we restrict our further discussions of QCD to gluon self-interaction, asymptotic freedom, and confinement.

Readers wishing to learn more about QCD should consult References [2] and [3] for basic treatments of the theory and the associated phenomena or Reference [1] for a more advanced and detailed discussion.

1.2.1 Gluon Self-Interaction

Because QCD is a non-abelian gauge theory, the gluons interact not only with the quarks but also with each other. One might naively anticipate this property from the simple fact that the strong interaction acts on color and, as we emphasized above, the gluons themselves carry color. The source of the self-interaction is best seen, however, by turning to the language of quantum field theory. The interaction Lagrangian density of QCD is [4]:

$$\begin{aligned} L_{int} = & -\tfrac{1}{2} g_0 (\bar{q}\gamma_\mu \lambda_a q) G_a{}^\mu + \tfrac{1}{2} g_0 f_{abc} (\partial^\mu G_a{}^\nu - \partial^\nu G_a{}^\mu) G_{b\mu} G_{c\nu} \\ & - \tfrac{1}{4} g_0^2 f_{abc} f_{ab'c'} G_b{}^\mu G_c{}^\nu G_{b'\mu} G_{c'\nu} + \tfrac{1}{2} g_0 f_{abc} (\eta_a^* \partial_\mu \eta_b) G_c{}^\mu \end{aligned} \tag{1.1}$$

In this expression, "q" is the fermion field operator for the quarks, "G" is the boson field operator for the gluons, and "η" is the field operator for Fadeev-Popov ghosts. The remaining symbols, other than the standard derivative operator, are simply constants or parameters: "g_0" is the coupling constant, "λ_a" are the Gell-Mann matrices (representations of the SU(3) generators), and "f_{abc}" are the SU(3) structure constants. The Greek indices "μ" and "ν" run over the four dimensions of Minkowski space. The Latin indices "a", "b", and "c" run over the eight components of the SU(3) generator algebra. With these definitions in place, we can proceed to determine the physics hidden in Equation 1.1.

The first term in the interaction Lagrangian density contains two quark field operators and a gluon field operator. Thus, it describes a fermion-fermion-boson interaction vertex of the form familiar from abelian gauge theories such as QED. This vertex is portrayed in Figure

1.1 (a). The second and third terms, however, have no counterparts in abelian theories. The second contains a derivative coupling between three gluon fields. Thus, it produces a three-gluon interaction vertex of the form shown in Figure 1.1 (b). The third term contains four gluon fields and produces the four-gluon interaction vertex shown in Figure 1.1 (c). The fourth term describes a coupling between a gluon and two Fadeev-Popov ghosts [25, 83]. This vertex is not relevant to our current purpose so it is not portrayed graphically. Obviously, this proliferation of tree level vertices greatly increases the number of Feynman diagrams that must be included in any QCD calculation.

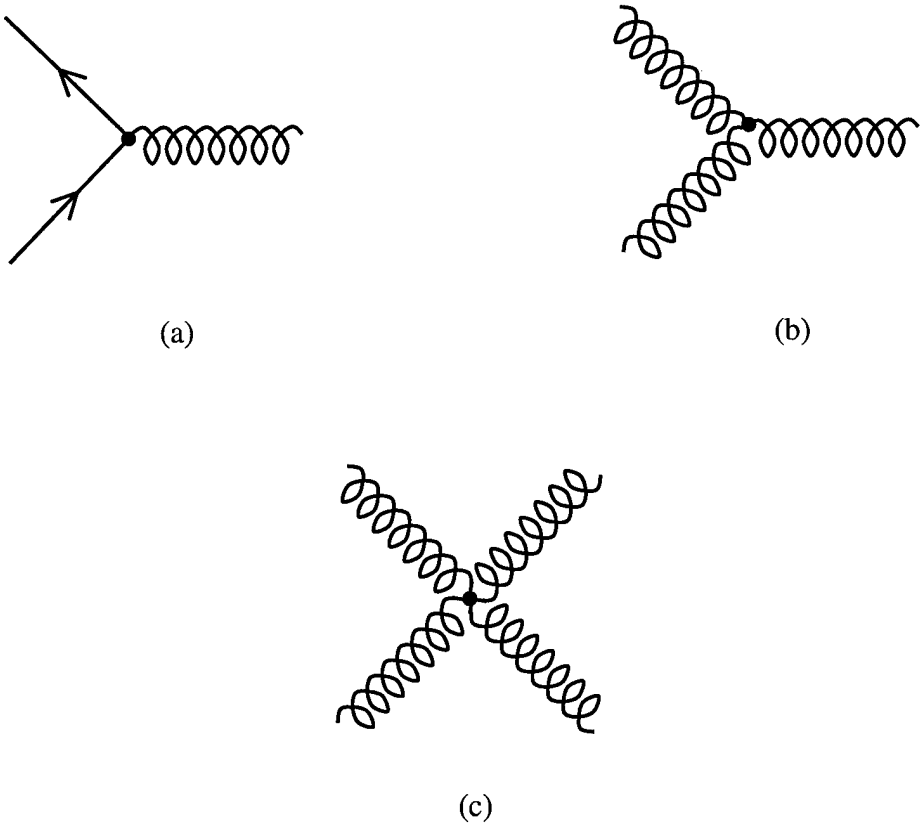

Figure 1.1: Tree-level vertices for QCD. (a) Quark-quark-gluon vertex. (b) Three-gluon vertex. (c) Four-gluon vertex.

At higher orders, the situation only becomes more complicated. At one loop, for example, we obtain three possible corrections to the gluon propagator rather than one as in QED (see Figure 1.2). Similarly, there are two one-loop corrections to the quark-quark-gluon vertex rather than the single correction found in QED (see Figure 1.3).

Although this by no means constitutes the complete set of Feynman diagrams required to perform QCD calculations, it is sufficient to lead us to an inescapable conclusion. Calculations in QCD are made enormously complicated by the presence of gluon self-interactions. Because of the large number of diagrams contributing to a given process, leading order calculations can become quite formidable and those beyond next-to-leading order can be prohibitively difficult.

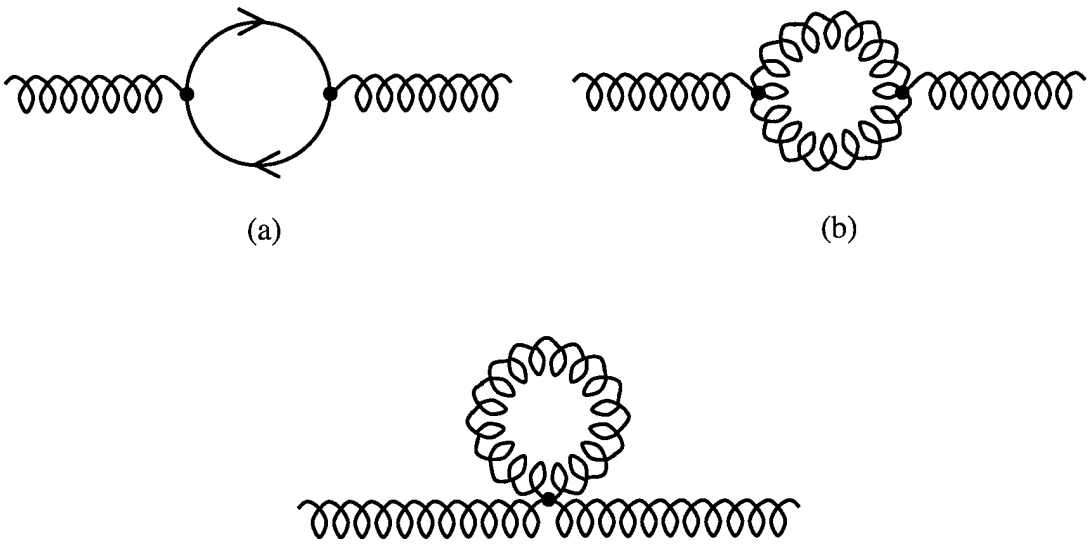

Figure 1.2: Gluon self-energy corrections at one loop. (a) Fermion loop correction analogous to QED. (b) Boson loop correction arising from three-gluon vertices. (c) Boson loop correction arising from a four-gluon vertex. The boson loops have no analogy in QED.

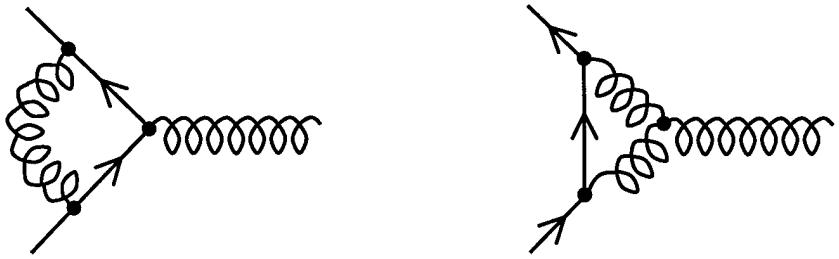

(a) (b)

Figure 1.3: One-loop corrections to the quark-quark-gluon vertex. (a) Correction analogous to QED. (b) Correction arising from a three-gluon vertex. The latter has no analogy in QED.

1.2.2 Asymptotic Freedom

The property of asymptotic freedom is best understood through analysis of the QCD coupling constant. Using renormalization group methods, one can derive the following expression for the running coupling constant [5]:

$$\alpha_s(Q^2) = \frac{12\pi}{(33 - 2n_f)\log(Q^2/\Lambda^2)} \tag{1.2}$$

In this expression, Q represents the energy scale of the reaction under study and n_f represents the number of quark flavors with masses less than Q. Obviously, n_f can be no greater than six. The parameter Λ is a constant of integration known as the QCD scale. Experiment has set the value of this parameter at approximately 200 MeV [6], but it is important to note that its exact value varies with n_f. We will comment on the physical meaning of the Λ parameter later in this section.

At this point, however, we simply consider the shape of the function that defines the coupling constant. Figure 1.4 contains a plot of $\alpha_s(Q^2)$ versus Q^2. Since the distance and

time scales associated with a given interaction are both on the order of 1/Q, the plot also includes a secondary scale showing $\alpha_s(Q^2)$ versus $1/Q^2$.

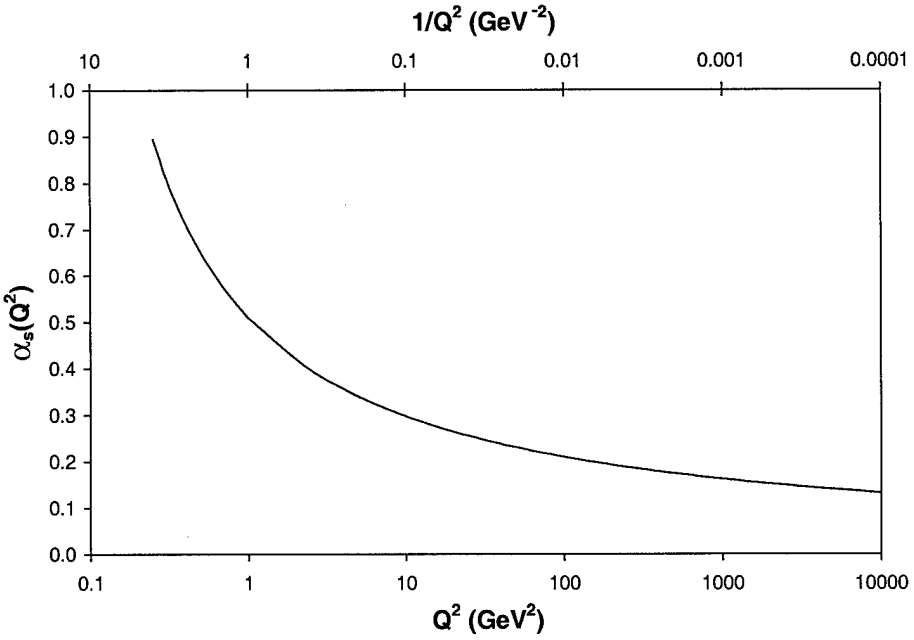

Figure 1.4: The QCD coupling constant as a function of Q^2. A secondary scale showing the coupling as a function of $1/Q^2$ is also included. This plot uses the parameters $n_f = 5$ and $\Lambda = 200$ MeV and the domain $0.5 \text{ GeV} \leq Q \leq 100 \text{ GeV}$.

Inspection of this curve shows that at small Q^2, or large distance and long time, the QCD coupling is extremely strong. As Q^2 increases, or the distance and time scales become smaller, however, the coupling becomes progressively weaker. It is this reduction in coupling strength that is known as asymptotic freedom. It derives its name from the idea that, in the asymptotic regime of very large Q^2, or very short distance and time, the coupling becomes so weak that the quarks and gluons effectively behave as free particles.

This behavior of the running coupling constant limits our ability to apply conventional techniques to QCD calculations. Such techniques almost always involve the use of a

covariant perturbation expansion in powers of the coupling constant. The validity of such an approach, however, is predicated upon the assumption that the coupling constant is a small parameter. Figure 1.4 clearly shows that, in QCD, this assumption is only valid for sufficiently large Q^2. In fact, it is valid only when Q is somewhat larger than the Λ parameter of Equation 1.1. This is the reason that Λ is called the QCD scale. It represents the energy scale at which the coupling constant of the strong interaction truly becomes strong.

In practice, it is usually assumed that perturbative techniques are applicable to QCD when Q is larger than about 1GeV. For this reason, reactions involving heavy quarks provide the perfect laboratory for the study of perturbative QCD. Perturbation theory is always applicable to such systems because the scale of the reaction can be no smaller than the heavy quark's mass, which is greater than 1 GeV by definition.

1.2.3 Confinement

In our discussion of asymptotic freedom, we saw that the QCD coupling becomes progressively stronger as the distance between the interacting particles increases. In fact, it is energetically impossible to separate them beyond a certain distance on the order of $1/\Lambda$, or about 1 fm. Upon reaching this scale, the colored particles will arrange themselves into colorless bound states known as hadrons. At low energies, the interacting particles might simply bind with each other. At higher energies, however, hadronization usually occurs through a very interesting process known as fragmentation. Qualitatively, this process is somewhat analogous to electromagnetic bremsstrahlung. Just as a decelerating electron radiates photons, a quark decelerated by strong interactions with other colored particles will

radiate hadrons. One of these hadrons will contain the original quark. Because these processes occur at such small distance and time scales, quarks and gluons are never experimentally observed as free particles. Since our fundamental particles are effectively "confined" inside larger composite objects, this property is called confinement.

It is critical to emphasize that the observed bound states carry no net color. Hadrons with non-zero total color would be subject to the same confining forces as the individual quarks. Consequently, they would bind into progressively larger and larger composite particles until, at least in principle, all the colored matter in the universe was contained in one extended object. The available experimental evidence strongly contradicts the possibility of such behavior. Thus, although the requirement has never been rigorously proven, there is little doubt that quarks, anti-quarks, and gluons are confined inside colorless hadrons at distance and time scales larger than $1/\Lambda$.

Naively, one might suspect that any random colorless combination of quarks and anti-quarks could form a hadron. Experimentally, however, only two basic types of hadrons are found to exist. The first type, and the one most relevant to the analysis in this paper, consists of one quark and one anti-quark. Such two-particle hadrons are called mesons. They contain an equal mixture of color and anti-color so that no net color is present. Because a meson must remain colorless under arbitrary rotations in color space, however, its color wave function can not be the simple product of one color and the corresponding anti-color. Rather, it must be the linear combination shown in Table 1.3.

The second type of bound state can consist of three quarks or three anti-quarks. These three-particle hadrons are known as baryons and anti-baryons respectively. They contain equal portions of all three colors or all three anti-colors, which cancel to yield no net color. It

is in this cancellation that the term "color" has its source. Since the three possible values of this degree of freedom neutralize each other when combined, it was named in analogy to optics where the colors red, green, and blue mix to form white. Like those of the mesons discussed in the proceeding paragraph, the color wave functions of the baryons and anti-baryons must be invariant under arbitrary transformations in color space. Thus, they can only be the linear combinations listed in Table 1.3.

Particle Type	Color Wave Function
Meson	$\sqrt{\frac{1}{3}}(R\overline{R} + G\overline{G} + B\overline{B})$
Baryon	$\sqrt{\frac{1}{6}}(RGB - RBG + BRG - BGR + GBR - GRB)$
Anti-Baryon	$\sqrt{\frac{1}{6}}(\overline{RGB} - \overline{RBG} + \overline{BRG} - \overline{BGR} + \overline{GBR} - \overline{GRB})$

Table 1.3: Hadron color wave functions.

Because quarks are not observed as free particles, their masses can not be measured directly. Rather, the masses must be inferred from their influence on the properties of the observed hadrons. Accordingly, the masses obtained depend on the technique used to extract them from the experimental data [7]. For this reason, quark masses are regarded as parameters in theoretical calculations and are varied through a reasonable range in order to establish uncertainties in the result. We will apply this technique to calculations performed in Chapter 4.

1.3 Heavy Quarkonium Production

1.3.1 Definitions

We begin this section by defining some relevant terms. If a meson contains a quark and an anti-quark of the same flavor, the system is referred to as "quarkonium" in analogy to the electron-positron bound state known as "positronium". If the flavor is charm or bottom, the meson carries the additional description "heavy" to indicate that it possesses properties unique from those of lighter quarkonium states. These heavy bound states are frequently referred to as "charmonium" and "bottomonium" respectively. Note that the top quark was conspicuously omitted from the proceeding discussion. Its lifetime is too short to allow the formation of bound states so "toponium" does not exist.

The framework of group theory dictates that the color wave function for a system consisting of a quark and an anti-quark has only nine possible forms. Eight of these have some net color content like the gluon wave functions shown in Table 1.2. Because of this multiplicity, states of this type are known as "color octet" states. The remaining wave function carries no net color like that of the meson described in Table 1.3. It is referred to as a "color singlet" state. Due to the principle of confinement described in Section 1.2.3, only a quark and an anti-quark in a color singlet state can bind to form quarkonium.

1.3.2 Motivation

The study of heavy quarkonium states is interesting for several reasons. First of all, they are experimentally accessible. Many of them decay to muon pairs with an appreciable branching fraction. Because it is comparatively easy to trigger on muon pairs in high energy physics experiments, detailed studies of total and differential quarkonium production rates are

possible. Second, they allow the investigation of confinement. The properties and behavior of the heavy bound states can reveal information about the form of the confining potential. Additionally, a reduction in production rates under certain circumstances could indicate the presence of an unconfined state called the quark-gluon plasma [1]. Third, and most importantly for our purposes, the study of heavy quarkonium production betters our understanding of the relationship between the perturbative and non-perturbative aspects of QCD. As mentioned in the previous section, the energy scales associated with the production of heavy quark pairs are large enough to allow the application of perturbation theory. The process by which the heavy quarks bind to form a quarkonium state, however, is inherently non-perturbative.

Any model of heavy quarkonium production must successfully link the perturbative and non-perturbative portions of the process. Most theories agree that the two pieces can be separated and that the production rates can be factorized into the product of a short-distance factor describing the production of the heavy quark pair and a long-distance factor describing the formation of the bound state. The theories diverge, however, on exactly how this factorization should be accomplished. The three most prominent models suggest very different factorization techniques, which we shall address in turn. In order of increasing complexity, these theories are called the Color Evaporation Model, the Color Singlet Model, and the Nonrelativistic QCD Factorization Model.

1.3.3 Color Evaporation Model

In the Color Evaporation Model, the perturbative and non-perturbative portions of the quarkonium production process are considered to be completely uncorrelated. It predicts that there is no connection between the color and angular momentum quantum numbers with

which a heavy quark pair is produced and the quantum numbers of the quarkonium states it can form. The explanation for this seeming contradiction is the postulate that the exchange of soft gluons with the surrounding color field destroys all information about the original quantum state of the heavy quark pair and creates a finite probability for it to emerge asymptotically as any given quarkonium state. These soft interactions are assumed to be universal and to have only negligible effects on the dynamics of the heavy quark pair. As an example, the model predicts a non-zero probability that a pair of bottom quarks produced in a P-wave color octet state will become an S-wave color singlet through soft gluon exchange and emerge as a Y(1S) meson. The model takes its name from this seeming "evaporation" of the pair's color.

The short-distance factor in the Color Evaporation Model is the total or differential production rate for heavy quark pairs, calculated to the desired order in perturbation theory and summed over all possible color and angular momentum states. The long-distance factor is simply a number expressing the probability of forming a given bound state. This factor can not be calculated. Rather, it must be determined phenomenologically by fitting the short-distance factor to data.

Despite its simplicity, the Color Evaporation Model has been very successful in reproducing the available data on quarkonium production [8-13]. We will discuss this model in greater detail in Chapter 2.

1.3.4 Color Singlet Model

In contrast to the Color Evaporation Model, the Color Singlet Model suggests that the perturbative and non-perturbative portions of the quarkonium production process are completely correlated. In this model, a heavy quark pair can become a quarkonium state

only if it is initially produced as a color singlet. Furthermore, a color singlet pair has a non-zero probability to emerge as only those quarkonium states whose angular momentum quantum numbers match those it possesses at the time of its production. For example, in the Color Singlet Model, there is a finite probability for a pair of bottom quarks to emerge as a Y(1S) meson only if they are initially produced as an S-wave color singlet. Gluons can not adjust quantum numbers in this theory. They simply serve to generate the binding potential. The model takes its name from its concrete insistence upon the initial color singlet state.

In the Color Singlet Model, the short-distance factor is the total or differential production rate for heavy quark pairs, calculated to the desired order in perturbation theory but constrained to a color singlet state with a given set of angular momentum quantum numbers. The long-distance factor is a calculable quantity proportional to the bound state's wave function, or in some cases its first derivative, evaluated at the origin.

Although it has met with some success, the Color Singlet Model has not adequately reproduced all the available data on quarkonium production. Its predictions for S-wave production rates tend to be smaller than those measured by experiment [14]. Additionally, in P-wave calculations, infrared divergences call the validity of its factorization scheme into question [15]. Its most noticeable failure is the underestimation, by a factor of approximately fifty, of $\psi(2S)$ production rates at large transverse momentum [16]. The reader interested in learning more about the Color Singlet Model can find a comprehensive review in Reference [14] or follow its initial development in References [17-21]. To avoid confusion, however, he or she should be aware that some authors refer to this theory as the Charmonium Model.

1.3.5 Nonrelativistic QCD Factorization Model

The Nonrelativistic QCD Factorization Model occupies a position somewhere between the extremes presented by the other two models. It predicts that there is a non-zero probability for any heavy quark pair to form almost any quarkonium state but that the size of this probability depends on the pair's initial quantum state. For example, it suggests that, although both an S-wave color singlet bottom quark pair and a P-wave color octet bottom quark pair can emerge as a Y(1S) meson, the two processes do not occur with the same probability.

In the Nonrelativistic QCD Factorization Model, calculations are significantly more complicated than in the other two models. Rather than a single term containing the product of a long-distance factor and a short-distance factor, the theory requires an infinite sum of such terms running over all possible color and angular momentum states of the heavy quark pair. In each term, the short-distance factor is the perturbatively calculated total or differential production rate for heavy quark pairs in the appropriate state of color and angular momentum. The long-distance factor is a matrix element specifying the probability for the given state of the heavy quark pair to produce the quarkonium state in question. These factors can be calculated using QCD sum rules or lattice techniques.

The Nonrelativistic QCD Factorization Model is by far the most theoretically robust of the three models we have discussed. It has been successful in reproducing a wide variety of quarkonium production data, but this success has not been universal. Most notably, its predictions about quarkonium polarization properties have been contradicted by recent experimental results [22-24, 50]. For a more detailed treatment of the Nonrelativistic QCD

Factorization Model, which is also referred to as the Color Octet Model in the literature, the interested reader should consult References [26-29].

1.4 Initial Statement of Purpose

In this paper, we will test the validity of the Color Evaporation Model by comparing its predictions to the available data on hadroproduction of bottomonium. At each step in the process, we will also apply our tests to selected charmonium data. This secondary analysis serves two purposes. First, it will allow us to highlight any differences between the two heavy quarkonium systems. Second, since charmonium production in the Color Evaporation Model has already received extensive treatment, it will also allow us to examine the credibility of our approach by comparing our results with those obtained in earlier studies. After a more thorough discussion of the Color Evaporation Model in the next chapter, we will state this purpose in greater detail and discuss the organization of the thesis.

Chapter 2

The Color Evaporation Model

2.1 Origin and Evolution

The first heavy quarkonium state to be experimentally observed was the J/ψ. In 1974, it was detected independently in electron-positron collisions at the Stanford Linear Accelerator Center [30] and in a proton-on-beryllium fixed target experiment at Brookhaven National Laboratory [31]. Following its discovery, many attempts were made to devise a theoretical framework that could adequately describe the associated production dynamics. A concise review of the most significant of these ideas can be found in Reference [14]. Here, however, we focus only on those that paved the road to the Color Evaporation Model.

Our journey begins with a pair of suggestions made by Einhorn and Ellis in 1975 [32]. First, they offered the idea that gluon fusion could be the dominant parton-level process involved in the hadroproduction of charmonium. This conjecture, which would prove to be quite important, marked a clear departure from the other early theories, most of which emphasized the primacy quark - anti-quark annihilation or flavor excitation. Second, they proposed that the dynamics of J/ψ production might be essentially identical to those involved in the production of open charm quark pairs. They were not able to pursue this idea quantitatively because it required more sophisticated parton distribution functions than those available at the time. Despite this fact, it was a significant suggestion because it was the first indication that it might be possible to devise a theory of quarkonium production that formally

separated the process of heavy quark pair production from the process of bound state formation.

The next step in the model's development was taken almost simultaneously by Fritzsch [33] and by Halzen [34, 35]. In 1977, they independently produced very similar theories that contradicted the first suggestion of Einhorn and Ellis but systematically developed the second. Both asserted that the dominant parton-level process contributing to charmonium production is quark – anti-quark annihilation into a highly virtual gluon. The tree-level Feynman Diagram for this process is shown in Figure 2.1. Since color conservation requires any charm quark pair produced through this mechanism to be in a color octet state, the theories were forced to allow for readjustment of the pair's color wave function prior to bound state formation. Fritzsch and Halzen both assumed that this readjustment to a color singlet configuration could occur through soft gluon emission. Thus, their papers contain the initial proposals of the process we now refer to as color evaporation.

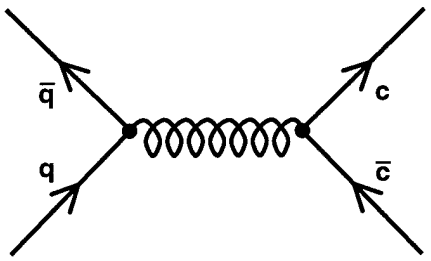

Figure 2.1: Tree-level Feynman diagram for charm quark pair production by $q\bar{q}$ annihilation into a single, highly virtual gluon.

With this mechanism in place, both theories proceeded to offer a scheme for calculating charmonium production rates in hadron-hadron collisions. Their approaches to this problem

can be summarized with three equations. Note, however, that we must alter the original notation in order to combine the essential features of the two theories. Bearing this caveat in mind, the first equation we must consider is:

$$\sigma_{c\bar{c}} \equiv \sigma_g(h_1 h_2 \rightarrow c\bar{c}X) = \frac{2}{3}\frac{\alpha_s^2}{\alpha^2 < q^2 >}\sigma_\gamma(h_1 h_2 \rightarrow \mu^+\mu^- X) \qquad (2.1)$$

In this expression, h_1 and h_2 represent the colliding hadrons in the initial state and $<q^2>$ refers to the average squared electric charge of the quarks participating in the reaction. The subscript "g" in the cross section on the left-hand side of the equation indicates that the charm quark pair results from a virtual gluon produced in the initial hadronic reaction. Similarly, the subscript "γ" in the cross section on the right-hand side of the equation indicates that the muon pair results from a virtual photon produced in the initial hadronic reaction. The other symbols have their conventional meanings. Thus, this equation suggests that the cross section for hadroproduction of a charm quark pair through the partonic process of Figure 2.1 can be obtained by simply rescaling the cross section for muon pair production with a factor based on the differences in color, coupling strength, and electric charge. Since experimental data on the hadroproduction of lepton pairs was available from a variety of experiments, this proposal offered a seemingly reasonable and accessible approach.

The second equation required for our summary of the two theories is:

$$\sigma_{[c\bar{c}]} = \int_{2M_c}^{2M_{D^0}} dM_{c\bar{c}} \frac{d\sigma_{c\bar{c}}}{dM_{c\bar{c}}} \qquad (2.2)$$

Here M_c is the mass of the charm quark, M_{D^0} is the mass of the D^0 meson, and $M_{c\bar{c}}$ is the invariant mass of the charm quark pair. The symbol "$[c\bar{c}]$" indicates a general bound state of the charmonium system. This notational convention of bracketing quarkonium states to

distinguish them from open heavy quark pairs will be employed throughout this thesis. Thus, Equation 2.2 says that the cross section for producing an unspecified charmonium state can be obtained by simply integrating Equation 2.1 over the energy interval from twice the mass of the charm quark to twice the mass of the D^0 meson. Since the D^0 is the lightest meson containing only one charm quark, this upper limit is conventionally called the "open charm threshold" or sometimes simply "threshold."

Equation 2.2 has three very important features that we must note before moving on to consider our third expression. First, it implies that, as suggested by Einhorn and Ellis, the dynamics of quarkonium production are identical to those of heavy quark pair production. Thus, this equation is the first example of what we referred to in Section 1.3 as a perturbative or short-distance factor for the calculation of quarkonium production rates. Second, it imposes the requirement that all charm quark pairs with masses below threshold must emerge asymptotically as charmonium states. This feature will be critical to the discussion in the next section. Finally, although we have expressed the equation in terms of total cross sections, it is equally valid for differential cross sections in dynamical variables such as P_T and X_F. The appropriate differential quantities can simply be substituted for the total cross sections on both sides of the equation.

The final equation we must extract from the work of Fritzsch and that of Halzen is:

$$\sigma_{n^{2S+1}L_J} = \frac{1}{N_{[c\bar{c}]}} \sigma_{[c\bar{c}]} \tag{2.3}$$

Here $\sigma_{n^{2S+1}L_J}$ is the cross section for production of a specific charmonium state such as J/ψ or η_c and $N_{[c\bar{c}]}$ is the number of different charmonium states with masses below threshold. Thus, this expression predicts that all charmonium states occur with equally probability

regardless of their mass or internal quantum numbers. It contains the first example of what we have previously called a non-perturbative or long-distance factor.

The model proposed by Fritzsch and by Halzen was very successful in describing many features of the available data on charmonium production, but its success was not universal. In 1978, Gluck, Owens, and Reya [36] and Babcock, Sivers, and Wolfram [37] independently demonstrated that the flaw in the theory was its failure to incorporate the gluon fusion process discussed in the work of Einhorn and Ellis. These two groups showed that the agreement between theory and data was significantly improved if both quark – anti-quark annihilation and gluon fusion were included in the theoretical calculations. This seemingly simple idea, however, had some non-trivial implications for the evolution of the Color Evaporation Model.

To understand the impact of adding the second production mechanism, we turn to the Feynman diagrams shown in Figure 2.2.

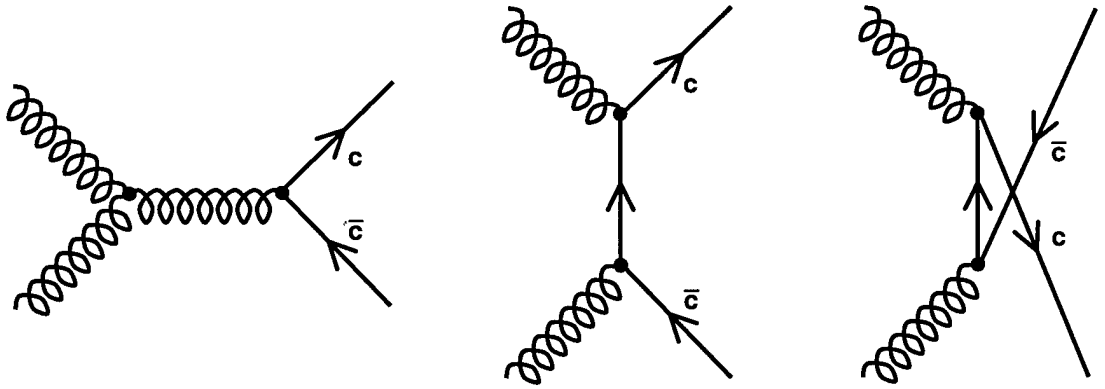

Figure 2.2: Tree-level Feynman diagrams for charm quark pair production by gluon fusion. (a) An s-channel process involving a three-gluon vertex. (b) A t-channel process. (c) A u-channel process.

Because of gauge invariance, three diagrams are required to describe heavy quark pair production through gluon fusion at lowest order. Since the first contains a three-gluon vertex, the second is a t-channel process, and the third is a u-channel process, the inclusion of these diagrams invalidates the QED analogy employed in constructing Equation 2.1. Thus, the model was forced to abandon the simple rescaling of lepton pair production data and turn to explicit calculations in perturbative QCD.

Accordingly, the Color Evaporation Model realized a more mature form by retaining Equations 2.2 and 2.3, but replacing Equation 2.1 with the following expression:

$$\sigma_{c\bar{c}} \equiv \sum_{q=u,d,s} \int dx_1 \int dx_2 [\, f_q(x_1,Q^2)\, f_{\bar{q}}(x_2,Q^2) + f_{\bar{q}}(x_1,Q^2)\, f_q(x_2,Q^2)]\hat{\sigma}(q\bar{q} \rightarrow c\bar{c}) + \int dx_1 \int dx_2 [\, f_g(x_1,Q^2)\, f_g(x_2,Q^2)]\hat{\sigma}(gg \rightarrow c\bar{c}) \tag{2.4}$$

Rather than explaining this equation in detail, we simply comment that it is an application of the now standard technique of calculating hadroproduction cross sections by convoluting the cross sections for the contributing parton-level processes with the appropriate parton distribution functions. The reader who is unfamiliar with this method can find an example in Chapter 4 of this paper or a detailed explanation in Reference [38].

This mature form of the Color Evaporation Model met with a great deal of success [39-41], but it was far from perfect. It correctly predicted the shapes of most dynamical distributions, but as experimental data began to show deviations from the 1/N rule of Equation 2.3, the correct method for normalizing the model's predictions became increasingly unclear. Thus, after the Color Singlet Model with its calculable long-distance factors and seemingly more sophisticated treatments of color and spin was proposed in 1980, the Color Evaporation Model fell from grace.

2.2 Resurrection and Generalization

The Color Singlet Model retained its position of prominence for more that a decade. As data became available at higher energies and larger values of transverse momentum, however, it slowly became evident that this model was seriously flawed (see Section 1.3.4). In their efforts to explain the new data, some physicists sought ways to improve the Color Singlet Model. Others offered entirely new theories such as the Non-relativistic QCD Factorization Model we have already discussed (see Section 1.3.5). A few, however, began to suspect that the Color Evaporation Model had been dismissed too hastily.

In 1994, Gavai, Kharzeev, Satz, Schuler, Sridhar, and Vogt proposed the resurrection of the Color Evaporation Model, but with a very significant generalization [12]. They dismissed the original model's requirement that all heavy quark pairs produced with invariant masses below threshold must emerge as quarkonium states. Instead, they suggested that such pairs had at least three different courses of action available to them. First, they could achieve a color singlet state through soft gluon emission and bind to form quarkonium states in accordance with the original model. Second, they could bind with light quarks produced elsewhere in the initial hadronic reaction to form heavy-flavored hadrons. Finally, pairs with invariant masses sufficiently close to threshold could gain enough energy through soft interactions with the color field to allow fragmentation into heavy-flavored hadrons. Thus, the generalized Color Evaporation Model predicts a finite, and in some cases quite large, probability for sub-threshold heavy quark pairs to emerge as heavy-flavored hadrons rather than quarkonium states.

In applying their generalized model, this group made two additional improvements over previous attempts to perform calculations with the Color Evaporation Model. First, they chose to abandon the 1/N in Equation 2.3 and determine the value of the long-distance factor entirely by normalizing the short-distance factor to data. Second, they took advantage of the improved perturbative QCD calculational techniques developed over the proceeding decade by using next-to-leading order results in their work. The product of these improvements was impressive agreement with the available data on both charmonium and bottomonium and new life for the Color Evaporation Model.

Soon after its resurrection, the model began to evolve into two similar but very distinct forms. For reasons that will become evident in the course of our discussion, one might refer to these as the minimal and maximal versions of the model. We will conclude our review of the history and current status of the Color Evaporation Model by describing these two versions and stating the most relevant results of each.

The minimal version of the model was most clearly articulated by Schuler and Vogt in 1996 [13]. They used the model only to analyze and predict the properties of cross sections for hadroproduction of heavy quarkonium states. Accordingly, their version can be summarized with just two equations. The first is:

$$\sigma_{nJ^{PC}} = F_{nJ^{PC}} \sigma_{<} \tag{2.5}$$

Here, the subscript "<" should be interpreted as "sub-threshold". We will retain this notational convention throughout the thesis. This expression announces that, as we would expect, the cross section for production of the quarkonium state described by the quantum numbers n, J, P, and C is the product of a corresponding long-distance factor, F, and a

general short-distance factor, $\sigma_<$. The former is obtained by normalizing the final result to data. The latter, however, must be calculated using the second equation:

$$\sigma_< = \int_{2M_Q}^{2M_{Q\bar{q}}} dM_{Q\bar{Q}} \frac{d\sigma_{Q\bar{Q}}}{dM_{Q\bar{Q}}} \tag{2.6}$$

Here, we have used the symbol "Q" to denote heavy quarks and the symbol "q" to denote light quarks. This expression, which is very similar to Equation 2.2, says that the short-distance factor is simply the heavy quark pair production cross section integrated over the energy interval between twice the heavy quark's mass and twice the mass of the lightest open-flavored meson that the heavy quark can form. The pair production cross section must be calculated to the desired order in perturbation theory using the method of Equation 2.4.

The long-distance factor, F, has two very important properties. First, since some percentage of the sub-threshold heavy quark pairs are expected to produce open-flavored hadrons instead of quarkonium states, the sum of the long-distance factor over all legitimate combinations of n, J, P, and C is less than one. Second, the long-distance factor is universal. The value determined from a given set of data is expected to remain valid for all other calculations. Accordingly, Schuler and Vogt were able to deduce the long-distance factors for several different charmonium and bottomonium states. Their results are summarized in Table 2.1. By extending these results to quarkonium states for which experimental data were not available, they were also able to estimate the percentage of sub-threshold heavy quark pairs that emerge as quarkonium states rather than heavy-flavored hadrons. The ranges at which they arrived are 8% to 10% for charm quark pairs and 17% to 32% for bottom quark pairs.

MESON	F_{LO} (%)	F_{NLO} (%)
J/ψ	5.50	2.50
ψ(2S)	0.77	0.35
Y(1S)	8.74	4.60
Y(2S)	4.56	2.40
Y(3S)	1.48	0.78

Table 2.1: Long-distance factors for the $J^{PC} = 1^{--}$ states of the Charmonium and bottomonium systems [13]. The subscript "LO" indicates a value obtained using a leading-order calculation of the short-distance factor. Similarly, the subscript "NLO" means that a next-to-leading-order calculation was used. These differences imply K-factors of 2.2 for charmonium and 1.9 for bottomonium.

The maximal version of the Color Evaporation Model was first presented in 1996 by Amundson, Eboli, Gregores, and Halzen [8]. They were drawn to the newly resurrected model by their work on rapidity gaps in deep inelastic scattering. Since the formation of rapidity gaps involves the neutralization of color, they felt that they might gain some insight into the process of gap formation by studying the more theoretically and experimentally well defined problem of color evaporation in heavy quarkonium production.

They began by imposing an additional constraint on the model. As we discussed in Chapter 1, a system of two heavy quarks has nine possible color wave functions but only one of these, the color singlet, permits the quarks to bind into a quarkonium state. Thus, this group used simple statistics to suggest that the probability for a sub-threshold heavy quark pair to emerge in a quarkonium state is 1/9 and the probability for it to emerge as heavy-flavored hadrons is 8/9. Note that this restriction to a universal quarkonium fraction contradicts the minimal version's prediction that the fraction is greater in the bottomonium system than in the charmonium system.

Because of this restriction, the maximal version of the model is able to make predictions about both quarkonium production rates and open-flavored meson production rates. The former are specified by the following equation:

$$\sigma_{nJ^{PC}} = \rho_{nJ^{PC}} \frac{1}{9} \sigma_{<} \tag{2.7}$$

The short-distance factor, $\sigma_{<}$, is identical to the one used in the minimal version of the model (Equation 2.6). The long-distance factor, however, is not the same. In the maximal version, we assume that only 1/9 of the short-distance factor results in quarkonium production. Thus, the long-distance factor, ρ, is the percentage of that 1/9 that emerges in the state specified by n, J, P, and C. Assuming that both the minimal and maximal versions are correct, their respective long-distance factors are related by $F = \rho/9$. It is important to note, however, that in the maximal version of the model the sum of the long-distance factor over all legitimate n, J, P, and C combinations must be unity.

The cross section for production of open-flavored mesons is predicted by the following equation:

$$\sigma_{M\overline{M}} = \frac{8}{9} \sigma_{<} + \sigma_{>} \tag{2.8}$$

In this expression, the subscript "$M\overline{M}$" refers to an open-flavored meson pair and, as one might suspect, the subscript ">" is to be interpreted as "above-threshold". Once again, $\sigma_{<}$ is specified by Equation 2.6. The new factor, $\sigma_{>}$, is given by:

$$\sigma_{>} = \int_{2M_{Q\bar{q}}}^{\sqrt{s}} dM_{Q\bar{Q}} \frac{d\sigma_{Q\bar{Q}}}{dM_{Q\bar{Q}}} \tag{2.9}$$

There are two important points about the maximal version's treatment of open-flavored meson production that we must mention before continuing. First, its developers state that, at least for charmonium, $\sigma_>$ is negligible and can be ignored in most calculations. We will discuss this point further in Chapter 4. Second, the model does not predict the production rates for specific open-flavored mesons. Rather, through Equation 2.8, it addresses only the inclusive open-flavored meson cross section.

Amundson, Eboli, Gregores, and Halzen have applied their version of the model to charmonium production data with extremely good results. They found that, with a universal long-distance factor of approximately $\rho_{J/\psi} = 0.47$, it could reproduce the available data on hadroproduction [9,11], photoproduction [9], and electroproduction (Z^0 decay) [10] of J/ψ mesons quite well. Despite these successes, however, the maximal version of the model must be tested against data on the bottomonium system and the remaining members of the charmonium system before its worth can be accurately assessed.

2.3 Detailed Statement of Purpose

We are now in a position to clarify the purpose stated in Section 1.4. Our primary intent is to test the predictions of the maximal version of the Color Evaporation Model developed by Amundson, Eboli, Gregores, and Halzen against the available hadroproduction data on the bottomonium system. As a secondary effort, we will also apply each test to the model's predictions for the charmonium system. The additional charmonium analysis will allow us to confirm and extend previous results and to highlight any differences between the two heavy quarkonium systems.

Our approach to this problem is organized as follows. In Chapter 3, we will assess the model's assertion that all the dynamics of heavy quarkonium production are contained in the short-distance factors by performing a detailed analysis of the available data. In Chapter 4, we will use Monte Carlo techniques to perturbatively calculate several short-distance factors, then determine the corresponding long-distance factors by normalizing our calculations to data. In Chapter 5, we will attempt to develop a universal equation to predict the long-distance factors for all quarkonium states in terms of a few basic parameters. Finally, in Chapter 6 we will summarize our results and discuss the possibilities for future work.

Chapter 3

Analysis of Production Dynamics

In this chapter, our task is to test the Color Evaporation Model's assertion that the dynamics of heavy quarkonium production are simply those of the production of heavy quark pairs. If this assertion is correct, all dynamical information must be contained in the model's short-distance factors. This fact permits us to perform our analysis using two different methods.

To understand the first technique, we consider the ratio of the production cross sections for two different quarkonium states. Since the short-distance factors for the two states are identical, we can use Equation 2.7 to obtain the following relation:

$$\frac{\sigma_{n'J'^{P'C'}}}{\sigma_{nJ^{PC}}} = \frac{\rho_{n'J'^{P'C'}} \frac{1}{9}\sigma_{<}}{\rho_{nJ^{PC}} \frac{1}{9}\sigma_{<}} = \frac{\rho_{n'J'^{P'C'}}}{\rho_{n'J'^{P'C'}}} \tag{3.1}$$

This expression predicts that the relative production rate of any two quarkonium states is simply the ratio of the corresponding long-distance factors. Thus, if the details of the dynamics are in the short-distance factors, these relative production rates must be independent of dynamical variables such as $\sqrt{s}$, P_T, and X_F. In Sections 3.1, 3.2, and 3.3, we will see if the experimental data supports this prediction.

The second method is based on the fact that the perturbative calculation used to determine the short-distance factors is averaged over all possible spin combinations of the initial state particles and summed over all possible spin combinations of the final state particles. Thus, since the model does not explicitly distinguish one spin state from another, it predicts that

quarkonium states should be produced with no preferred direction of polarization or spin alignment. We will compare this assertion to the available experimental data in Section 3.4.

3.1 Relative Production Rates as a Function of $\sqrt{s}$

In this section, we analyze plots of the relative production rates for various quarkonium states versus center of mass energy. If the Color Evaporation Model is correct, each ratio must remain essentially constant, within the experimental errors, as the center of mass energy increases. A significant change or fluctuation in any ratio, however, could indicate that the model is flawed.

3.1.1 Bottomonium

In the bottomonium system, experimental data is available only for the $J^{PC} = 1^{--}$ states, which are designated by Y(nS). We have arranged the data into three separate plots (Figures 3.1, 3.2 and 3.3). The exact ratios involved and the sources of the data are stated in the captions of the figures. Since the same symbol conventions are used in each plot, however, we will define them in advance rather than repeating the information in each caption. The square data points are from experiments using π^- beams on nuclear targets. The triangular data points are from experiments using proton beams on nuclear targets. The circular data points are from $p\bar{p}$ collider experiments. The dashed horizontal line on each plot represents the weighted mean of the data.

Inspection of the plots shows that a horizontal line fits the data reasonably well over two orders of magnitude in center of mass energy. A few of the error bars are large and some small fluctuations are visible, but the data on bottomonium production is generally consistent with the predictions of the Color Evaporation Model.

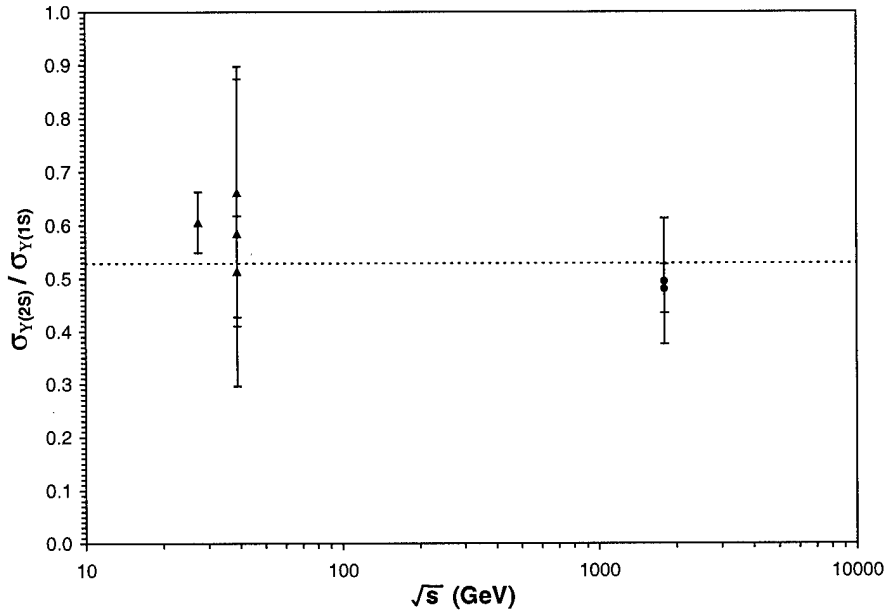

Figure 3.1: Plot of $\sigma_{Y(2S)} / \sigma_{Y(1S)}$ vs. $\sqrt{s}$ [22, 42-46].

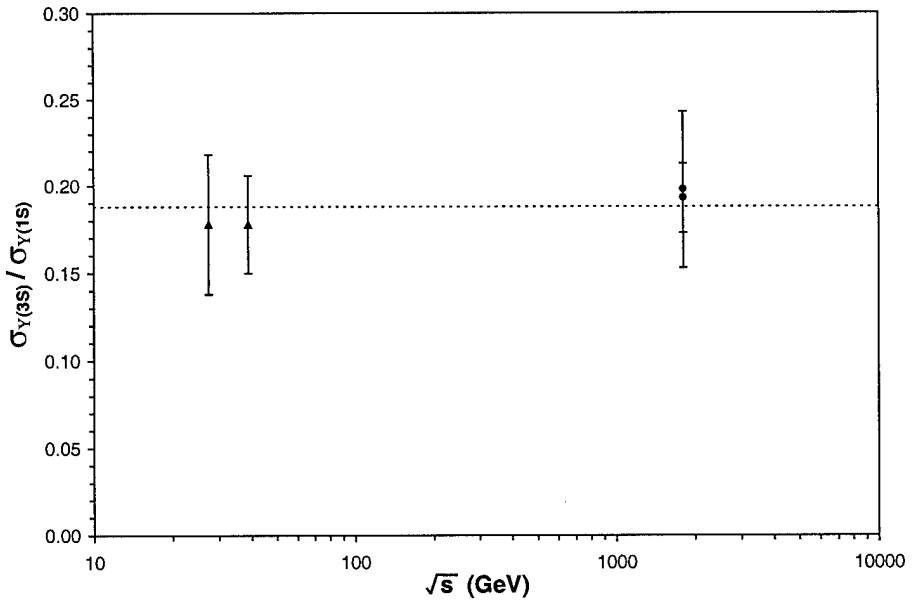

Figure 3.2: Plot of $\sigma_{Y(3S)} / \sigma_{Y(1S)}$ vs. $\sqrt{s}$ [22, 43, 45, 46].

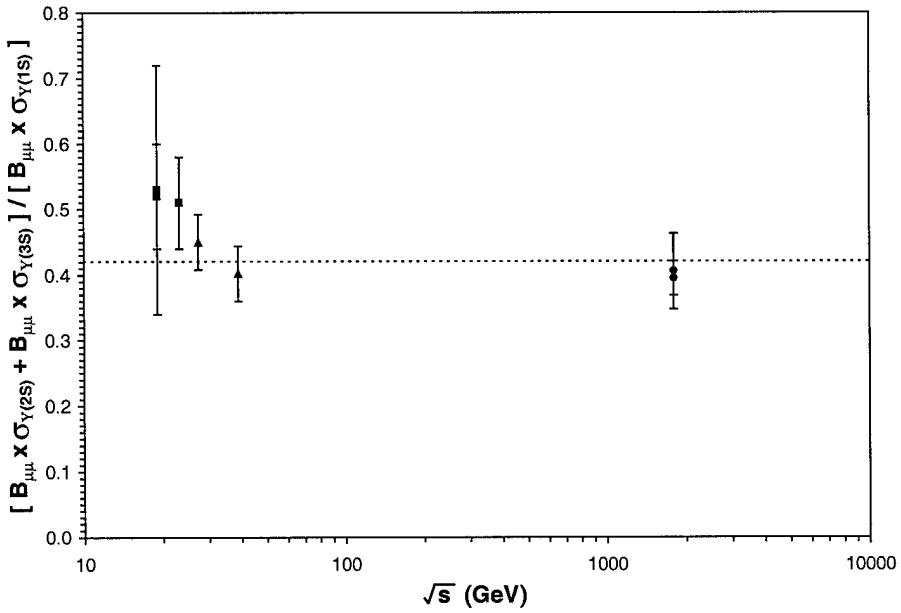

Figure 3.3: Plot of [$B_{\mu\mu}$ x $\sigma_{\Upsilon(2S)}$ + $B_{\mu\mu}$ x $\sigma_{\Upsilon(3S)}$] / [$B_{\mu\mu}$ x $\sigma_{\Upsilon(1S)}$] vs. $\sqrt{s}$ [22, 43, 45-48]. The symbol "$B_{\mu\mu}$" denotes the muonic branching ratio of the adjacent meson.

3.1.2 Charmonium

The charmonium system has been studied much more extensively than the bottomonium system. Thus, a greater variety of experimental data on charmonium production is available. This data includes measurements of the cross sections for the $J^{PC} = 1^{--}$ states denoted by J/ψ and ψ(2S), the $J^{PC} = 1^{++}$ state denoted $\chi_{c1}(1P)$, and the $J^{PC} = 2^{++}$ state denoted $\chi_{c2}(1P)$. Once again, we have arranged the data into three different plots (Figures 3.4, 3.5, and 3.6). The symbol conventions used in these plots are identical to those defined in the previous section, but with two additions. First, the diamond shaped data points are from experiments using π^+ beams on nuclear targets. Second, the data points marked with an "X" are from experiments using anti-proton beams on nuclear targets.

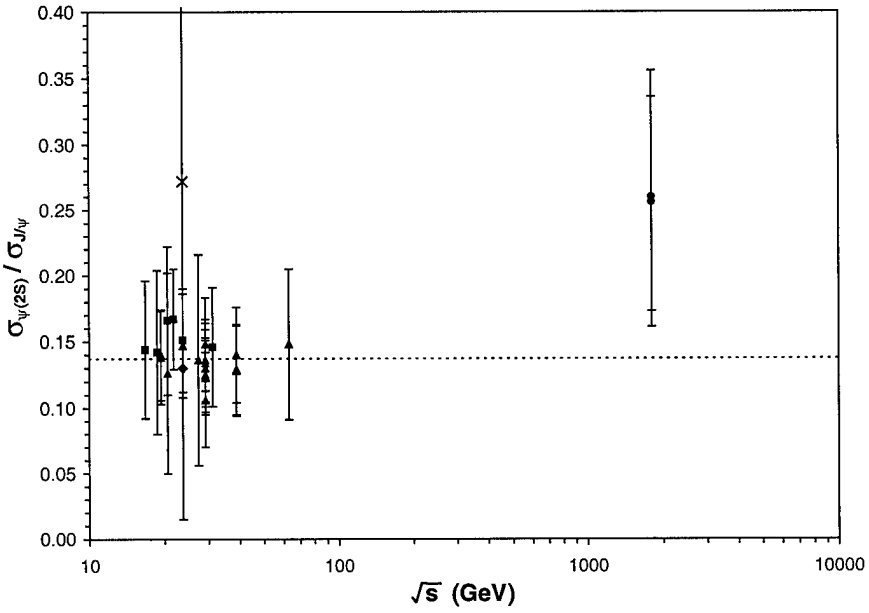

Figure 3.4: Plot of $\sigma_{\psi(2S)} / \sigma_{J/\psi}$ vs. $\sqrt{s}$ [14, 16, 42, 49-56].

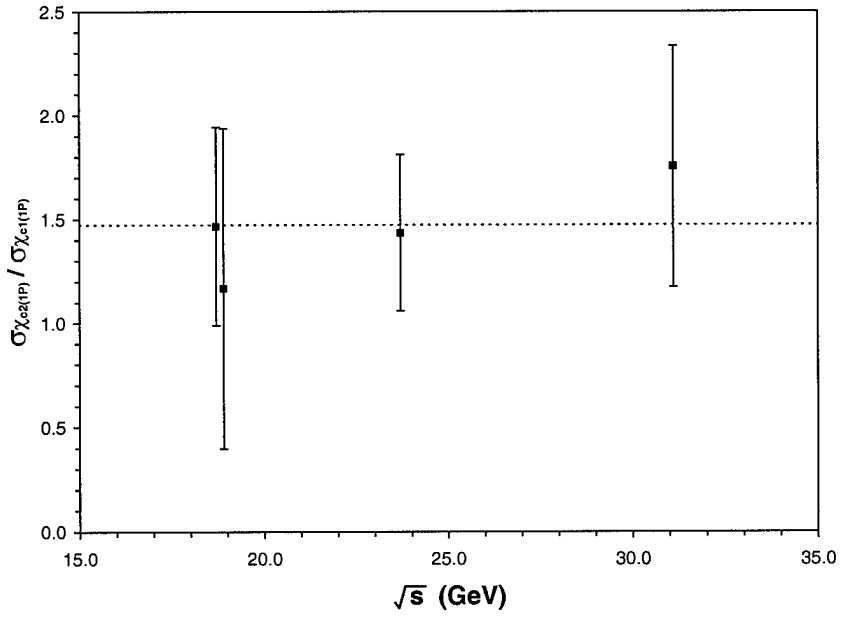

Figure 3.5: Plot of $\sigma_{\chi_{c2(1P)}} / \sigma_{\chi_{c1(1P)}}$ vs. $\sqrt{s}$ [14, 54, 57].

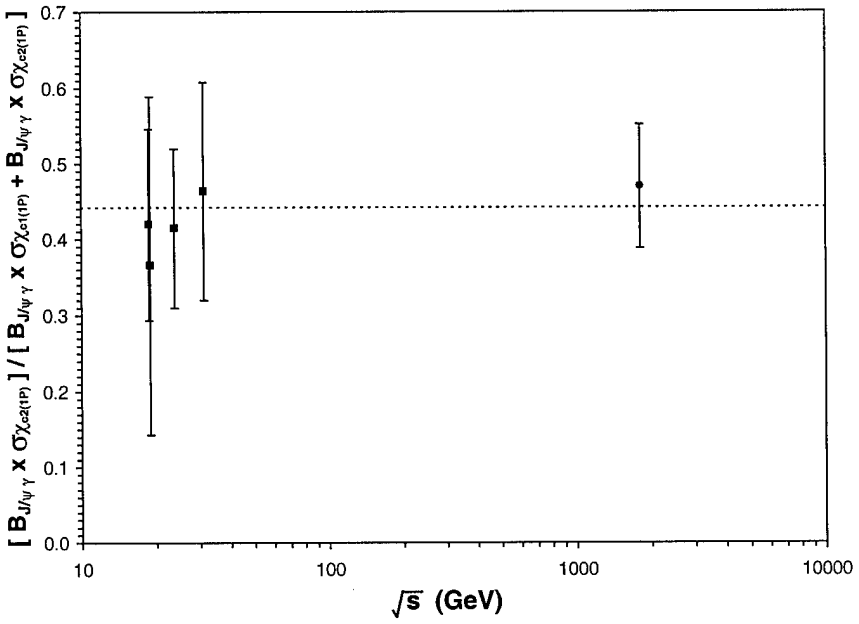

Figure 3.6: Plot of [$B_{J/\psi\,\gamma}$ x $\sigma_{\chi_{c2(1P)}}$] / [$B_{J/\psi\,\gamma}$ x $\sigma_{\chi_{c1(1P)}}$ + $B_{J/\psi\,\gamma}$ x $\sigma_{\chi_{c2(1P)}}$] vs. $\sqrt{s}$ [14, 54, 57, 58]. The symbol "$B_{J/\psi\,\gamma}$" denotes the adjacent meson's branching ratio to $J/\psi + \gamma$.

Once again, the plots show that a horizontal line fits the data reasonably well over two orders of magnitude in center of mass energy. Accordingly, we conclude that the charmonium data is generally consistent with the predictions of the Color Evaporation Model. We must, however, note one potentially significant exception. In Figure 3.4, the central values of the three data points that come from experiments involving beams of anti-protons are approximately twice as large as those from experiments using other beam types. Although all the data are essentially consistent within the experimental errors, this discrepancy is too large to ignore. Attempts to explain this feature of the data are beyond the scope for this paper but, before leaving the subject, we will make three observations.

First, although the anti-proton data points are larger than the others, they are self-consistent over two orders of magnitude in center of mass energy. Thus, when considered

independently, these three measurements do support our model's prediction that relative production rates are independent of dynamical variables. Second, the Color Evaporation Model predicts an increase in the individual cross sections when an anti-proton beam is used [9], but it expects the relative production rates to be unchanged. Thus, it can offer no explanation for the discrepancy we have observed. Finally, since we saw no evidence for similar behavior in the bottomonium system, the explanation could lie in the fact that the charm quark's mass is only slightly larger than the energy scale at which we expect perturbation theory to become valid. Accordingly, there may be circumstances under which some portions of the charmonium production dynamics are smeared into the non-perturbative regime.

3.2 Relative Production Rates as a Function of P_T

In this section, we will use two techniques to analyze the transverse momentum dependence of the relative production rates for various quarkonium states. The first method is identical to the one we employed in the previous section. We will plot the available data and consider the behavior of the relative production rates as the transverse momentum increases. If the rates remain constant, the data support the predictions of the Color Evaporation Model.

Our second technique is based on the fact that, if all quarkonium states have the same production dynamics, the shapes of their transverse momentum distributions must be the same. Thus, we will attempt to force all the distributions onto a common curve by simply adjusting their normalizations with an appropriate numerical constant. Inability to do so could indicate a flaw in the model's predictions.

3.2.1 Bottomonium

We begin by applying the first technique to the bottomonium system. The relevant plots are contained in Figures 3.7, 3.8, and 3.9. Note that, due to the nature of the available data, these figures do not present the actual transverse momentum distributions. Rather, the data points represent the ratios of cross sections that have been integrated over transverse momentum from the indicated minimum value to 20 GeV. Following the convention of the previous section, the dashed horizontal line on each plot represents the weighted mean of the data.

Inspection of these figures shows that the relative production rates of the Y(nS) mesons do not exhibit significant fluctuations as transverse momentum is increased. There is a tendency for deviations from the mean at large values of p_t, but the direction and magnitude of these deviations vary. Thus, we conclude that the data is essentially consistent with the predictions of the Color Evaporation Model.

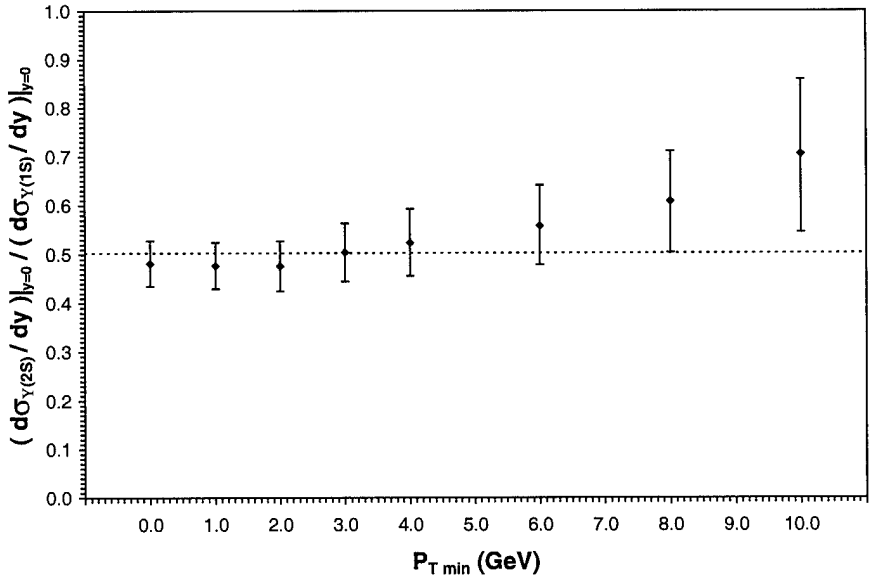

Figure 3.7: Plot of $(d\sigma_{Y(2S)}/dy)|_{y=0}$ / $(d\sigma_{Y(1S)}/dy)|_{y=0}$ vs. $P_{T\,min}$ [22].

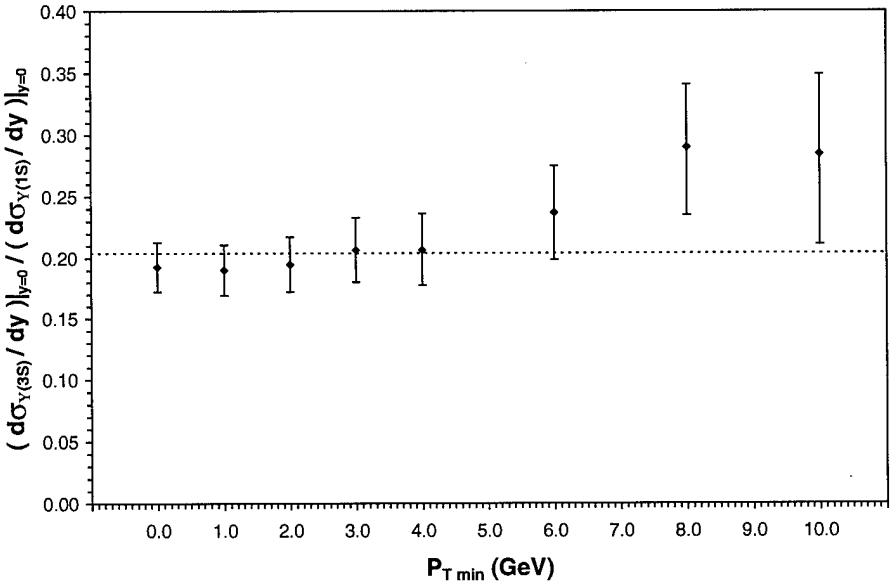

Figure 3.8: Plot of $(d\sigma_{Y(3S)}/dy)|_{y=0} / (d\sigma_{Y(1S)}/dy)|_{y=0}$ vs. $P_{T\,min}$ [22].

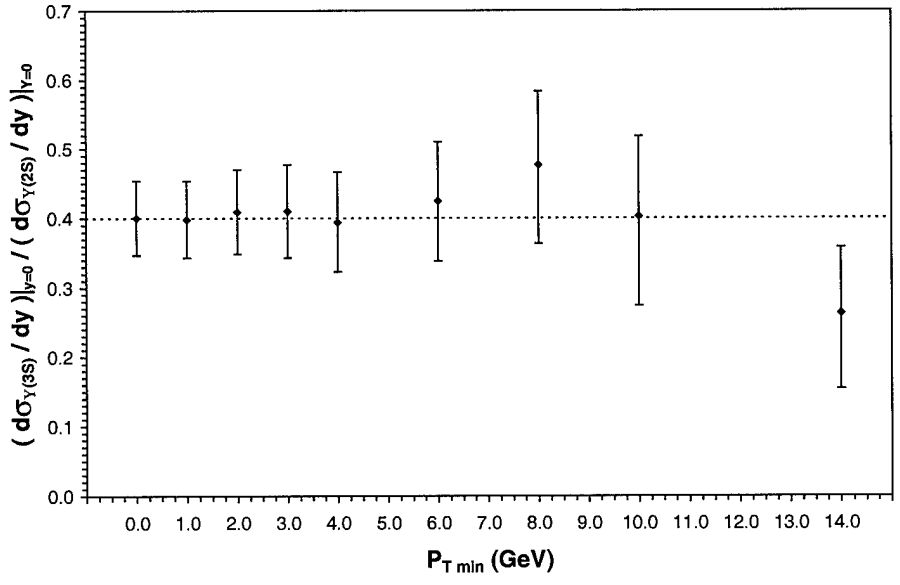

Figure 3.9: Plot of $(d\sigma_{Y(3S)}/dy)|_{y=0} / (d\sigma_{Y(2S)}/dy)|_{y=0}$ vs. $P_{T\,min}$ [22].

Next, we turn to our second method. In Figure 3.10, we have plotted the transverse momentum distributions of all three Y(nS) mesons. The distributions for Y(2S) and Y(3S) have been rescaled as indicated in the figure's caption. This chart makes it quite obvious that the three distributions have essentially the same shape, thereby lending additional support to the Color Evaporation Model's predictions.

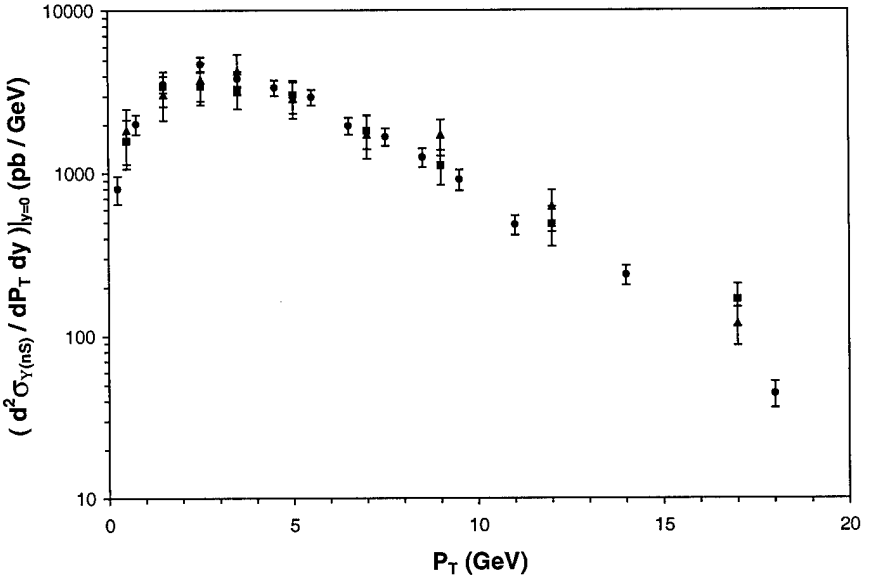

Figure 3.10: Plot of $(d^2\sigma_{Y(nS)}/dP_T dy)|_{y=0}$ vs. P_T for n = 1, 2, 3 [22]. The Y(1S) distribution is represented by the circular data points. The Y(2S) distribution, which has been multiplied by a constant factor of 2.0, is represented by the square data points. The Y(3S) distribution, which has been multiplied by constant factor of 5.4, is represented by the triangular data points.

3.2.2 Charmonium

Data on the transverse momentum distributions of bottomonium states is rather scarce. In the charmonium system, however, just the opposite is true. Thus, as our focus shifts to the latter, we will take advantage of the relative abundance of data by applying our analysis techniques

to two data sets: one from a $p\bar{p}$ collider experiment and one from a p-Au fixed target experiment.

Once again, our first method is to search for significant fluctuations in relative production rates as transverse momentum is increased. The plots required for this analysis are contained in Figures 3.11 and 3.12. As in the previous section, the data points represent the ratios of integrated cross sections. The limits of the integrations are stated in the captions of the figures. Both plots show deviations from the mean at the upper ends of their domains but, just as we noted in our analysis of the bottomonium data, the directions and magnitudes of the deviations are not consistent. Thus, we conclude that the charmonium data generally exhibits the behavior predicted by the Color Evaporation Model.

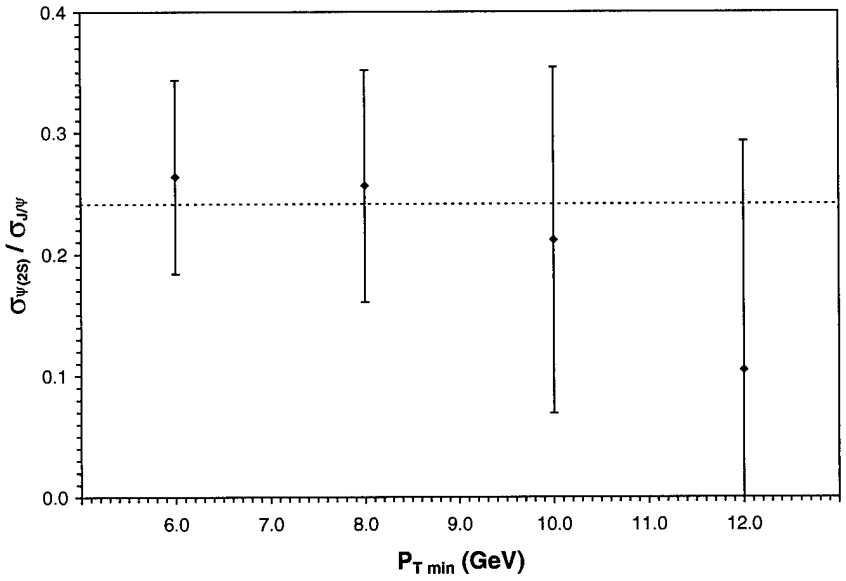

Figure 3.11: Plot of $\sigma_{\psi(2S)} / \sigma_{J/\psi}$ vs. $P_{T\,min}$. The data points represent the ratios of cross sections integrated over transverse momentum from $P_{T\,min}$ to 14 GeV. The measurements were made in a $p\bar{p}$ collider experiment [56].

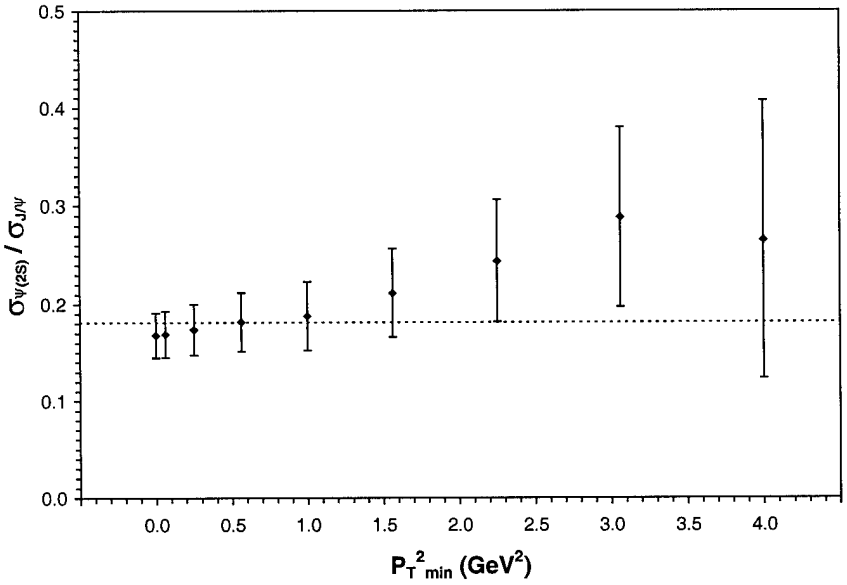

Figure 3.12: Plot of $\sigma_{\psi(2S)} / \sigma_{J/\psi}$ vs. $P_T^2{}_{min}$. The data points represent the ratios of cross sections integrated over transverse momentum squared from $P_T^2{}_{min}$ to 5.0625 GeV^2. The measurements were made in a fixed target experiment using a proton beam on a gold target [49].

As in the previous section, our second technique is to compare the shapes of the transverse momentum distributions for different quarkonium states by globally adjusting their normalizations. The results obtained by applying this method to our two sets of charmonium data are shown in Figures 3.13 and 3.14. In the $p\bar{p}$ collider data (Figure 3.13), the J/ψ and ψ(2S) transverse momentum distributions clearly have almost identical shapes. In the fixed target data (Figure 3.14), however, the tail of the ψ(2S) distribution contains a noticeable fluctuation. Since this behavior is confined to two data points and we have included only the lower limit on the systematic error given for the ψ(2S) distribution, we tend to suspect that this represents an anomaly in the measurement rather than a true deviation from the expected shape. Thus, we conclude that the charmonium data are essentially consistent with the predictions of our model.

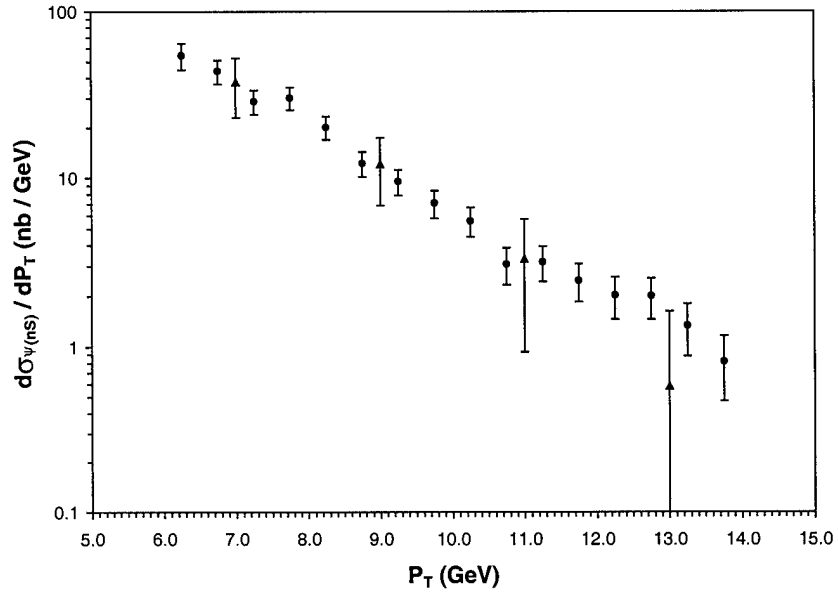

Figure 3.13: Plot of $d\sigma_{\psi(nS)}/dP_T$ vs. P_T for n = 1, 2 [56]. The J/ψ distribution is represented by the circular data points. The ψ(2S) distribution, which has been multiplied by a constant factor of 3.6, is represented by the triangular data points.

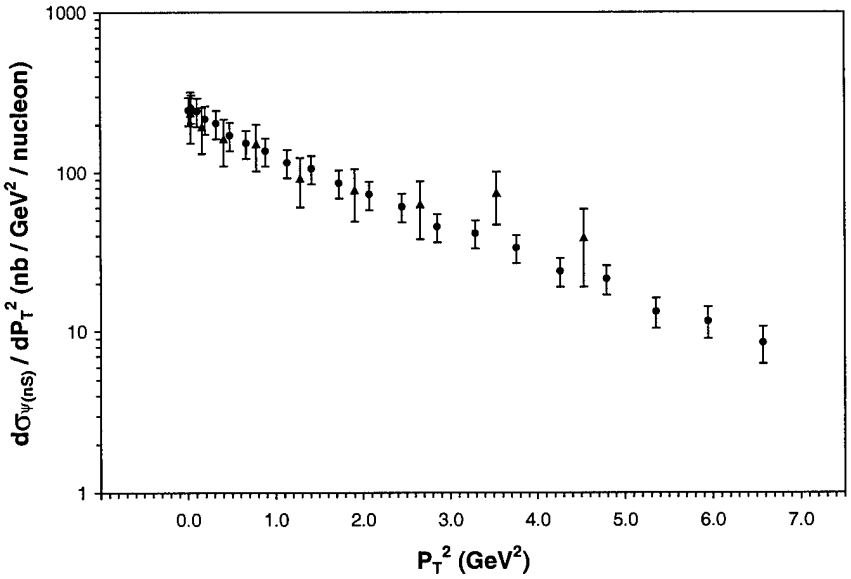

Figure 3.14: Plot of $d\sigma_{\psi(nS)}/dP_T^2$ vs. P_T^2 for n = 1, 2 [49]. The J/ψ distribution is represented by the circular data points. The ψ(2S) distribution, which has been multiplied by a constant factor of 6.5, is represented by the triangular data points.

3.3 Relative Production Rates as a Function of X_F

Next, we turn our attention to the X_F distributions of heavy quarkonium states. We will analyze the available data using the same techniques we applied to the transverse momentum distributions in the previous section.

3.3.1 Bottomonium

We begin by considering the relative production rates of the Y(nS) states. The relevant plots are contained in Figures 3.15, 3.16, and 3.17. Note that these figures are based on the ratios of actual differential cross sections rather than the integrated cross sections forced upon us by the nature of the available data in our analysis of the transverse momentum distributions. Inspection of these plots makes it quite obvious that the relative production rates of bottomonium states are independent of X_F. Thus, the Color Evaporation Model's predictions are confirmed.

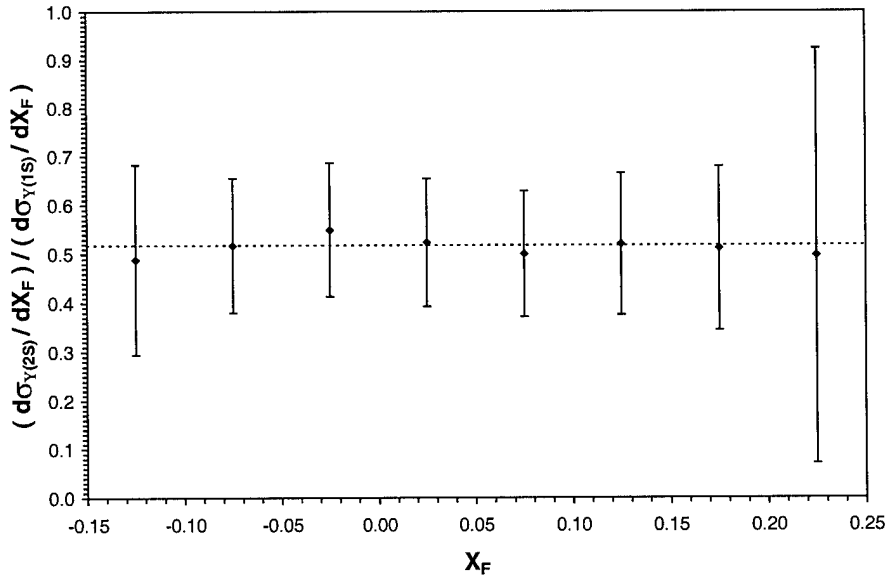

Figure 3.15: Plot of $(d\sigma_{Y(2S)}/dX_F) / (d\sigma_{Y(1S)}/dX_F)$ vs. X_F [43].

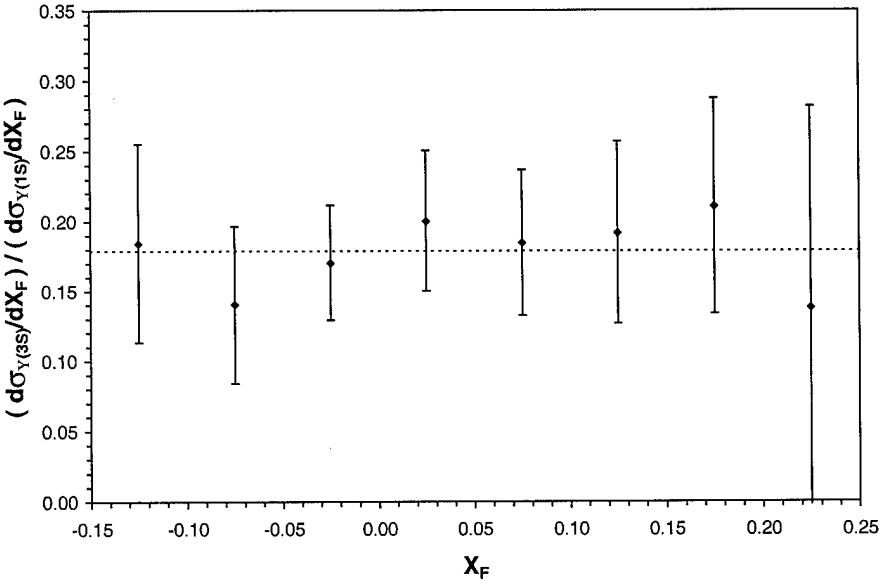

Figure 3.16: Plot of $(d\sigma_{Y(3S)}/dX_F) / (d\sigma_{Y(1S)}/dX_F)$ vs. X_F [43].

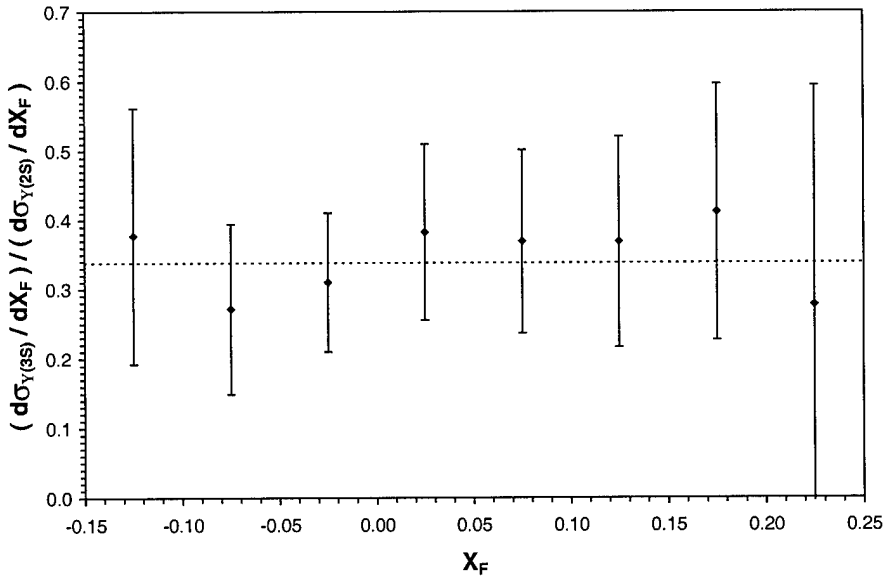

Figure 3.17: Plot of $(d\sigma_{Y(3S)}/dX_F) / (d\sigma_{Y(2S)}/dX_F)$ vs. X_F [43].

Next, we consider the shapes of the X_F distributions of the Y(nS) states. These distributions are plotted in Figure 3.18 with normalizations adjusted in accordance with our now familiar technique. Obviously, all three have the same shape as predicted by the Color Evaporation Model.

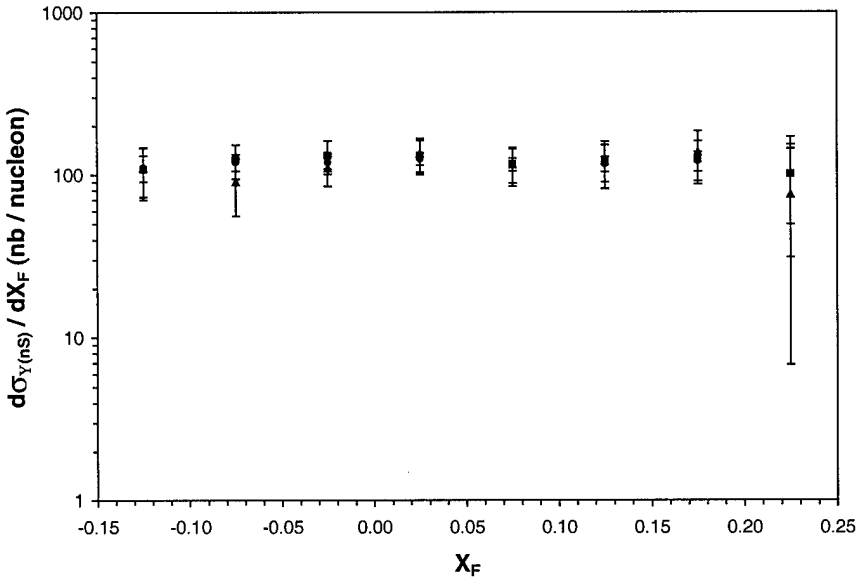

Figure 3.18: Plot of $d\sigma_{Y(nS)}/dX_F$ vs. X_F for n = 1, 2, 3 [43]. The Y(1S) distribution is represented by the circular data points. The Y(2S) distribution, which has been multiplied by a constant factor of 2.0, is represented by the square data points. The Y(3S) distribution, which has been multiplied by constant factor of 5.4, is represented by the triangular data points.

3.3.2 Charmonium

Once again, we will take advantage of the abundance of data on the charmonium system by considering two sets of data. The first set, which was produced by a fixed target experiment using a proton beam, is confined to the region around $X_F = 0$. The second, which comes from a fixed target experiment using a π^- beam, addresses the domain of large, positive X_F.

The relative production rates contained in these two data sets are plotted in Figures 3.19 and 3.20.

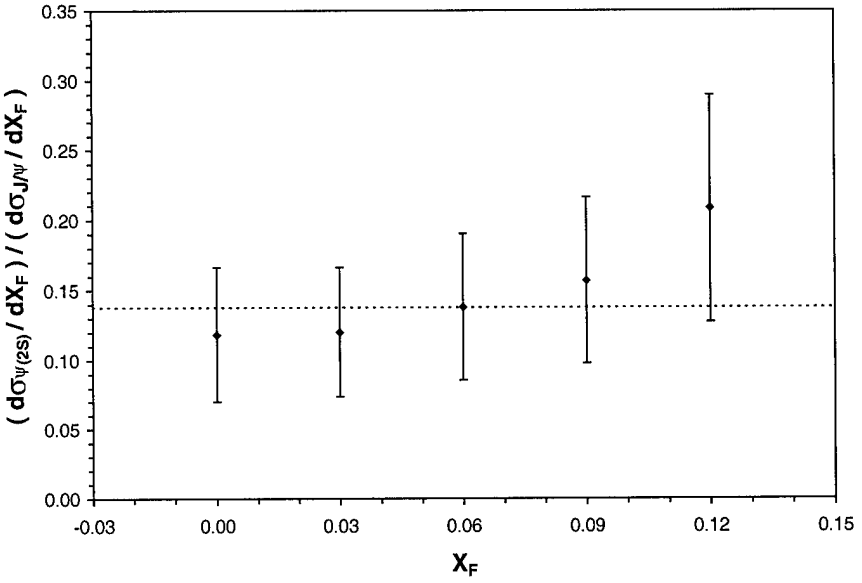

Figure 3.19: Plot of $(d\sigma_{\psi(2S)}/dX_F) / (d\sigma_{J/\psi}/dX_F)$ vs. X_F. The measurements were made in a fixed target experiment using a proton beam on a gold target [49].

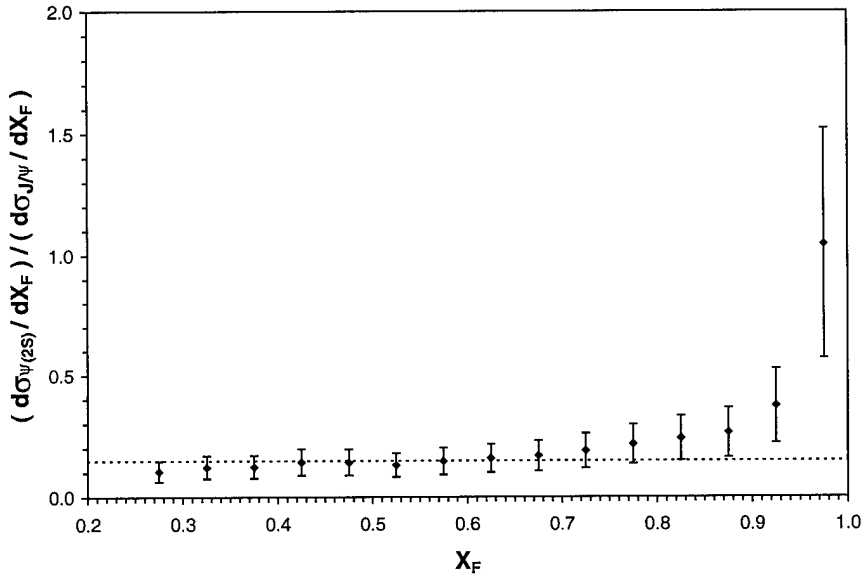

Figure 3.20: Plot of $(d\sigma_{\psi(2S)}/dX_F) / (d\sigma_{J/\psi}/dX_F)$ vs. X_F. The measurements were made in a fixed target experiment using a π^- beam on a tungsten target [55].

The relative production rate of the $\psi(2S)$ and J/ψ states remains essentially constant for small and moderate values of X_F as predicted by the Color Evaporation Model. As X_F approaches 1.0, however, the rate begins to grow very rapidly. This behavior contradicts the expectations of our model and seems to indicate that additional, or perhaps completely different, dynamics are present in the limit of very large X_F. A detailed investigation of these new dynamics is beyond the scope of this paper, but we will make two comments before leaving the subject.

First, the analysis in Section 3.1 considered a much more diverse collection of data but detected no significant differences between the behavior of data produced with proton beams and data produced with pion beams. Thus, we are inclined to believe that the discrepancy noted above is a feature of the large X_F limit rather than a function of beam type. Second, as we mentioned at the end of Section 3.1, the comparatively small mass of the charm quark could blur the line between perturbative and non-perturbative effects under certain circumstances. Thus, the large X_F behavior we have observed might be the result of non-perturbative effects for which our model does not account. Since large X_F data are not available for the bottomonium system, however, we do not know if this behavior is unique to charmonium system or if it is a universal feature of all quarkonium states.

Next, we turn our attention to the shapes of the individual X_F distributions. The relevant plots are contained in Figures 3.21 and 3.22. As we might now suspect, they show that the J/ψ and $\psi(2S)$ distributions have similar shapes at small and moderate X_F but that they move apart as X_F becomes very close to 1.0. Thus, we conclude that the charmonium data support the predictions of the Color Evaporation Model at most values of X_F. In the large X_F limit, however, it appears that the model is invalid, or at least incomplete.

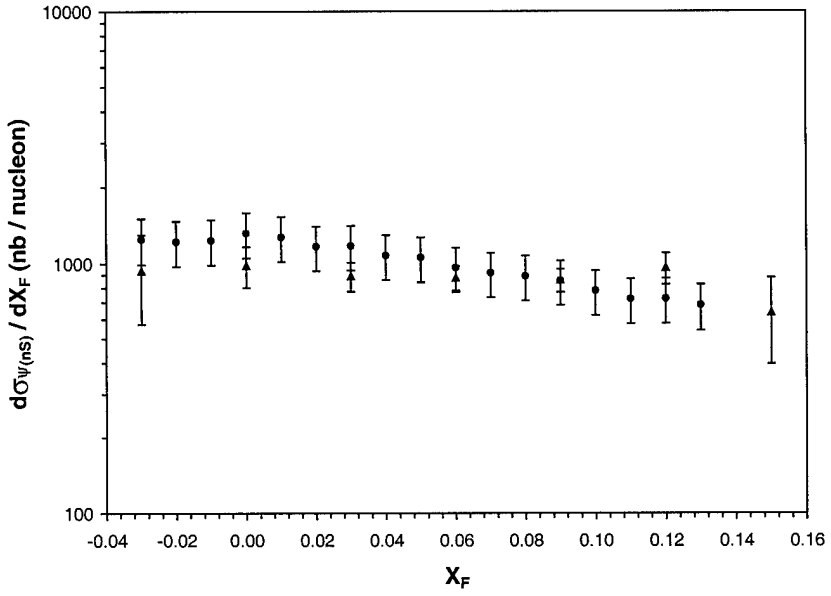

Figure 3.21: Plot of $d\sigma_{\psi(nS)}/dX_F$ vs. X_F for n = 1, 2 [49]. The J/ψ distribution is represented by the circular data points. The ψ(2S) distribution, which has been multiplied by a constant factor of 6.5, is represented by the triangular data points.

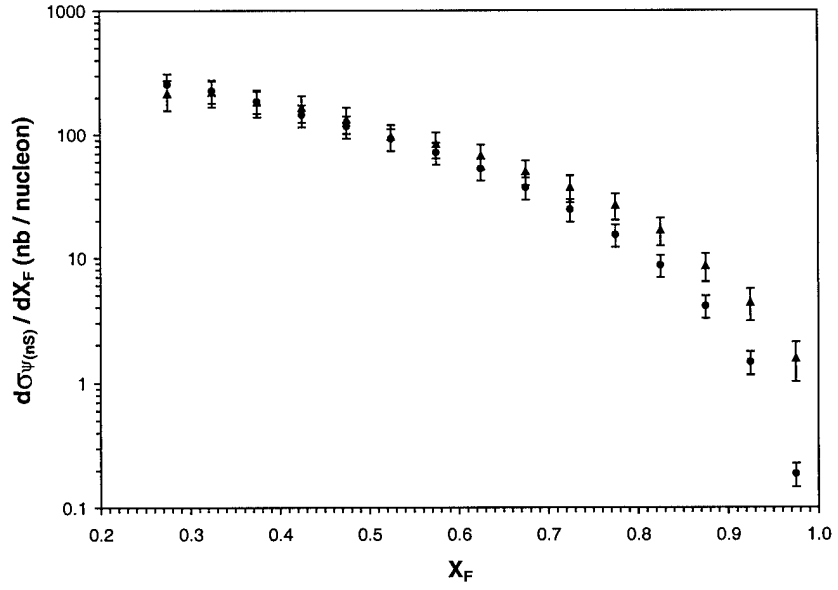

Figure 3.22: Plot of $d\sigma_{\psi(nS)}/dX_F$ vs. X_F for n = 1, 2 [55]. The J/ψ distribution is represented by the circular data points. The ψ(2S) distribution, which has been multiplied by a constant factor of 8.0, is represented by the triangular data points.

3.4 Polarization and Spin Alignment

Finally, we turn our attention to the polarization and spin alignment of quarkonium states. These properties are usually studied through analysis of the angular distributions of muon pairs produced in quarkonium decays. Because the results of these studies are most often stated in terms of something called the polarization parameter, however, we must define this quantity before we consider the data. We begin by defining "θ*" as the angle between the positive muon's direction in the decaying meson's rest frame and the decaying meson's direction in the center-of-mass frame of the colliding hadrons. Since this angle can be a bit difficult to visualize, we have portrayed it graphically in Figure 3.23.

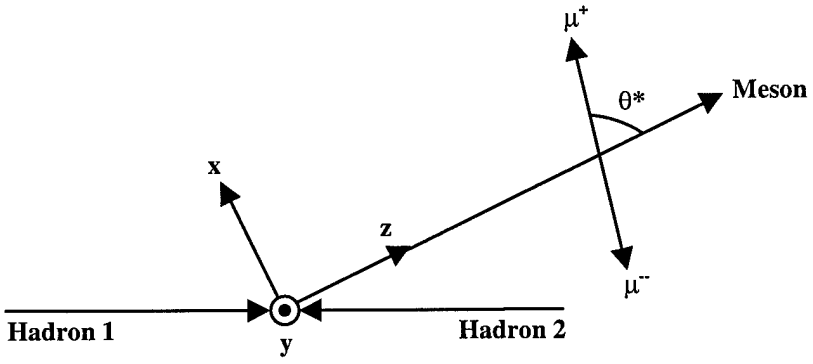

Figure 3.23: Definition of the angle "θ*" [59].

The decay distribution in this angle satisfies the following proportionality relation [23]:

$$\frac{d\Gamma}{d\cos\theta^*} \propto 1+\alpha\cos^2\theta^* \qquad (3.2)$$

The polarization parameter we seek is "α", the coefficient of the term containing the angular dependence in Equation 3.2. A measurement of $\alpha = +1$ indicates that the decaying mesons have fully transverse polarization. Similarly, a measurement of $\alpha = -1$ indicates fully

longitudinal polarization. The Color Evaporation Model, however, predicts that the mesons will be completely unpolarized. This state corresponds to $\alpha = 0$.

3.4.1 Bottomonium

The study of polarization in the bottomonium system has been very limited. In fact, only one set of data is currently available and it addresses only the Y(1S) meson [22]. Since the results are preliminary, the authors of the study simply state the fractions of Y(1S) decays that exhibit longitudinal polarization for various ranges of transverse momentum rather than giving detailed distributions for the polarization parameter. These fractions are listed in Table 3.1.

P_T Range (GeV)	Γ_L / Γ
$2 \leq P_T \leq 20$	0.37 ± 0.04
$8 \leq P_T \leq 20$	0.32 ± 0.11

Table 3.1: Fraction of Y(1S) mesons carrying longitudinal polarization for two different ranges of P_T [22].

The polarization of a massive particle can be expressed in terms of three linearly independent basis states. One of these basis states corresponds to longitudinal polarization and the others represent the two orthogonal directions available for transverse polarization. Thus, if 1/3 of a group of mesons is found to be longitudinally polarized and 2/3 are found to be transversely polarized, the polarizations are equally distributed between the available states and the group has no overall preferred direction of spin alignment. Accordingly, the longitudinal polarization fractions stated in Table 3.1 allow us to conclude that, within the experimental errors, the Y(1S) mesons are unpolarized. This result supports the predictions of the Color Evaporation Model.

3.4.2 Charmonium

The polarization properties of the charmonium system have been studied in much greater detail. Accordingly, data on the transverse momentum and X_F dependence of the polarization parameter is available. Figure 3.24 shows the transverse momentum dependence of prompt J/ψ mesons produced in $p\bar{p}$ collisions.

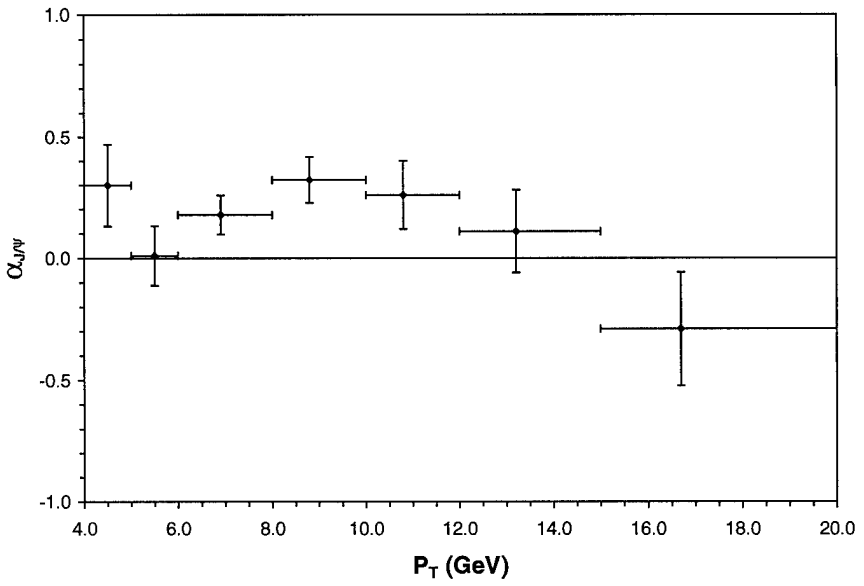

Figure 3.24: Plot of $\alpha_{J/\psi}$ vs. P_T [23].

In conjunction with this plot, we can also consider the single data point given in Reference [50]: $\alpha_{J/\psi} = -0.09 \pm 0.12$ in the range 0.0 GeV $\leq P_T \leq$ 3.5 GeV. It is difficult to draw a conclusion from this information. The polarization parameter is clearly not zero across the entire transverse momentum spectrum. Thus, the mesons are not completely unpolarized as our model predicts. The parameter's variation from zero, however, is neither large nor consistent. Thus, the mesons are not strongly polarized in any given direction. Accordingly,

we conclude that this data neither supports nor contradicts the expectations of the Color Evaporation Model.

Next, we turn our attention to a different charmonium state. Figure 3.25 shows the transverse momentum dependence of prompt $\psi(2S)$ mesons produced in $p\bar{p}$ collisions. At moderate values of transverse momentum, the data is consistent with zero polarization. As P_T increases, however, there is a tendency toward longitudinal polarization. Despite these observations, the data remains rather inconclusive because the error bars span almost the entire range of the polarization parameter. Thus, we once again conclude that the charmonium polarization data neither supports nor contradicts our model.

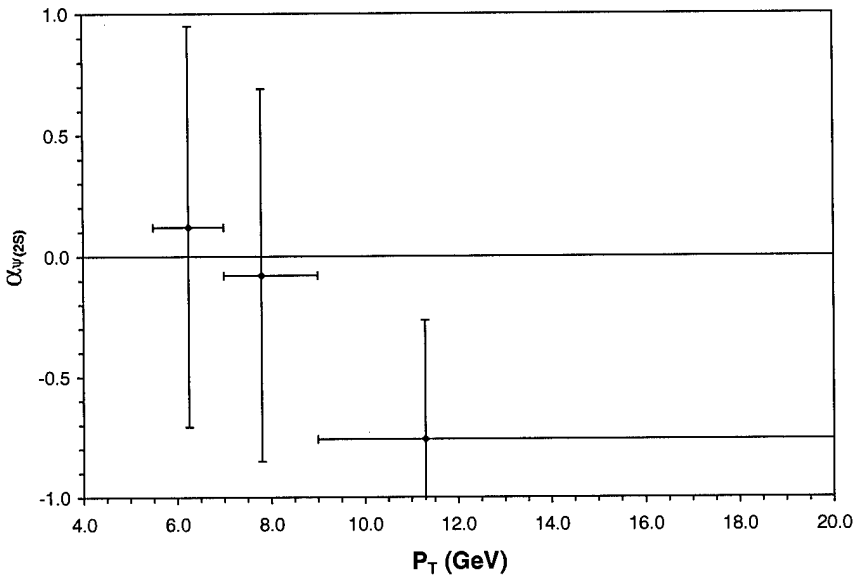

Figure 3.25: Plot of $\alpha_{\psi(2S)}$ vs. P_T [24].

Finally, we consider the X_F distribution of J/ψ mesons. The data, which is shown in Figure 3.26, was produced by a fixed target experiment using a π^- beam on a tungsten target.

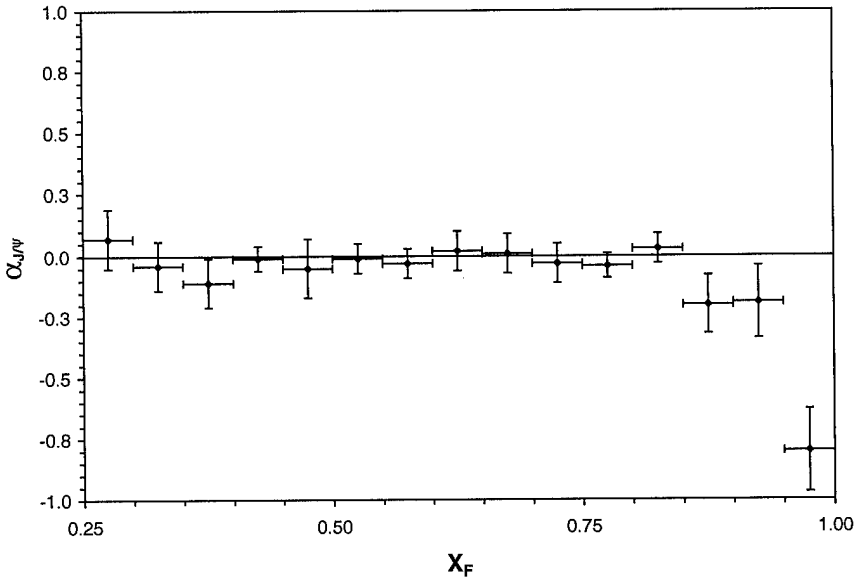

Figure 3.26: Plot of $\alpha_{J/\psi}$ vs. X_F [60].

At small and moderate values of X_F, the data is clearly consistent with zero polarization. As X_F approaches 1.0, however, the mesons seem to exhibit almost fully longitudinal polarization. Thus, we conclude that our model makes accurate predictions over the majority of the X_F domain, but that it becomes invalid in the limit of very large X_F. This is completely analogous to the conclusion reached in Section 3.3.2. Since the implications of this situation are addressed in that section, we will not repeat them here.

3.5 Conclusions

In this chapter, we have analyzed the Color Evaporation Model's assertion that the dynamics of heavy quarkonium production are completely contained in the short-distance factors by comparing three of its predictions to a representative sample of the available data. First, we have tested the prediction that the relative production rates of various quarkonium states are independent of $\sqrt{s}$, P_T, and X_F. Second, we have sought confirmation of the model's claim

that the P_T and X_F distributions of all quarkonium states have the same shape. Finally, we examined the prediction the quarkonium states are produced with no preferred direction of polarization or spin alignment.

The bottomonium data, though rather limited in scope, fully supported all three of these predictions. The charmonium data was generally supportive of the model's expectations, but its support was not universal. In fact, we noted two situations in which the charmonium data directly contradicted the model's predictions. First, in Section 3.1.2, we discovered that the relative production rate of J/ψ and $\psi(2S)$ mesons measured by experiments using anti-proton beams is significantly larger than the rate measured by experiments using other beam types. Then, in Sections 3.3.2 and 3.4.2, we saw that, for J/ψ and $\psi(2S)$ mesons, none of our three expectations are met in the limit of very large X_F. This asymmetry between the two heavy quark systems invites the interpretation that the model's predictions for the charmonium system are somehow spoiled by the comparatively light mass of the charm quark. Since this mass is only slightly larger than the energy scale at which we expect perturbation theory to fail, it may not be possible to completely isolate the production dynamics of charmonium in the perturbative portion of the model. We will be alert for further indications of this behavior as we continue our analysis.

Chapter 4

Determination of Long-Distance Factors for Observed Quarkonium States

In this chapter, we will attempt to determine the non-perturbative, long-distance factors for the sub-threshold $J^{PC} = 1^{--}$ mesons in both the bottomonium and charmonium systems. We will begin by using computer-based Monte Carlo techniques to calculate the appropriate short-distance factors. Then, we will obtain the long-distance factors by normalizing our calculations to the available data. Finally, we will compare our results with those presented in the original development of both the minimal and maximal versions of the Color Evaporation Model.

4.1 Calculation of Short-Distance Factors

As discussed in Chapter 2, the short-distance factors of the Color Evaporation Model are simply the cross sections for production of heavy quark pairs calculated to the desired order in perturbation theory. Because these factors contain all the information on the dynamics of the production process, however, a separate calculation must be performed for each type of data one wishes to study. For example, the short-distance factors required to predict the X_F distributions of quarkonium states produced in hadron-hadron collisions are not the same as those required for the analysis of total photoproduction cross sections as a function of center-of-mass energy. Thus, since we can not hope to attain universal applicability from a single

calculation, we will confine our efforts to the one category of data that contains recent and detailed results on both heavy quark systems: transverse momentum distributions of quarkonium states produced in $p\bar{p}$ collisions.

With this constraint in place, our task reduces to calculating the P_T distributions for hadroproduction of heavy quark pairs. We will perform the calculation to leading order using basic parton-model techniques of the type described in Equation 2.4. This scheme has two main ingredients: cross section formulae for the contributing parton-level processes and parameterizations of the appropriate parton distribution functions. We will discuss each of these components separately.

Beginning with the first ingredient, we must exercise great care in determining which parton-level reactions to include in our calculation. Naively, one is inclined to choose the order α_s^2 processes $q\bar{q} \rightarrow Q\bar{Q}$ and $gg \rightarrow Q\bar{Q}$, which were included in Equation 2.4 and depicted in Figures 2.1 and 2.2. This choice, however, is incorrect. Because our calculation scheme assumes that the initial state partons have no intrinsic transverse momentum, a heavy quark pair produced by either of these mechanisms must have zero net P_T. Thus, these processes can make no contribution to our transverse momentum distributions.

Instead, the leading order processes for the evaluation of transverse momentum distributions are the order α_s^3 reactions $q\bar{q} \rightarrow gQ\bar{Q}$, $qg \rightarrow qQ\bar{Q}$, and $gg \rightarrow gQ\bar{Q}$. Because a total of 28 tree-level Feynman diagrams contribute to these three processes (see Appendix A), the explicit expressions for the parton-level cross sections are enormously long. In the interest of brevity, we will not include them here. This omission will in no way impair the

reader's ability to understand our results. Those who are interested, however, can find reasonably concise forms of the spin-averaged, squared amplitudes in Reference [69].

By selecting these three processes, we have allowed our heavy quark pairs to acquire non-zero transverse momentum, but we are left with a subtler problem. The intrinsic transverse momentum of the initial state partons and the results of the soft gluon resummation required to treat infrared divergences are expected to have a substantial impact on the lower end of the P_T distributions. Since our parton-model technique accounts for neither of these effects, the results of our calculation will only be reliable in the region $P_T > M_Q$. We must keep this limitation in mind throughout our analysis.

The second major component we must consider is the parton distribution functions for the proton and the anti-proton. An enormous variety of distributions are available in the literature. Each of these has its own advantages and disadvantages so one must carefully select the set that is most appropriate for the calculation being performed. In the present case, 23 of the 28 contributing Feynman diagrams have gluons in the initial state. Thus, it is critical that we select a parameterization that emphasizes the accuracy of the gluon distributions. The set that best fits this description is the CTEQ-4M parameterization [70].

Now that we have selected a set of parton distribution functions, we must carefully choose the values of the variables on which these functions depend. For our purposes, there are three such parameters: the mass of the appropriate heavy quark, the QCD scale with five active flavors, and the momentum scale that characterizes the hadronic reaction. In treating the last of the three, a distinction is sometimes made between the renormalization scale (μ_R), which is used in the evaluation of the strong coupling constant, and the factorization scale (μ_F), which is used in the evolution of the parton distribution functions. In the current

calculation, however, there is no need to distinguish between the two. Thus, the single relevant momentum scale will be denoted by the more familiar label "Q^2".

The values we have selected for the three key parameters are consolidated in Table 4.1. The heavy quark masses are in the same ranges as those advocated by earlier works on the Color Evaporation Model [8-13]. The expressions used to define the momentum scales, which essentially correspond to the square of the average of the transverse masses of the heavy quark and the heavy anti-quark, are similar to those recommended by Reference [72]. The value of the QCD scale with five active quark flavors is mandated by our choice of parton distribution functions [70].

System	M_Q (GeV)	Q^2	$\Lambda^{(5)}_{QCD}$ (GeV)
Bottomonium	4.75	$\frac{1}{2}[(P_T^2)_b + (P_T^2)_{\bar{b}}] + M_b^2$	0.202
Charmonium	1.20	$4\{\frac{1}{2}[(P_T^2)_c + (P_T^2)_{\bar{c}}] + M_c^2\}$	0.202

Table 4.1: Input parameters for the calculation of short-distance factors.

Before leaving this subject, we note that the results of our calculations are actually rather insensitive to the choice of parton distribution functions when the values of the three input parameters are selected appropriately. For example, we repeated the bottomonium calculations described in Section 4.3 using the GRV 94 HO parameterization [71]. With the input variables changed to $M_b = 4.775$ GeV, $Q^2_{GRV} = (\frac{1}{2}Q_{CTEQ})^2$, and $\Lambda^{(5)}_{QCD} = 0.131$ GeV (the mandated value for GRV 94 HO), the results differed by less than one percent.

Since we have now determined the contributing parton-level processes and selected an appropriate set of parton distribution functions, we can state the equation that will govern the calculation of our short-distance factors:

$$\begin{aligned}\sigma_{Q\overline{Q}} \equiv & \sum_{q=u,d,s} \int dx_1 \int dx_2 [\, f_q(x_1,Q^2)\, f_{\overline{q}}(x_2,Q^2) + f_{\overline{q}}(x_1,Q^2)\, f_q(x_2,Q^2)]\, \hat{\sigma}(q\overline{q} \rightarrow gQ\overline{Q}) + \\ & \sum_{q=u,d,s} \int dx_1 \int dx_2 [\, f_q(x_1,Q^2)\, f_g(x_2,Q^2) + f_g(x_1,Q^2)\, f_q(x_2,Q^2)]\, \hat{\sigma}(qg \rightarrow qQ\overline{Q}) + \\ & \sum_{\overline{q}=\overline{u},\overline{d},\overline{s}} \int dx_1 \int dx_2 [\, f_{\overline{q}}(x_1,Q^2)\, f_g(x_2,Q^2) + f_g(x_1,Q^2)\, f_{\overline{q}}(x_2,Q^2)]\, \hat{\sigma}(\overline{q}g \rightarrow \overline{q}Q\overline{Q}) + \\ & \int dx_1 \int dx_2 [\, f_g(x_1,Q^2)\, f_g(x_2,Q^2)]\, \hat{\sigma}(gg \rightarrow gQ\overline{Q})\end{aligned} \tag{4.1}$$

Throughout this equation, $f_{parton}(x_a, Q^2)$ refers to the CTEQ-4M parameterization of the appropriate parton distribution function. In the next section, we will discuss the application of Monte Carlo techniques to the evaluation of Equation 4.1.

4.2 Monte Carlo Simulation

To calculate the required short-distance factors, we constructed a computer-based Monte Carlo simulation that produces the leading order transverse momentum distributions and integrated cross sections for a specified type of heavy quark pair subject to a user-defined set of initial conditions. Because a detailed knowledge of our modeling technique is not essential to gaining an understanding of our results, we will give only a general overview of the simulation. The reader interested in a more thorough treatment of Monte Carlo techniques should consult Chapter 11 of Reference [38].

In each iteration, our simulation randomly generates a heavy quark pair production event in the kinematical range allowed by the stated set of initial conditions, then estimates the corresponding value of Equation 4.1 and records it in a histogram according to its associated

transverse momentum. Each event consists of six parameters: one value of the initial state partonic center-of-mass energy ($\sqrt{\hat{s}}$), one value of the relative longitudinal momentum fraction of the initial state partons (x_1 - x_2), and one value each for three of the angles and one of the momenta that define the final state phase space. After a very large number of iterations, the P_T distribution can be read off directly from the histogram. The integrated cross sections are obtained by taking a weighted average of the results from all the events.

The FORTRAN program that performs these calculations is not completely original. Rather, it is almost entirely a collection of pre-existing blocks of code drawn from a variety of sources and linked together to serve our purpose. Thus, we must enumerate these components and acknowledge the corresponding sources before we proceed to analyze our results.

Our base program, which manages the other components and assembles the various factors required to predict the cross sections, is a modified version of code produced by E. Gregores for the original work on the maximal version of the Color Evaporation Model [8-11]. We used the MADGRAPH package [61] to build functions that generate our spin and color averaged, squared amplitudes by calling HELAS subroutines [62]. The flux and phase space factors are determined using subroutines written by O. J. P. Eboli. These were also employed in the original work on the maximal version of our model. The six-dimensional Monte Carlo integration is performed by a program called VEGAS [63], which was designed by G. P. Lepage. The histograms for our transverse momentum distributions are produced using the HBOOK program [64] of the CERN Program Library [65]. Finally, the required values of the strong coupling constant and the CTEQ-4M parton distribution functions are obtained using another CERN Program Library component entitled PDFLIB [66-68].

4.3 Bottomonium Results

In this section, we will determine the long-distance factors for the Y(1S), Y(2S), and Y(3S) states of the bottomonium system to leading order by fitting our calculated short distance-factors to experimental data. By manipulating the model, we will also be able to obtain a very good approximation of the next-to-leading order values. Throughout the analysis, we will respect the limitations discussed in Section 4.1 by confining our calculations to the region $P_T > 6$ GeV.

We begin by rewriting Equation 2.7 in the following form:

$$K\rho_{n^3S_1^{PC}} = 9\frac{\sigma_{n^3S_1^{PC}}}{\sigma_<} \tag{4.2}$$

Note that we have inserted a K factor into this expression in recognition of the fact that our short-distance factors were calculated to leading order only. By substituting the integrated sub-threshold cross section from our Monte Carlo simulation for $\sigma_<$ and the appropriate bottomonium data from Reference [22] for $\sigma_{n^3S_1^{PC}}$, we can use this equation to obtain numerical predictions for the quantity $K\rho_{n^3S_1^{PC}}$. Performing this operation yields the following values for our leading order long-distance factors: $K\rho_{Y(1S)} = 0.6233$, $K\rho_{Y(2S)} = 0.3483$, and $K\rho_{Y(3S)} = 0.1479$.

Next, we will attempt to convert these numbers into next-to-leading order results by finding the approximate value of the K factor. If we assume that the K factor for the $b\bar{b}$ pair production cross section is the same both above and below threshold, we can rewrite Equation 2.8 in the following form:

$$K = \frac{\sigma_{M\bar{M}}}{\frac{8}{9}\sigma_{<} + \sigma_{>}} \tag{4.3}$$

The quantity $\sigma_{<}$ can once again be replaced with the integrated sub-threshold cross section from our Monte Carlo simulation. The quantity $\sigma_{>}$, however, can not be treated quite so simply. From Chapter 2, we recall that the maximal version of the Color Evaporation Model suggests that the above-threshold cross section is negligible. Rather than directly accepting this assertion, we will test its validity before deciding how to manage the corresponding term in our equation.

In Figure 4.1, we have plotted the $b\bar{b}$ pair production cross section from our Monte Carlo simulation as a function of the upper limit imposed on the invariant mass of the pair. The leftmost data point on the curve is the result obtained with the upper limit set equal to threshold.

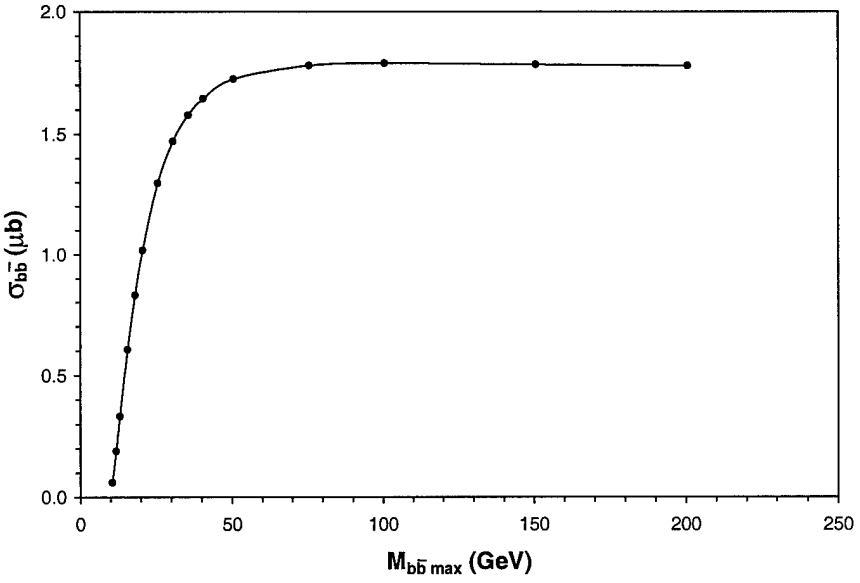

Figure 4.1: Plot of $\sigma_{b\bar{b}}$ vs. $M_{b\bar{b}\,max}$.

Inspection of this plot shows that the above-threshold cross section is actually quite large. We obviously can not ignore its contribution to our K factor. Accordingly, we will replace the quantity $\sigma_>$ in Equation 4.3 with the integrated above-threshold cross section from our Monte Carlo simulation.

Finally, we must find appropriate data to provide a value for the quantity $\sigma_{M\overline{M}}$. Our best option is the B meson data of Reference [73], but we must exercise care in how we apply it. The data represents the cross section for production of B^+ and B^0 mesons only, but our calculated cross sections also include contributions from b quarks that fragment into other open-flavored bottom hadrons, such as B_s^0 and $\overline{\Lambda}_b^0$. Thus, we must extract only the B^+ and B^0 contribution from our calculation. To do so, we will make use of the b quark fragmentation fractions measured in Reference [74].

By assembling all the components discussed in the proceeding paragraphs, we can rewrite Equation 4.3 in the following form:

$$K = \frac{\sigma_{B^+/B^0}}{(f_u + f_d)(\frac{8}{9}\sigma_< + \sigma_>)} \tag{4.4}$$

In this expression, the symbols "f_u" and "f_d" represent the fragmentation fractions that yield B^+ and B^0 mesons respectively. Inserting the numerical values, we obtain the result $K = 1.84$.

By dividing this K factor out of our leading order long-distance factors, we can obtain a very good approximation for the next-to-leading order values. The results of this operation are consolidated in Table 4.2. To facilitate comparison, they are stated in the language of

both the maximal and minimal versions of the Color Evaporation Model. As discussed in Chapter 2, the respective long-distance factors are related by $F = \rho/9$.

Meson	ρ_{LO} (%)	ρ_{NLO} (%)	F_{LO} (%)	F_{NLO} (%)
Y(1S)	62.33	33.88	6.93	3.76
Y(2S)	34.83	18.93	3.87	2.10
Y(3S)	14.78	8.03	1.64	0.89

Table 4.2: Long distance factors for the sub-threshold $J^{PC} = 1^{--}$ mesons of the bottomonium system.

Our long-distance factors agree quite well with the original results of the minimal version of the model, which are listed in Table 2.1. The small differences between the two sets of numbers can be attributed to the fact that the data set used in our calculation [22] is more recent and more detailed than those used in the original work [43-45, 75]. The differences in the two sets of results simply mirror the differences in the data. This agreement with previous results is an encouraging validation of our technique.

Since no previous bottomonium results exist for the maximal version of the model, a comparison is not possible. We can, however, make one observation. Note that the sum of the percentages in the first column of Table 4.2 is greater than 100 percent. Thus, at leading order, the maximal version of the model makes the rather nonsensical prediction that the sum of the cross sections for the three Y states is greater than the total sub-threshold quarkonium cross section. At next-to-leading order, the contribution of the Y states is reduced to about 60 percent. Although this next-to-leading order correction removes the unitarity problem, we still have cause for concern. The bottomonium system is expected to contain at least 14 sub-threshold bound states and may contain more than 20. Thus, it seems highly unlikely that

three states would account for 60 percent of the total quarkonium cross section. This observation leads us to doubt the maximal version's prediction that only 1/9 of the sub-threshold bottom quark pairs emerge bound into bottomonium states. The correct fraction for the bottomonium system is almost certainly larger. We will return to this issue in Chapter 5. Before leaving the subject, however, we note that this observation does not invalidate our calculation of the K factor. Although that calculation employed the factor of 8/9 we have just refuted (see Equation 4.3), the result is not sensitive to changes in this fraction because, as we saw in Figure 4.1, the above-threshold contribution completely dominates the sub-threshold factor in which the fraction appears.

As a final test of our results, we plot our predictions for the P_T distributions of all three Y states and compare them to the data of Reference [22]. These charts are contained in Figures 4.2, 4.3, and 4.4.

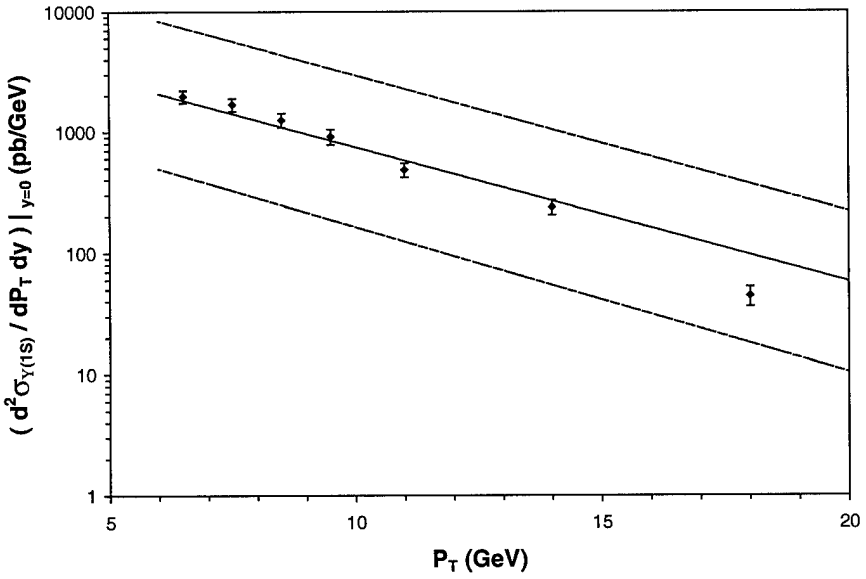

Figure 4.2: Plot of $(d^2\sigma_{\Upsilon(1S)}/dP_T dy)|_{y=0}$ vs. P_T. The data points represent experimental measurements from Reference [22]. The lines are the theoretical predictions of the Color Evaporation Model.

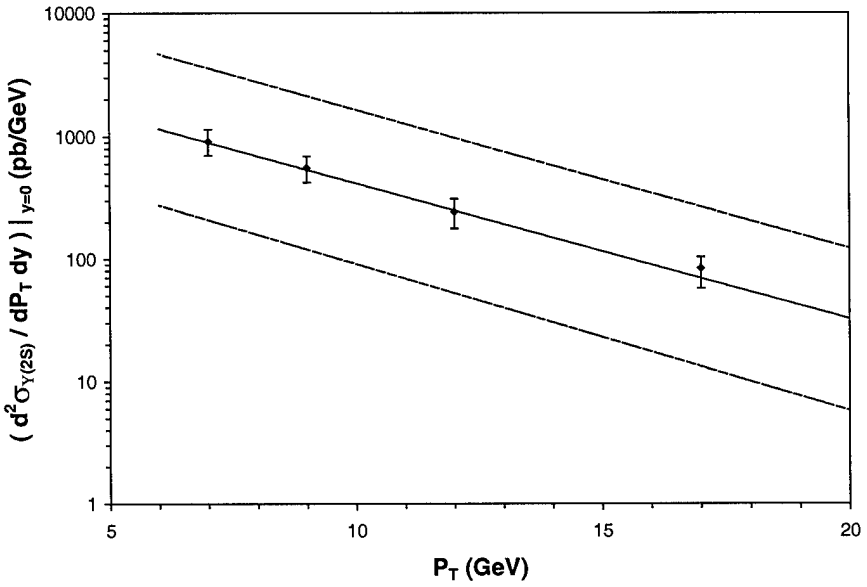

Figure 4.3: Plot of $(d^2\sigma_{\Upsilon(2S)}/dP_T dy)|_{y=0}$ vs. P_T. The data points represent experimental measurements from Reference [22]. The lines are the theoretical predictions of the Color Evaporation Model.

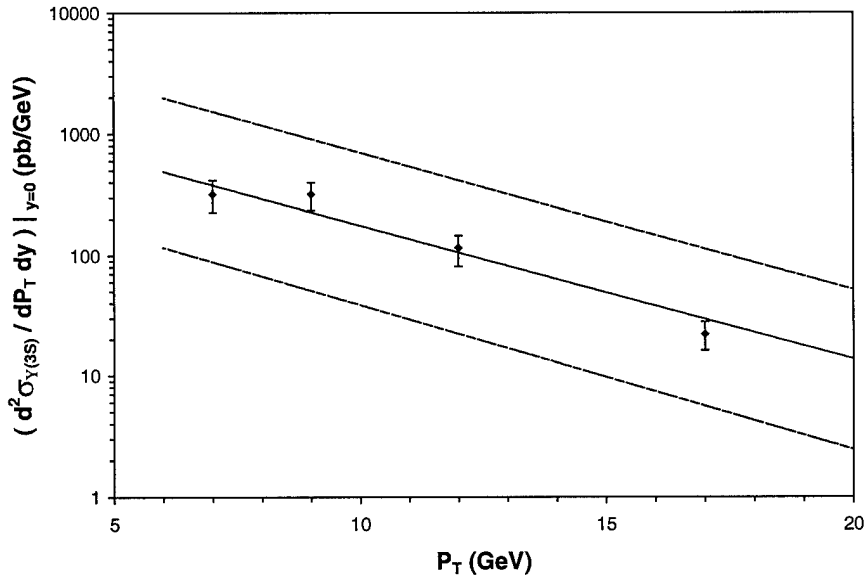

Figure 4.4: Plot of $(d^2\sigma_{\Upsilon(3S)}/dP_T dy)|_{y=0}$ vs. P_T. The data points represent experimental measurements from Reference [22]. The lines are the theoretical predictions of the Color Evaporation Model.

In each plot, the solid line represents our central prediction. It is simply a smooth curve fitted to the product of the P_T distribution histogram from our Monte Carlo simulation and the appropriate value of F_{LO} from Table 4.2. The dotted lines give estimates of the theoretical error in our results following the techniques described in References [15], [76], and [77]. They were obtained by the same fitting procedure mentioned above, but with the P_T distributions recalculated using extreme values of the parameters introduced in Table 4.1. The upper limit was produced using the values $M_b = 4.50$ GeV, $Q^2 = (\frac{1}{2}Q_0)^2$, and $\Lambda^{(5)}_{QCD} = 0.300$ GeV. For the lower limit, we used the values $M_b = 5.00$ GeV, $Q^2 = (2Q_0)^2$, and $\Lambda^{(5)}_{QCD} = 0.150$ GeV. In assessing the validity of these error estimates, we must bear in mind that our parton distribution functions were developed using a fixed value of the QCD scale. Thus, the technique of varying $\Lambda^{(5)}_{QCD}$ without corresponding adjustments in the distribution functions ignores the correlation between the two. Accordingly, the true errors are almost certainly smaller than those depicted on our plots. The agreement between the data and our central prediction is impressive.

4.4 Charmonium Results

Next, we perform a similar analysis on the charmonium system. Our initial intent is to determine the long-distance factors for the J/ψ and ψ(2S) mesons to leading order. We will achieve this goal using the now familiar technique of fitting our calculated short distance-factors to experimental data. We will also attempt to obtain an approximation of the next-to-leading order values. Due to the limitations on the validity of our calculation discussed in Section 4.1, we will confine our analysis to the region $P_T > 2$ GeV.

Once again, our starting point is Equation 4.2. By substituting the integrated sub-threshold cross section from our Monte Carlo simulation for $\sigma_<$ and the appropriate charmonium data from Reference [16] for $\sigma_{nJ^{PC}}$, we obtain the following leading order long-distance factors: $K\rho_{J/\psi} = 0.4646$ and $K\rho_{\psi(2S)} = 0.1188$.

Unfortunately, we can not calculate the K factor for $c\bar{c}$ pairs using the technique we employed to find the $b\bar{b}$ K factor in the previous section. To do so, we would have to substitute D meson data for $\sigma_{M\bar{M}}$ in Equation 4.3. Because all the available data on the hadroproduction of D mesons was produced at rather low center-of-mass energies (generally less than 40 GeV), however, the measured P_T distributions are almost entirely confined to the region of low transverse momentum where our calculations are not reliable. Thus, instead of computing our K factor directly, we will borrow the result K = 2.2 from the minimal version of the Color Evaporation Model [13]. Since our bottomonium results agreed almost exactly with those of the minimal version, we expect our charmonium results to be very similar as well. Accordingly, it is reasonable to assume that the $c\bar{c}$ K factor from the minimal version of the model is a good approximation of the value we require.

Despite the fact that we can not explicitly determine our K factor, it is informative to consider the quantity $\sigma_>$ from Equation 4.3 before we leave the subject entirely. In the previous section, we found that, contrary to the predictions of the maximal version of the Color Evaporation Model, the cross section for production of bottom quark pairs is much larger in the above-threshold region than in the sub-threshold region. We will perform a similar analysis for charm quark pairs. In Figure 4.5, we have plotted the $c\bar{c}$ pair production cross section from our Monte Carlo simulation as a function of the upper limit imposed on

the invariant mass of the pair. The leftmost data point on the curve is the result obtained with the upper limit set equal to threshold.

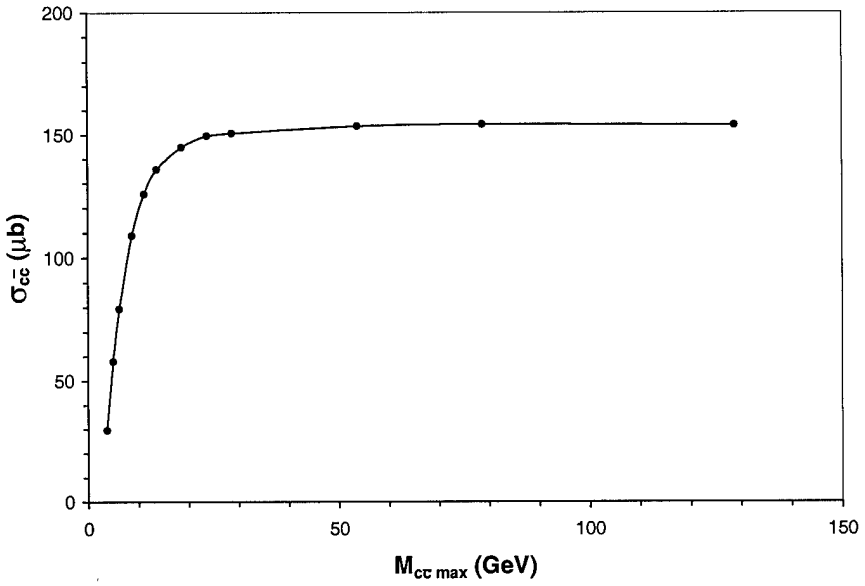

Figure 4.5: Plot of $\sigma_{c\bar{c}}$ vs. $M_{c\bar{c}\,max}$.

Inspection of this plot shows that the above-threshold $c\bar{c}$ cross section is much too large to neglect. Since the approximation $\sigma_< \cong 0$ appears to have been used several times in the original work on the maximal version of the model [8, 9], the corresponding numerical results must be viewed with a certain degree of skepticism.

Next, we obtain approximate next-to-leading order results by dividing the borrowed K factor out of our leading order long-distance factors. The results are consolidated in Table 4.3. Once again, we have stated them in the language of both versions of the model in order to facilitate comparison.

Meson	ρ_{LO} (%)	ρ_{NLO} (%)	F_{LO} (%)	F_{NLO} (%)
J/ψ	46.46	21.12	5.16	2.35
ψ(2S)	11.88	5.40	1.32	0.60

Table 4.3: Long distance factors for the sub-threshold $J^{PC} = 1^{--}$ mesons of the charmonium system.

Our J/ψ long-distance factor is in good agreement with the original result of the minimal version of the Color Evaporation Model, which is given in Table 2.1. Our ψ(2S) long-distance factor, however, is larger than the minimal version's original result by approximately a factor of two. Although this difference is much larger than the small deviations we noted in our bottomonium predictions, the explanation can once again be found by comparing the data sets used in the calculations. In the original work on the minimal version of the model [13], the charmonium long-distance factors were determined using the data consolidated in Reference [14]. This data was drawn exclusively from fixed target experiments that employed proton and pion beams. In our calculation, however, we used data produced in $p\bar{p}$ collisions [16]. As we discovered in Section 3.1.2, the use of an anti-proton beam causes the relative ψ(2S) – J/ψ production rate to increase by approximately a factor of two. The difference between our ψ(2S) long-distance factor and the minimal version's original result is simply another manifestation of this behavior. This difference, however, does not limit the predictive power of our result. When analyzing data produced with proton and pion beams, one can obtain very good results by simply dividing our ψ(2S) long-distance factor by two.

Turning our attention to the maximal version of the Color Evaporation Model, we recall from Chapter 2 that its original prediction for the J/ψ long-distance factor was $\rho_{J/\psi} = 0.47$. Although the original papers [8-11] do not state whether this is to be considered a leading order or next-to-leading order value, it agrees almost exactly with our leading order result. The original work on the maximal version does not state a value for the ψ(2S) long-distance factor so comparison of our second result is not possible.

Next, we consider the maximal version's assertion that only 1/9 of the sub-threshold charm quark pairs emerge bound into charmonium states. From the second column of Table 4.3, we see that the maximal version expects the J/ψ and ψ(2S) states to contribute just over 25 percent of the total sub-threshold quarkonium cross section. Since the charmonium system is expected to contain only eight sub-threshold bound states, it is very reasonable to assume that two of them should account for one quarter of the total cross section. Thus, we have discovered no reason to doubt that 1/9 is the correct fraction for the charmonium system. We will consider this issue in more detail in the next chapter.

Finally, we plot our predictions for the P_T distributions of both charmonium states and compare them to the data of Reference [16]. These charts are given in Figures 4.6 and 4.7. Our main predictions, which are represented by the solid lines, were produced using the same technique described in the previous section's analysis of bottomonium. The error estimates, however, were treated in a slightly different manner.

The mass of the charm quark is generally assumed to lie between 1.2 GeV and 1.8 GeV. Since our main prediction was obtained using a mass value from the lower end of this range, we have not used it as the central point about which to vary our three critical parameters as we did in our bottomonium analysis. Rather, we have elected to display the error range by

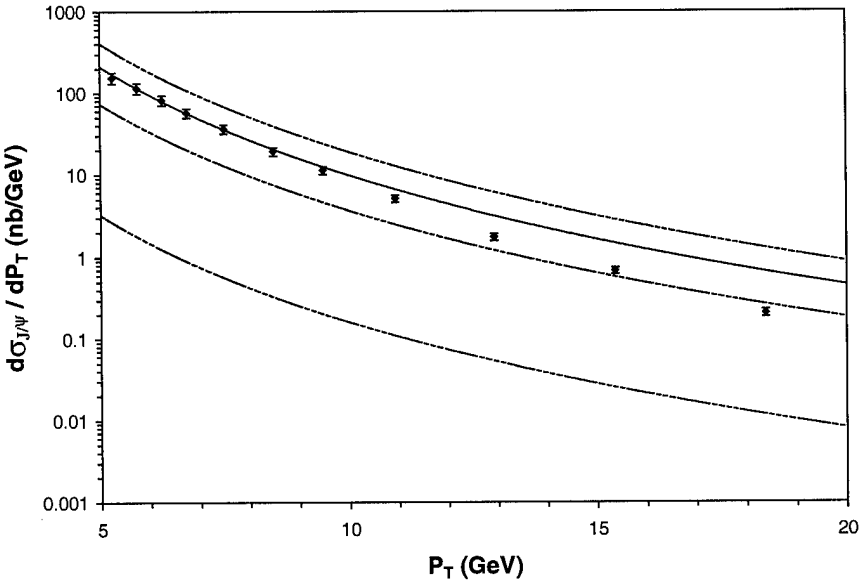

Figure 4.6: Plot of $d\sigma_{J/\psi}/dP_T$ vs. P_T. The data points represent experimental measurements from Reference [16]. The lines are the theoretical predictions of the Color Evaporation Model.

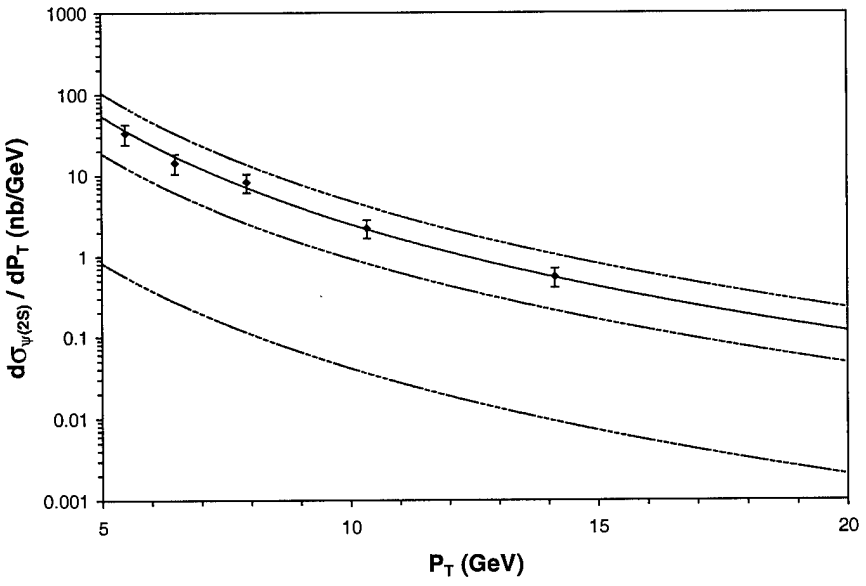

Figure 4.7: Plot of $d\sigma_{\psi(2S)}/dP_T$ vs. P_T. The data points represent experimental measurements from Reference [16]. The lines are the theoretical predictions of the Color Evaporation Model.

including three dashed lines on each plot. The middle dashed line was obtained using the central values of all three parameters: $M_c = 1.50$ GeV, $Q^2 = Q_0^2$, and $\Lambda^{(5)}_{QCD} = 0.202$ GeV. It represents the midpoint of our error range. As in the previous section, the upper and lower dashed lines were obtained using extreme values of the parameters. The upper limit was produced using $M_c = 1.20$ GeV, $Q^2 = (\frac{1}{2}Q_0)^2$, and $\Lambda^{(5)}_{QCD} = 0.300$ GeV. For the lower limit, we used the values $M_c = 1.80$ GeV, $Q^2 = (2Q_0)^2$, and $\Lambda^{(5)}_{QCD} = 0.150$ GeV. Thus, as we would expect, our main prediction lies inside the error range but not at its center. As in the bottomonium case, the agreement between the data and our predictions is impressive.

4.5 Conclusions

The most important results of this chapter are the leading order and next-to-leading order values of the long-distance factors for the $J^{PC} = 1^{--}$ states of the bottomonium and charmonium systems. These factors are consolidated in Table 4.4 for easy reference.

Meson	ρ_{LO} (%)	ρ_{NLO} (%)	F_{LO} (%)	F_{NLO} (%)
Y(1S)	62.33	33.88	6.93	3.76
Y(2S)	34.83	18.93	3.87	2.10
Y(3S)	14.78	8.03	1.64	0.89
J/ψ	46.46	21.12	5.16	2.35
ψ(2S)	11.88	5.40	1.32	0.60

Table 4.4: Consolidated list of the long-distance factors calculated in this chapter. The ψ(2S) factor should be reduced by 45 to 50 percent when analyzing a hadronic reaction that does not include an anti-proton in the initial state.

Our long-distance factors agree very well with the available results from earlier work on both the maximal and minimal versions of the Color Evaporation Model. Despite the agreement of the final results, however, we discovered two cases in which the assertions of the maximal version seem to be incorrect. First, we saw that, in both heavy quarkonium systems, the above-threshold pair production cross section is definitely not negligible. Thus, previous maximal version calculations that ignored the above-threshold contribution are called into question. Second, we found that, although the prediction that only 1/9 of sub-threshold heavy quark pairs form quarkonium states seems reasonable in the charmonium system, this fraction is almost certainly too small to accurately describe the bottomonium system. We will address this point in greater detail in the next chapter.

Chapter 5

Prediction of Long-Distance Factors for Unobserved Quarkonium States

When we first introduced the Color Evaporation Model in Chapter 1, we noted that it does not include a system for calculating the non-perturbative, long-distance factors. Accordingly, these factors must be determined empirically following procedures similar to those we employed in Chapter 4. Although these techniques are effective, the model's reliance on them is a substantial limitation. The production cross sections for the vast majority of quarkonium states have not been experimentally measured. Thus, the current versions of the model can make detailed predictions for only a very small portion of the spectrum.

Obviously, the model's utility would be greatly enhanced by the introduction of a universal equation that predicts the long-distance factors of all quarkonium states in terms of a few basic parameters, such as mass and internal quantum numbers. Although it seems unlikely that such an expression could be derived from first principles, it might be possible to construct one empirically. An equation that generates long-distance factors which accurately reproduce the data on the observed quarkonium states might yield very good estimates of the factors for the unobserved states as well. In this chapter, we will attempt to find such an equation.

Before we begin, however, we must make an important distinction. Most experimental results state values for inclusive quarkonium cross sections. In other words, the mesons counted in the measurements include those that result from the de-excitation of heavier quarkonium states and from the decays of other hadrons in addition to those that are directly produced in the initial hadronic reaction. In most cases, it is prohibitively difficult to remove all of these secondary contributions from the data. Thus, although predictions of the cross sections for direct or prompt quarkonium production might be the most theoretically interesting, predictions of the inclusive cross sections are much more useful in experimental and phenomenological applications. Accordingly, the equation we hope to find is one that generates the long-distance factors required to predict the inclusive cross sections for the unobserved states. Since the long-distance factors we produced in Chapter 4 were determined by normalizing our calculations to inclusive data, this choice will also facilitate comparison of our equation's predictions with our previous results.

5.1 Explicit Forms of the Long-Distance Factor

We are not the first to undertake this task. Thus, prior to beginning our own search for an equation that correctly predicts the long-distance factors, we will review the successes and failures of those who have gone before. As a reference point, we will use the following equation.

$$\sigma_{n J^{PC}} = \rho_{n J^{PC}} \beta_Q \sigma_{<} = \rho_{n J^{PC}} \sigma_{[Q\bar{Q}]} \tag{5.1}$$

This expression is simply a modification of Equation 2.7. Its general intent is unchanged but, in light of the results obtained in the last chapter, we have removed the requirement for the total quarkonium cross section to equal 1/9 of the sub-threshold pair production cross section.

In its place, we have inserted a system-dependent fraction denoted "β_Q". Thus, $\sigma_{[Q\bar{Q}]}$ still represents some fraction of $\sigma_<$, but this fraction is now allowed to vary from system to system.

When the Color Evaporation Model was first resurrected, it was suggested that the long-distance factor for a given state might be proportional to the wave function of the heavy quark pair evaluated at the origin [12]. Although there is some theoretical justification for this idea, the wave function at the origin is definitely not a basic parameter of the type we want to use in our equation. Thus, since this technique is not in the same category as the one we intend to design, we will not consider its predictions in detail.

A method with an intent more similar to our own can be found in the original work on the maximal version of the Color Evaporation Model [8]. It offered the following technique for predicting long-distance factors:

$$\rho_{nJ^{PC}} = \frac{(2J+1)}{\sum_i (2J_i+1)} \tag{5.2}$$

In this expression, and those that follow, the summation index "i" runs over all sub-threshold quarkonium states. Equation 5.2 implies that simple statistical counting of spin states might correctly predict the long-distance factors. It is easy to see, however, that its results do not reproduce the data. In Equation 3.1, we noted that the relative production rate of two quarkonium states is equal to the ratio of their long distance factors. Thus, since all the Y states have the same total angular momentum, Equation 5.2 predicts that their relative production rates are all equal to 1.0. It makes the same prediction for the relative production rate of the J/ψ and ψ(2S) mesons. By looking back at Figures 3.1, 3.2, and 3.4, however, we

immediately note that the experimentally measured values of these relative rates are all less than 0.7 and most are less than 0.5. Thus, the technique expressed by Equation 5.2 must be regarded as incomplete.

Edin, Ingelman, and Rathsman suggested the inclusion of a factor to suppress the radially excited states [78]. More specifically, they recommended dividing the spin-counting factor by the main quantum number in accordance with the following equation:

$$\rho_{nJ^{PC}} = \frac{(2J+1)/n}{\sum_i (2J_i+1)/n_i} \tag{5.3}$$

This addition does yield improved predictions, but this improvement is far too small to bring the results into agreement with data. For example, Equation 5.3 predicts that the relative production rate of the J/ψ and ψ(2S) mesons is 0.5. In Figure 3.4, however, we saw that the experimental measurements of this rate all fall between 0.1 and 0.3.

Another approach was suggested by Mangano [79]. His method assumes that the quarkonium state produced will always be the heaviest one with a mass less than the invariant mass of the heavy quark pair. This idea can be summarized as follows:

$$\rho_{nJ^{PC}} = \frac{(2J+1)\frac{\Delta M}{M}}{\sum_i (2J_i+1)\frac{\Delta M_i}{M_i}} \tag{5.4}$$

In this expression, ΔM represents the mass splitting between the quarkonium state under study and the next heavier state. If the state under consideration is the heaviest in the system, the difference between threshold and the state's mass is used instead. This technique predicts some relative production rates quite well. For example, it yields a relative production rate of

0.49 for the Y(1S) and Y(2S) mesons, which agrees quite nicely with the average experimental value of 0.53 (see Figure 3.1). In other cases, however, its results are rather poor. It predicts a relative rate of 0.46 for the Y(1S) and Y(3S) mesons, which is much larger than experimental average of 0.19 (see Figure 3.2) Thus, although this method is much more successful than the others we have discussed, it is still not satisfactory for our purposes.

Having gained a bit of intuition from our analysis of earlier efforts, we now begin our own attempts to develop a technique for predicting long-distance factors. As stated earlier, our equation should depend only on fundamental quarkonium parameters such as mass, total width, and the quantum numbers n, J, P, and C. Extensive trial and error with various seemingly logical combinations of these parameters has led us to the following expression:

$$\rho_{nJ^{PC}} = \frac{(2J+1)\, e^{-\left(\frac{M}{2M_Q}\right)^2} e^{-n\left(\frac{n-1}{N+1}\right)}}{\sum_i (2J_i+1)\, e^{-\left(\frac{M_i}{2M_Q}\right)^2} e^{-n_i\left(\frac{n_i-1}{N_i+1}\right)}} \tag{5.5}$$

This equation consists of three major components. The first is the statistical spin counting factor that has appeared in every method we have considered. The second is an exponential suppression of heavier states. The scale in this suppression factor is set by M_Q, the mass of the heavy quark. The final component is an exponential suppression of radial excitations. Here, the notation may require a bit of clarification. The symbol "n" designates the main quantum number, but the symbol "N" denotes the number of sub-threshold quarkonium states having the same J, P, C, and L quantum numbers as the state under consideration. For example, the Y(1S) meson has n = 1 and N = 3. In the next two sections, we will test

Equation 5.5's ability to predict the long-distance factors for the bottomonium and charmonium systems and analyze its implications for the Color Evaporation Model.

5.2 Bottomonium Results

The level scheme for the sub-threshold portion of the bottomonium system is shown in Figure 5.1. In plotting these levels, we have used the experimentally measured masses for the observed states [80]. The masses of the unobserved states were taken from Reference [81], where they were calculated using a Buchmuller-Tye potential [82]. At this point, we have not included the possibility of D-wave states. We will, however, address their impact later in this section.

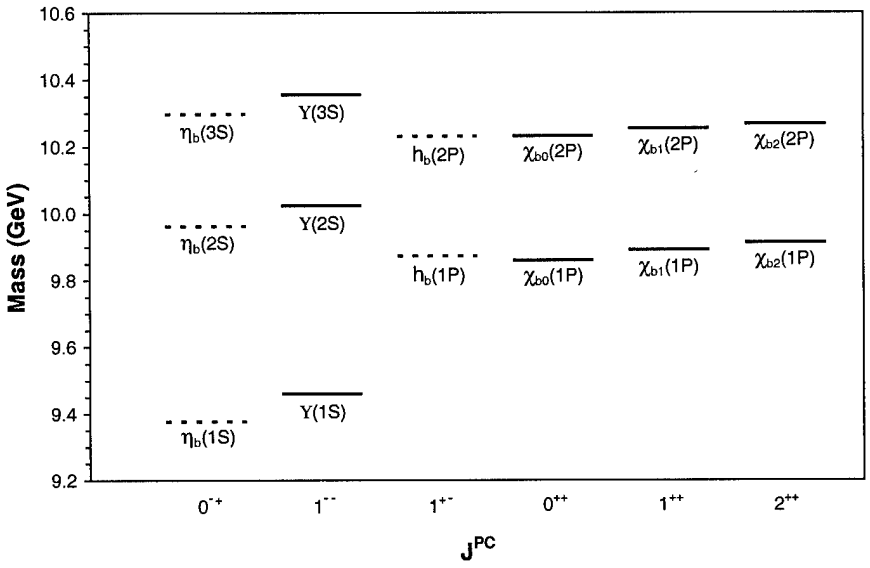

Figure 5.1: The level scheme of the bottomonium system, excluding D-wave states. Experimentally observed states are represented by solid lines. States that have yet to be observed are represented by dashed lines.

We have used Equation 5.5 to predict the long-distance factors for all 14 of the bottomonium states shown in this level diagram. The results, stated in the language of the

revised maximal version of the Color Evaporation Model (Equation 5.1), are consolidated in Table 5.1. The table also includes the values of the parameters J, M, n, and N used for each state. The masses of the quarkonium states are those used in the construction of Figure 5.1. As in Chapter 4, the bottom quark mass was set to $M_b = 4.75$ GeV.

Meson	J	M (GeV)	n	N	ρ (%)
$\eta_b(1S)$	0	9.377	1	3	4.42
$\eta_b(2S)$	0	9.963	2	3	2.36
$\eta_b(3S)$	0	10.298	3	3	0.81
Y(1S)	1	9.46037	1	3	13.03
Y(2S)	1	10.02330	2	3	7.00
Y(3S)	1	10.3553	3	3	2.39
$h_b(1P)$	1	9.873	1	2	11.93
$h_b(2P)$	1	10.231	2	2	5.65
$\chi_{b0}(1P)$	0	9.8598	1	2	3.99
$\chi_{b1}(1P)$	1	9.8919	1	2	11.88
$\chi_{b2}(1P)$	2	9.9132	1	2	19.70
$\chi_{b0}(2P)$	0	10.2321	2	2	1.88
$\chi_{b1}(2P)$	1	10.2552	2	2	5.62
$\chi_{b2}(2P)$	2	10.2685	2	2	9.34

Table 5.1: Long-distance factors for the bottomonium system.
The values shown are the predictions of Equation 5.5.

Next, we test the accuracy of these predictions by comparing the resulting relative production rates to experimental data. In Figures 5.2, 5.3, and 5.4, we have redrawn the plots of relative production rate versus center-of-mass energy that were used in the analysis of Chapter 3 but added solid lines to show the rates predicted using the long-distance factors from Table 5.1. Our predictions match the data very well.

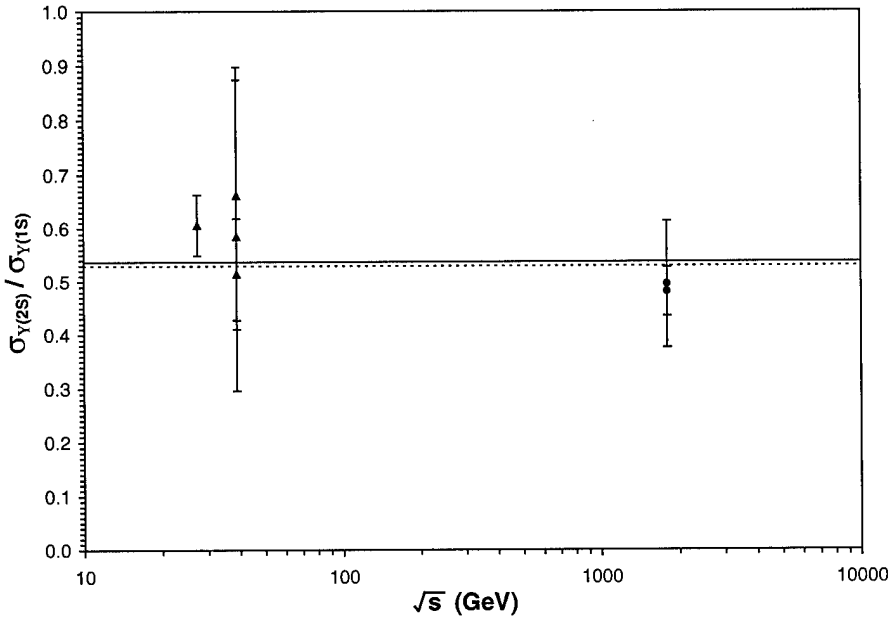

Figure 5.2: Plot of $\sigma_{Y(2S)}/\sigma_{Y(1S)}$ vs. $\sqrt{s}$ [22, 42-46]. The dashed line represents the weighted mean of the data. The solid line is the prediction of Equation 5.5.

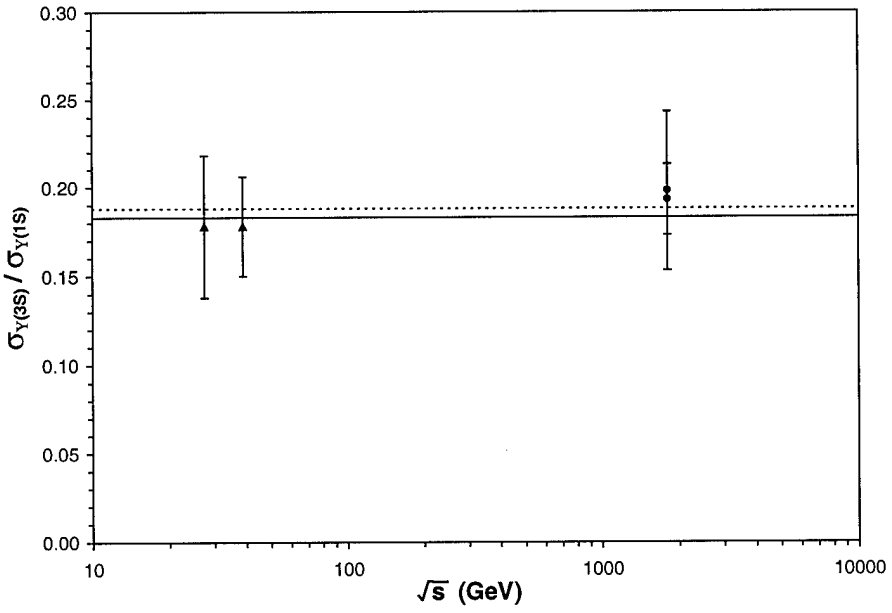

Figure 5.3: Plot of $\sigma_{Y(3S)}/\sigma_{Y(1S)}$ vs. $\sqrt{s}$ [22, 43, 45, 46]. The dashed line represents the weighted mean of the data. The solid line is the prediction of Equation 5.5.

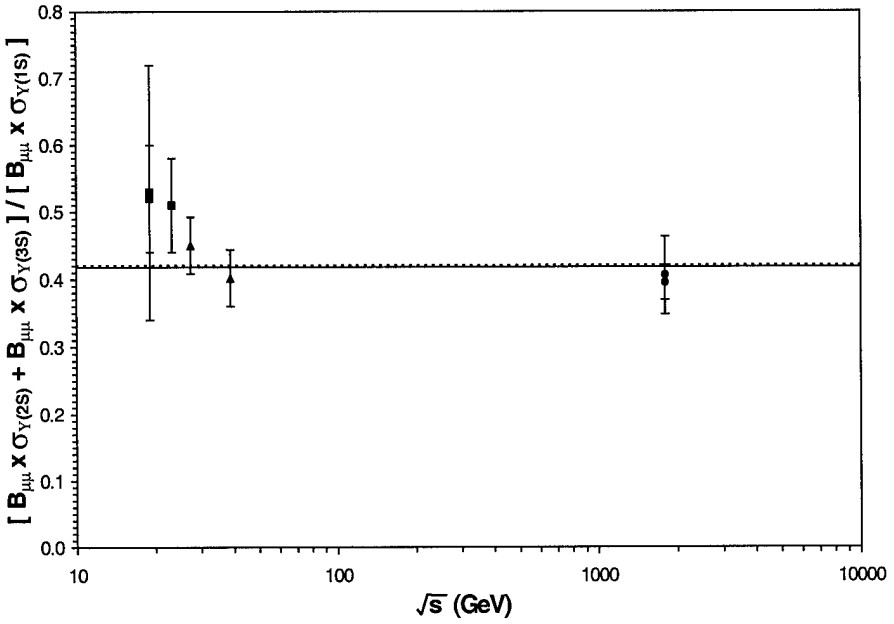

Figure 5.4: Plot of $[B_{\mu\mu} \times \sigma_{Y(2S)} + B_{\mu\mu} \times \sigma_{Y(3S)}] / [B_{\mu\mu} \times \sigma_{Y(1S)}]$ vs. $\sqrt{s}$ [22, 43, 45-48]. The dashed line represents the weighted mean of the data. The solid line is the prediction of Equation 5.5. The symbol "$B_{\mu\mu}$" denotes the muonic branching ratio of the adjacent meson.

We can combine these results with those of the previous chapter to estimate β_b, the percentage of sub-threshold bottom quark pairs that emerge as bottomonium states. By equating the right-hand sides of Equations 5.1 and 2.5, we obtain the relation:

$$\beta_Q = \frac{F_{nJ^{PC}}}{\rho_{nJ^{PC}}} \tag{5.6}$$

Using the next-to-leading order values of $F_{nJ^{PC}}$ calculated in Chapter 4 and the values of $\rho_{nJ^{PC}}$ from Table 5.1, this equation yields the average result $\beta_b = 0.32$. This agrees quite well with the prediction of the original work on the minimal version of the model [13], which suggested that the appropriate fraction is between 17 and 32 percent. As expected, however, it sharply contradicts the un-revised maximal version's prediction of $\beta_b = 0.11$ [8].

The existence of D-wave bottomonium states is uncertain. It is interesting, however, to consider the impact that their presence would have on our analysis. To do so, we introduced the spin-singlet $\eta_b(1D)$ state and the three spin-triplet $Y_J(1D)$ states as shown in Figure 5.5, then repeated our calculations. Once again, we assigned these unobserved states the mass values predicted in Reference [81].

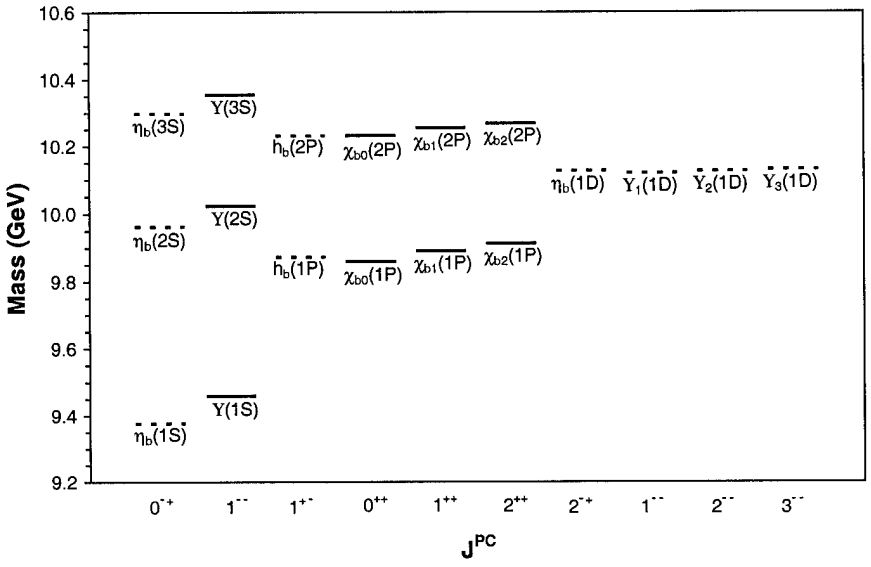

Figure 5.5: The level scheme of the bottomonium system, including D-wave states. Experimentally observed states are represented by solid lines. States that have yet to be observed are represented by dashed lines.

The new values of all the long-distance factors resulting from this calculation can be found in the consolidated listing at the end of this section (Table 5.2). Note that inclusion of the L = 2 states did not change the numerical values of the minimal version's long-distance factors. Nor did it alter the predicted relative production rates. It did, however, change the quarkonium fraction to $\beta_b = 0.56$. This rather significant increase implies that the production cross sections for the D-wave bottomonium states are comparatively large. By

extension, if the n = 2 D-wave states and the n = 1 F-wave states are included in the spectrum, the quarkonium fraction could approach 100 percent.

We conclude this section by tabulating all our results in the language of both versions of the Color Evaporation Model. This consolidated list of long-distance factors is given in Table 5.2.

Meson	ρ (%) ($L < 2$)	F (%) ($L < 2$)	ρ (%) ($L \leq 2$)	F (%) ($L \leq 2$)
$\eta_b(1S)$	4.42	1.41	2.52	1.41
$\eta_b(2S)$	2.36	0.76	1.35	0.76
$\eta_b(3S)$	0.81	0.26	0.46	0.26
$\Upsilon(1S)$	13.03	4.17	7.44	4.17
$\Upsilon(2S)$	7.00	2.24	4.00	2.24
$\Upsilon(3S)$	2.39	0.76	1.36	0.76
$h_b(1P)$	11.93	3.82	6.81	3.82
$h_b(2P)$	5.65	1.81	3.23	1.81
$\chi_{b0}(1P)$	3.99	1.28	2.28	1.28
$\chi_{b1}(1P)$	11.88	3.80	6.78	3.80
$\chi_{b2}(1P)$	19.70	6.30	11.25	6.30
$\chi_{b0}(2P)$	1.88	0.60	1.08	0.60
$\chi_{b1}(2P)$	5.62	1.80	3.21	1.80
$\chi_{b2}(2P)$	9.34	2.99	5.33	2.99
$\eta_b(1D)$	--	--	10.72	6.00
$\Upsilon_1(1D)$	--	--	6.44	3.60
$\Upsilon_2(1D)$	--	--	10.73	6.00
$\Upsilon_3(1D)$	--	--	15.01	8.40

Table 5.2: Long-distance factors for the bottomonium system. The values shown are the combined predictions of Equation 5.5 and Equation 5.6.

5.3 Charmonium Results

Next, we perform an identical analysis on the charmonium system. The level scheme for the sub-threshold portion of this system is shown in Figure 5.6. All the masses used in this diagram are experimental measurements taken from Reference [80]. The D-wave and other large L charmonium states are all expected to lie above threshold so, in this system, the issue of their inclusion does not arise.

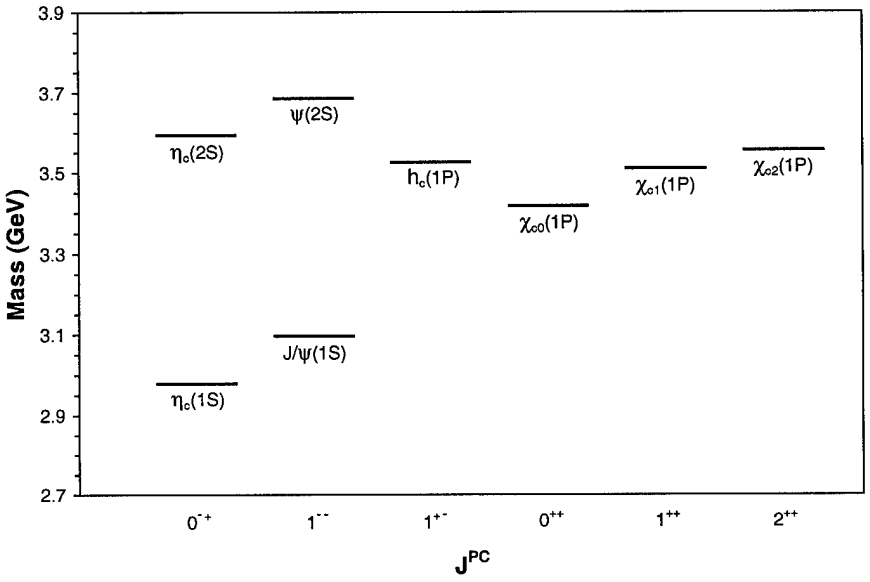

Figure 5.6: The level scheme of the charmonium system.

We have used Equation 5.5 to predict the long-distance factors for all 8 of the charmonium states shown in our level diagram. The results, stated in the language of the maximal version of the Color Evaporation Model (Equation 5.1), are consolidated in Table 5.3. The table also includes the values of the parameters J, M, n, and N used for each state. The masses of the quarkonium states are those used in the construction of Figure 5.1. As in Chapter 4, the charm quark mass was set to $M_c = 1.20$ GeV.

Meson	J	M (GeV)	n	N	ρ (%)
$\eta_c(1S)$	0	2.9798	1	2	9.03
$\eta_c(2S)$	0	3.594	2	2	2.30
$J/\psi(1S)$	1	3.09688	1	2	23.95
$\psi(2S)$	1	3.68600	2	2	6.15
$h_c(1P)$	1	3.52614	1	1	14.62
$\chi_{c0}(1P)$	0	3.4173	1	1	5.56
$\chi_{c1}(1P)$	1	3.51053	1	1	14.90
$\chi_{c2}(1P)$	2	3.55617	1	1	23.49

Table 5.3: Long-distance factors for the charmonium system.
The values shown are the predictions of Equation 5.5.

Next, we test the accuracy of these predictions by comparing the resulting relative production rates to experimental data. In Figures 5.7, 5.8, and 5.9, we have redrawn the plots of relative production rate versus center-of-mass energy that were used in the analysis of Chapter 3 but added a solid line to show the rate predicted using the long-distance factors from Table 5.3. Note, however, that the plot of the relative $J/\psi - \psi(2S)$ production rate (Figure 5.7) contains two solid lines. The upper line represents our prediction for quarkonium production methods that involve an anti-proton beam in the initial state. It is the direct ratio of our calculated long-distance factors. The lower line represents our prediction for quarkonium production in the absence of an anti-proton beam. To obtain it, we divided the $\psi(2S)$ long-distance factor by two as suggested in Section 4.4. Once again, our predictions match the data very well.

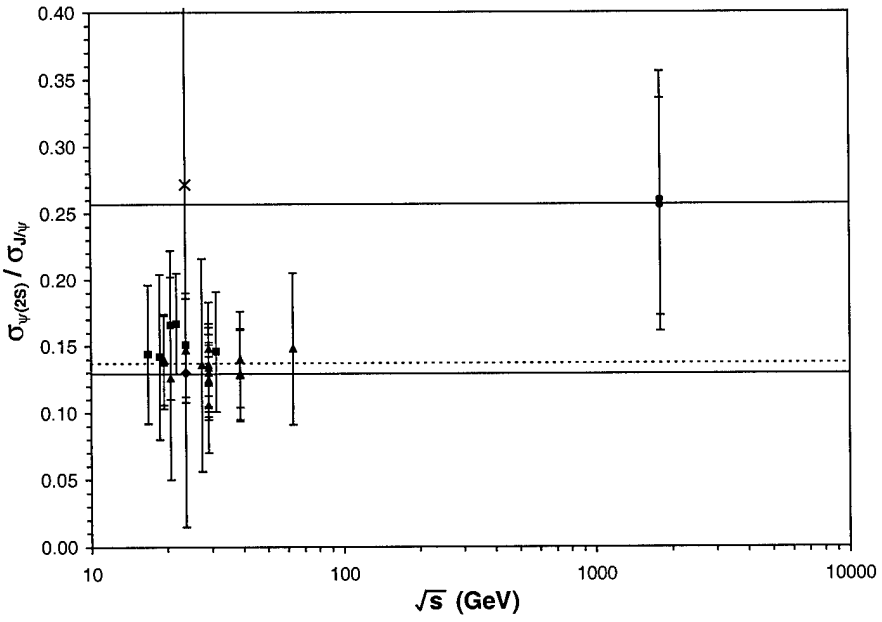

Figure 5.7: Plot of $\sigma_{\psi(2S)} / \sigma_{J/\psi}$ vs. $\sqrt{s}$ [14, 16, 42, 49-56]. The dashed line represents the weighted mean of the data. The solid line is the prediction of Equation 5.5.

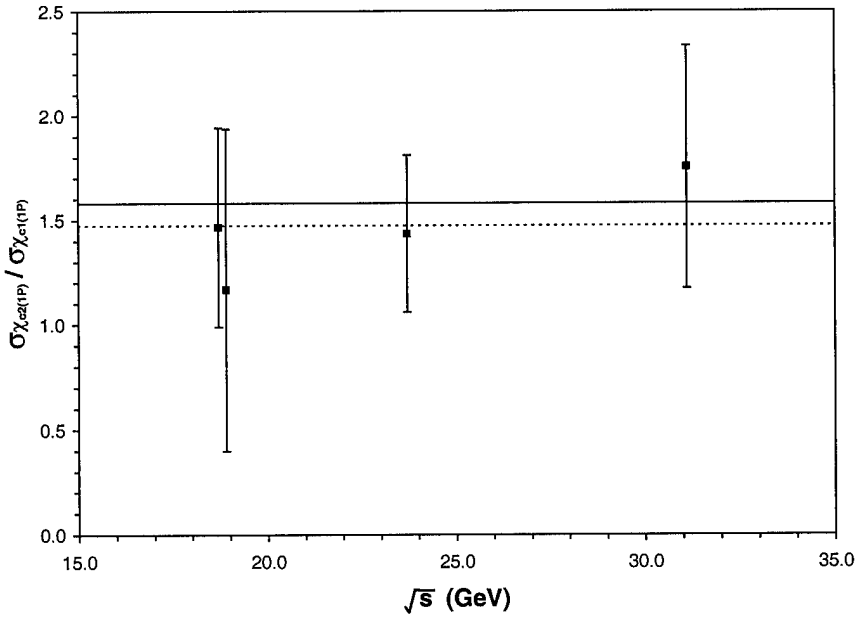

Figure 5.8: Plot of $\sigma_{\chi_{c2(1P)}} / \sigma_{\chi_{c1(1P)}}$ vs. $\sqrt{s}$ [14, 54, 57]. The dashed line represents the weighted mean of the data. The solid line is the prediction of Equation 5.5.

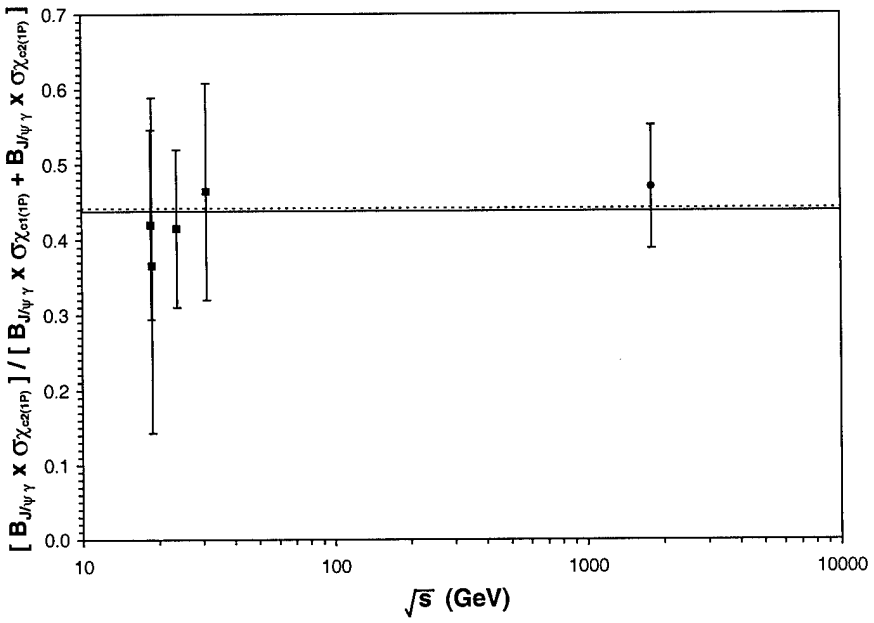

Figure 5.9: Plot of $[B_{J/\psi\,\gamma} \times \sigma_{\chi_{c2(1P)}}] / [B_{J/\psi\,\gamma} \times \sigma_{\chi_{c1(1P)}} + B_{J/\psi\,\gamma} \times \sigma_{\chi_{c2(1P)}}]$ vs. $\sqrt{s}$ [14, 54, 57, 58]. The dashed line represents the weighted mean of the data. The solid line is the prediction of Equation 5.5. The symbol "$B_{J/\psi\,\gamma}$" denotes the adjacent meson's branching ratio to $J/\psi + \gamma$.

Finally, we use Equation 5.6 to obtain an estimate of β_c, the percentage of sub-threshold charm quark pairs that emerge as quarkonium states. With the next-to-leading order values of $F_{n^{J^{PC}}}$ calculated in Chapter 4 and the values of $\rho_{n^{J^{PC}}}$ from Table 5.3, we obtain the average result $\beta_c = 0.10$. This value is in good agreement with the predictions of the original work on both the minimal and maximal versions of the Color Evaporation Model.

As mentioned at the beginning of this section, there is no need to consider the impact of higher L states in the charmonium system. Thus, we once again conclude by tabulating our results in the language of both versions of the Color Evaporation Model. This consolidated list of charmonium long-distance factors is given in Table 5.4.

Meson	ρ (%)	F (%)
$\eta_c(1S)$	9.03	0.90
$\eta_c(2S)$	2.30	0.23
$J/\psi(1S)$	23.95	2.40
$\psi(2S)$	6.15	0.62
$h_c(1P)$	14.62	1.46
$\chi_{c0}(1P)$	5.56	0.56
$\chi_{c1}(1P)$	14.90	1.49
$\chi_{c2}(1P)$	23.49	2.35

Table 5.4: Long-distance factors for the charmonium system. The values shown are the predictions of Equation 5.5.

5.4 Conclusions

We have succeeded in constructing an equation that predicts the long-distance factors for all heavy quarkonium states in terms of a few basic parameters (Equation 5.5). Granted, our expression is not grounded in physical principle or mathematical rigor. It is simply a collection of factors we have grouped together with no justification other than their ability to produce the desired numerical results. Despite the simplicity of our technique, however, the long-distance factors produced by our equation do agree quite nicely with the available data on the observed states of both heavy quarkonium systems. This suggests that they might produce reasonable approximations of the cross sections and relative production rates for the unobserved states as well. Accordingly, our equation can be counted among the resources available to the theorist in need of a numerical value for use in a quarkonium calculation or the experimentalist looking for an estimate of the result to expect from a quarkonium measurement.

An immediate application of our equation was the ability to predict the fraction of sub-threshold heavy quark pairs that emerge as quarkonium states. For the charmonium system, our estimated fraction was 10 percent. For the bottomonium system, however, we estimated that the fraction was at least 30 percent and that, depending on the number and type of higher L states assumed to have masses below threshold, it could be as high as 100 percent. Thus, we refute the universal fraction of 1/9 that the maximal version of the Color Evaporation Model predicted using color counting arguments. The model should be adjusted to allow the quarkonium fraction to vary from system to system as we suggested in Equation 5.1.

Chapter 6

Summary and Conclusion

At this point, we have met our primary intent of testing the predictions of the maximal version of the Color Evaporation Model against the available hadroproduction data on the bottomonium system. We have also accomplished our secondary objective of testing the model's predictions for the charmonium system. As expected, the additional charmonium analysis has allowed us to examine the validity of previous results and to identify differences between the two heavy quarkonium systems. We now conclude by recalling our most significant results one chapter at a time, highlighting the original contributions made by this thesis, and offering suggestions for future work on this topic.

6.1 Summary of Results

6.1.1 Chapter 3

In Chapter 3, we discovered that the available experimental data generally supports the Color Evaporation Model's assertion that the dynamics of heavy quarkonium production are simply those of heavy quark pair production and thus, they are contained entirely within the perturbative, short-distance factors. We based this conclusion on three pieces of evidence. First, the relative production rates for different quarkonium states are generally independent of dynamical variables such as $\sqrt{s}$, P_T, and X_F. Second, the differential distributions for different quarkonium states have essentially the same shapes. Finally, quarkonium states are produced with no consistently preferred direction of polarization or spin alignment.

We did, however, note two isolated, but potentially significant, cases where the data on the charmonium system contradicted the model's predictions. First, the relative production rate of J/ψ and ψ(2S) mesons measured by experiments using anti-proton beams is twice as large as the rate measured by experiments using other beam types. Second, for J/ψ and ψ(2S) mesons, all three of the pieces of evidence cited above become invalid in the limit of very large X_F. This behavior suggests that, because the mass of the charm quark is only slightly larger than the energy scale at which we expect perturbation theory to fail, it may not be possible to completely isolate the production dynamics of charmonium in the perturbative portion of the model.

6.1.2 Chapter 4

In Chapter 4, we extracted leading order and next-to-leading order long-distance factors from the available data on experimentally observed quarkonium states. The results of this effort are consolidated in Table 4.4. They agree quite well with the long-distance factors produced in other works on the Color Evaporation Model.

Despite this numerical agreement, our results contradicted two of the tenets of the maximal version of the model. First, the above-threshold pair production cross section is not negligible in either heavy quark system. Thus, we are suspicious of all previous calculations that ignored the above-threshold contribution. Second, although the prediction that only 1/9 of sub-threshold heavy quark pairs form quarkonium states seems reasonable in the charmonium system, the quarkonium fraction for the bottomonium system is probably much larger.

6.1.3 Chapter 5

In Chapter 5, we constructed a universal equation to predict the long-distance factors for all quarkonium states in terms of a few basic parameters. Although our technique was not sophisticated, our equation successfully reproduced the available data on the observed states of both heavy quarkonium systems. This implies that it might accurately predict the properties of the unobserved states as well.

By using our equation to predict the fraction of sub-threshold heavy quark pairs that emerge as quarkonium states in each system, we discovered further evidence that the maximal version's universal quarkonium fraction of 1/9 is not correct. Our estimated fraction for charmonium was 10 percent. For bottomonium, however, we found that the fraction was at least 30 percent and that, depending on the number and type of higher L states assumed to have masses below threshold, it could be as high as 100 percent.

6.2 Summary of Contributions Made by this Project

The majority of the results in this thesis do not constitute new and original contributions to the body of scientific knowledge. Rather, they are almost exclusively confirmations, refutations, or slight extensions of previous works. The lone exception is Equation 5.5, our universal technique for predicting long-distance factors. Although this contribution is small, its ability to provide estimates for the cross sections of unobserved quarkonium states may prove useful in some applications. Accordingly, our equation can be counted among the resources available to the theorist in need of a numerical value for use in a quarkonium calculation or the experimentalist looking for an estimate of the result to expect from a quarkonium measurement.

6.3 Suggestions for Further Work

As a starting point, we suggest the immediate removal of two ideas from the maximal version of the Color Evaporation Model. First, any implication that the above-threshold pair production cross section can be ignored when estimating the production rate for open-flavored mesons should be stricken from the model. Second, the universal quarkonium fraction of 1/9 should be replaced with a system dependent fraction in accordance with Equation 5.1.

Next, we suggest that our technique for predicting the long-distance factors of unobserved quarkonium states (Equation 5.5) be challenged when appropriate data becomes available. If our equation's predictions agree with the initial data on newly observed states, its utility will be confirmed. If they do not agree, however, the new results can be used to modify and improve the equation.

We also recommend an investigation to explain the increase of the relative charmonium production rates observed in anti-proton reactions. The answer could be revealed by the simple study of additional quarkonium production data from fixed target experiments using anti-proton beams. More likely, however, the explanation will require a better understanding of the non-perturbative aspects of QCD.

Finally, and perhaps most importantly, we suggest a detailed study of the behavior of quarkonium systems at large X_F. If the phenomena we observed are limited to the charmonium system, they might be explained by non-perturbative effects. If similar behavior is observed in large X_F bottomonium data, however, the Color Evaporation Model could require significant revision.

We have offered four suggestions for further work on the Color Evaporation Model. The first two are rather simple. The third and fourth, however, are critical. If these two issues can not be sufficiently resolved, the Color Evaporation Model will eventually lose its status as a candidate for the basic theory of quarkonium production and be relegated to the role of a useful phenomenological tool.

Appendix A

Relevant Feynman Diagrams

This appendix contains the 28 tree-level Feynman diagrams that contribute to the three processes used for the calculations described in Chapter 4. They are shown in the format generated by the MADGRAPH package [61]. Although every light quark is labeled "u" and every heavy quark is labeled "b" in this depiction, the diagrams are equally valid under appropriate substitution of the other quark flavors.

A.1 Diagrams for the Process $q\bar{q} \rightarrow gQ\bar{Q}$

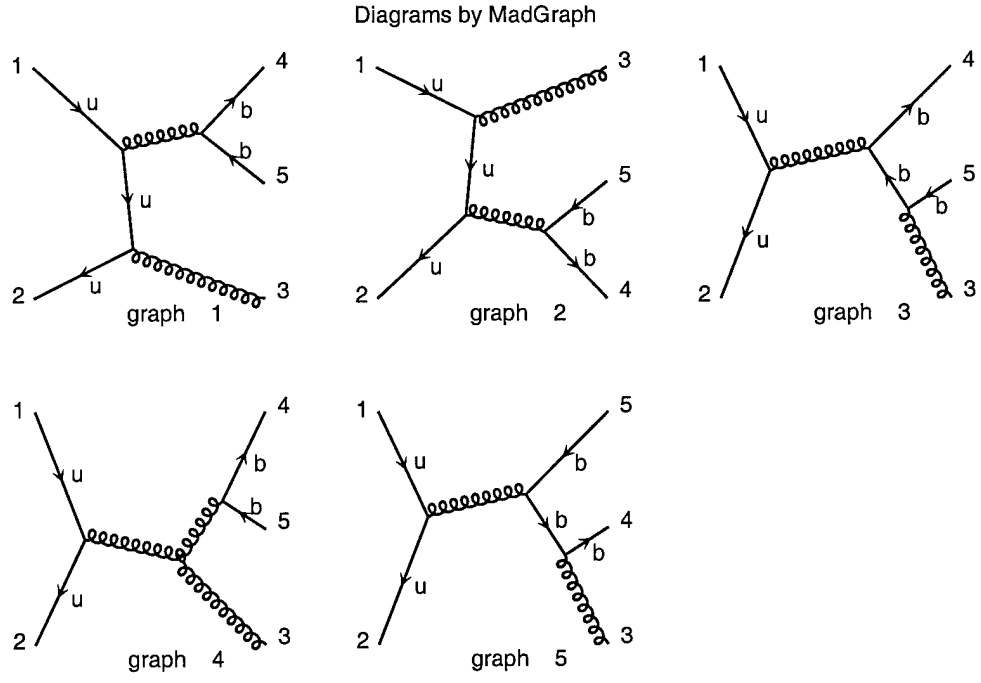

A.2 Diagrams for the Process $gg \to gQ\overline{Q}$

Diagrams by MadGraph

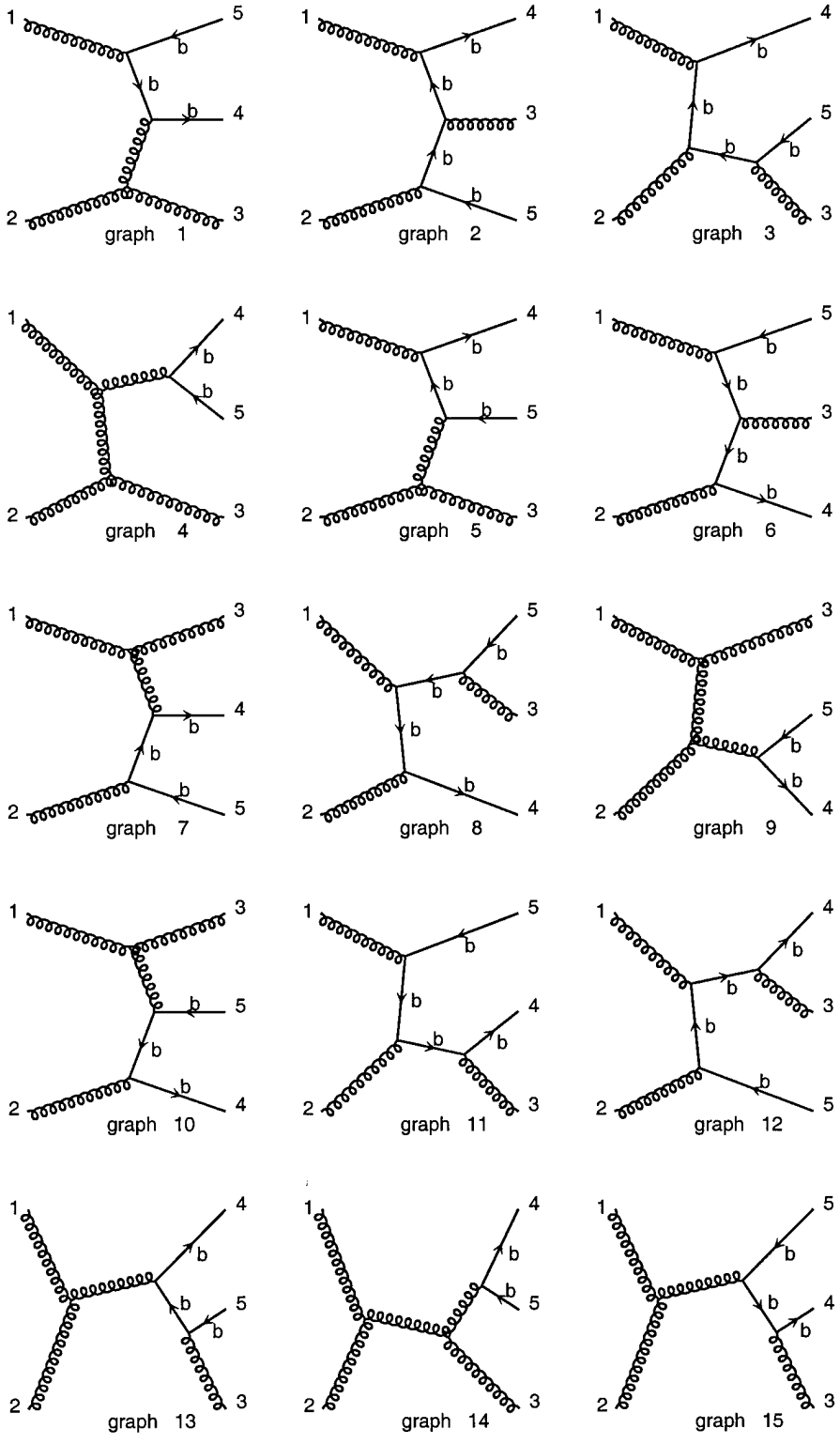

Diagrams by MadGraph

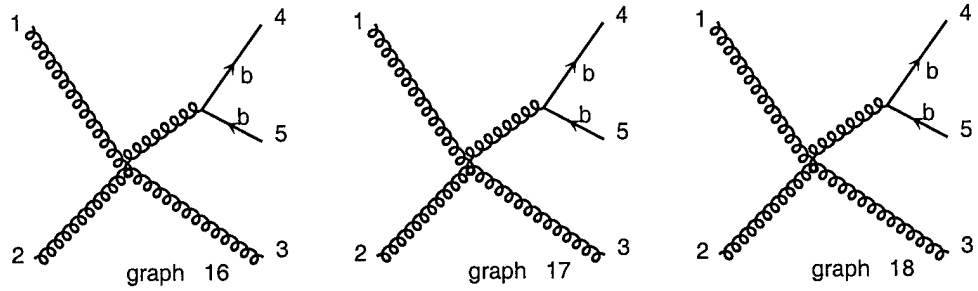

A.3 Diagrams for the Process $qg \rightarrow qQ\overline{Q}$

Diagrams by MadGraph

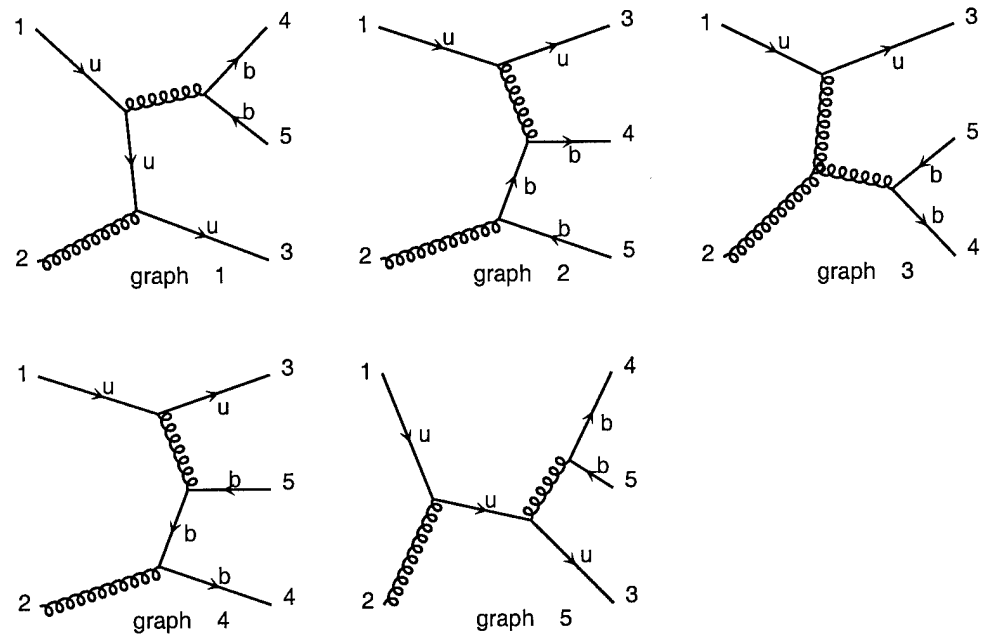

References

[1] R. K. Ellis, W. J. Stirling and B. R. Webber, *QCD and Collider Physics* (Cambridge University Press, Cambridge, 1996).

[2] F. Halzen and A. D. Martin, *Quarks and Leptons: An Introductory Course in Modern Particle Physics* (John Wiley and Sons, New York, 1984).

[3] O. Nachtmann, *Elementary Particle Physics: Concepts and Phenomena* (Springer-Verlag, Berlin, 1990).

[4] K. Huang, *Quarks, Leptons, and Gauge Fields*, 2nd ed. (World Scientific, Singapore, 1992), p. 254.

[5] S. Weinberg, *The Quantum Theory of Fields, Volume II: Modern Applications* (Cambridge University Press, Cambridge, 1996), p. 156.

[6] I. Hinchliffe, Eur. Phys. J. C **3**, 81 (1998).

[7] A. Manohar, Eur. Phys. J. C **3**, 337 (1998).

[8] J. F. Amundson, O. J. P. Eboli, E. M. Gregores and F. Halzen, Phys. Lett. **372B**, 127 (1996).

[9] J. F. Amundson, O. J. P. Eboli, E. M. Gregores and F. Halzen, Phys. Lett. **390B**, 323 (1997).

[10] O. J. P. Eboli, E. M. Gregores and F. Halzen, Phys. Lett. **395B**, 113 (1997).

[11] O. J. P. Eboli, E. M. Gregores and F. Halzen, Phys. Rev. D **60**, 117501 (1999).

[12] R. Gavai, D. Kharzeev, H. Satz, G. A. Schuler, K. Sridhar and R. Vogt, Int. J. Mod. Phys. **A10**, 3043 (1995).

[13] G. A. Schuler and R. Vogt, Phys. Lett. **387B**, 181 (1996).

[14] G. A. Schuler, *Quarkonium Production and Decays*, CERN-TH.7170/94 (1994).

[15] G. A. Schuler, Z. Phys. C **71**, 317 (1996).

[16] F. Abe *et al.* (CDF Collaboration), Phys. Rev. Lett. **79**, 572 (1997).

[17] B. Guberina, J. H. Kuhn, R. D. Peccei and R. Ruckl, Nucl. Phys. **B174**, 317 (1980).

[18] E. L. Berger and D. Jones, Phys. Rev. D **23**, 1521 (1981).

[19] R. Baier and R. Ruckl, Phys. Lett. **102B**, 364 (1981).

[20] R. Baier and R. Ruckl, Z. Phys. C **19**, 251 (1983).

[21] R. Gastmans, W. Troost and T. T. Wu, Nucl. Phys. **B291**, 731 (1987).

[22] CDF Collaboration, Measurement *of the Y(1S), Y(2S), and Y(3S) Cross Sections and the Polarization of the Y(1S) State in Run Ib*, http://www-cdf.fnal.gov/physics/new/bottom/cdf5027/cdf5027.html (unpublished).

[23] CDF Collaboration, *Measurement of Prompt J/ψ Production Polarization at CDF*, http://www-cdf.fnal.gov/physics/new/bottom/cdf5029/cdf5029.html (unpublished).

[24] CDF Collaboration, *Measurement of Production Polarization in* $\psi(2S) \rightarrow \mu^+ \mu^-$, http://www-cdf.fnal.gov/physics/new/bottom/cdf4876/cdf4876.html (unpublished).

[25] L. D. Faddeev and V. N. Popov, Phys. Lett. **25B**, 29 (1967).

[26] G. T. Bodwin, E. Braaten and G. P. Lepage, Phys. Rev. D **51**, 1125 (1995).

[27] P. Cho and A. K. Leibovich, Phys. Rev. D **53**, 150 (1996).

[28] P. Cho and A. K. Leibovich, Phys. Rev. D **53**, 6203 (1996).

[29] E. Braaten, S. Fleming and T. C. Yuan, Ann. Rev. Nucl. Part. Sci. **46**, 197 (1996).

[30] J. E. Augustin *et al.*, Phys. Rev. Lett. **33**, 1406 (1974).

[31] J. J. Aubert *et al.*, Phys. Rev. Lett. **33**, 1404 (1974).

[32] M. B. Einhorn and S. D. Ellis, Phys. Rev. D **12**, 2007 (1975).

[33] H. Fritzsch, Phys. Lett. **67B**, 217 (1977).

[34] F. Halzen, Phys. Lett. **69B**, 105 (1977).

[35] F. Halzen and S. Matsuda, Phys. Rev. D **17**, 1344 (1978).

[36] M. Gluck, J. F. Owens and E. Reya, Phys. Rev. D **17**, 2324 (1978).

[37] J. Babcock, D. Sivers and S. Wolfram, Phys. Rev. D **18**, 162 (1978).

[38] V. D. Barger and R. J. N. Phillips, *Collider Physics*, 2nd Ed. (Addison-Wesley, Reading, 1997).

[39] M. Gluck and E. Reya, Phys. Lett. **79B**, 453 (1978).

[40] V. D. Barger, W. Y. Keung and R. J. N. Phillips, Phys. Lett. **91B**, 253 (1980).

[41] V. D. Barger, W. Y. Keung and R. J. N. Phillips, Z. Phys. C **6**, 169 (1980).

[42] T. Alexopoulos *et al.* (E771 Collaboration), Phys. Lett. **374B**, 271 (1995).

[43] G. Moreno *et al.* (E605 Collaboration), Phys. Rev. D **43**, 2815 (1991).

[44] T. Yoshida *et al.*, Phys. Rev. D **39**, 3516 (1989).

[45] K. Ueno *et al.*, Phys. Rev. Lett. **42**, 486 (1979).

[46] F. Abe *et al.* (CDF Collaboration), Phys. Rev. Lett. **75**, 4358 (1995).

[47] M. Grossmann-Handschin *et al.* (NA10 Collaboration), Phys. Lett. **179B**, 170 (1986).

[48] S. Falciano *et al.* (NA10 Collaboration), Phys. Lett. **158B**, 92 (1985).

[49] M. H. Schub *et al.* (E789 Collaboration), Phys. Rev. D **52**, 1307 (1995).

[50] T. Alexopoulos *et al.* (E771 Collaboration), Phys. Rev. D **55**, 3927 (1997).

[51] M. C. Abreu *et al.* (NA38 Collaboration), Phys. Lett. **444B**, 516 (1998).

[52] M. C. Abreu *et al.* (NA38 Collaboration), Phys. Lett. **466B**, 408 (1999).

[53] L. Antoniazzi *et al.* (E705 Collaboration), Phys. Rev. D **46**, 4828 (1992).

[54] V. Koreshev *et al.* (E672 and E706 Collaborations), Phys. Rev. Lett. **77**, 4294 (1996).

[55] J. G. Heinrich *et al.* (E615 Collaboration), Phys. Rev. D **44**, 1909 (1991).

[56] F. Abe *et al.* (CDF Collaboration), Phys. Rev. Lett. **69**, 3704 (1992).

[57] L. Antoniazzi *et al.* (E705 Collaboration), Phys. Rev. Lett. **70**, 383 (1993).

[58] CDF Collaboration, *Measurement of the Ratio of Production of χ_{c1} to χ_{c2}*, http://www-cdf.fnal.gov/physics/new/bottom/cdf3121/cdf3121.html (unpublished).

[59] V. Papadimitriou, *Charm and Beauty Production and Polarization at CDF*, presented at Les Rencontres de Physique de la Vallée d'Aoste: Results and Perspectives in Particle Physics (February 29, 2000).

[60] C. Biino *et al.* (E615 Collaboration), Phys. Rev. Lett. **58**, 2523 (1987).

[61] T. Stelzer and W. F. Long, Comp. Phys. Comm. **81**, 357 (1994).

[62] H. Murayama, I. Watanabe and K. Hagiwara, *HELAS: Helicity Amplitude Subroutines for Feynman Diagram Evaluations*, KEK-91-11 (1992).

[63] G. P. Lepage, *VEGAS: An Adaptive Multidimensional Integration Program*, CLNS-80/447 (1980).

[64] CERN Information Technology Division, *HBOOK: Statistical Analysis and Histogramming, Reference Manual*, CERN Program Library Long Writeups Y250 (1998) (available at http://wwwinfo.cern.ch/asdoc/Welcome.html).

[65] CERN Information Technology Division, *CERNLIB overview*, http://wwwinfo.cern.ch/asd/cernlib/overview.html.

[66] H. Plothow-Besch, Int. J. Mod. Phys. **A10**, 2901 (1995).

[67] H. Plothow-Besch, Comp. Phys. Comm. **75**, 396 (1993).

[68] H. Plothow-Besch, *PDFLIB: Nucleon, Pion, and Photon Parton Density Functions, Parton Density Functions of the Nucleus, and α_s Calculations, Users' Manual, Version 8.04*, CERN-ETT/TT/2000.04.17 (2000) (available at http:// wwwinfo.cern.ch/asdoc/Welcome.html).

[69] R. K. Ellis and J. C. Sexton, Nucl. Phys. **B282**, 642 (1987).

[70] H. L. Lai *et al.* (CTEQ Collaboration), Phys. Rev. D **55,** 1280 (1997).

[71] M. Gluck, E. Reya and A. Vogt, Z. Phys. C **67**, 433 (1995).

[72] M. L. Mangano, P. Nason and G. Ridolfi, Nucl. Phys. **B405**, 507 (1993).

[73] CDF Collaboration, *Measurement of the B Meson Differential Cross Section for Run 1A and 1B Using the Exclusive Decay $B^{\pm} \rightarrow J/\psi K^{\pm}$*, http://www-cdf.fnal.gov/ physics/new/bottom/cdf3634/cdf3634.html (unpublished).

[74] T. Affolder *et al.* (CDF Collaboration), Phys. Rev. Lett. **84**, 1663 (2000).

[75] F. Abe *et al.* (CDF Collaboration), Phys. Rev. Lett. **75**, 4358 (1995).

[76] G. Altarelli, M. Diemoz, G. Martinelli and P. Nason, Nucl. Phys. **B308**, 724 (1988).

[77] S. Frixione, M. L. Mangano, P. Nason and G. Ridolfi, Nucl. Phys. **B431**, 453 (1994).

[78] A. Edin, G. Ingelman and J. Rathsman, Phys. Rev. D **56**, 7317 (1997).

[79] M. L. Mangano, in *Proceedings of the 10^{th} Topical Workshop on Proton–Antiproton Collider Physics, Batavia, IL, 1995*, edited by R. Raja and J. Yoh (American Institute of Physics, College Park, 1996).

[80] C. Caso *et al.* (Particle Data Group), Eur. Phys. J. C **3**, 1 (1998).

[81] E. J. Eichten and C. Quigg, Phys. Rev. D **49**, 5845 (1994).

[82] W. Buchmuller and S. H. H. Tye, Phys. Rev. D **24**,132 (1981).

[83] M. E. Peskin and D. V. Schroeder, *An Introduction to Quantum Field Theory* (Perseus, Reading, 1995), pp. 512-517.